BULK HETEROJUNCTION ORGANIC SOLAR CELLS AND THIN FILM ELECTRODE BUFFER LAYERS: SYNTHESIS, PREPARATION AND CHARACTERIZATION

Ph.D. Thesis

By

Elhadi Abdalla Adam Arbab

Supervisor: Prof. Genene Tessema Mola

A thesis submitted for the fulfillment of the requirements for

Doctor of Philosophy of Science

In

Physics

School of Chemistry and Physics

College of Agriculture, Engineering and Science

University of KwaZulu-Natal

Pietermaritzburg Campus

South Africa

September 2016

ABSTRACT

Solution processed bulk heterojunction organic solar cells (BHJ-OSCs) have gained considerable attention during the last two decades and have become one of the future photovoltaic technologies in the production of inexpensive electricity power. This Ph.D. thesis deals with the fabrication and characterization of BHJ-OSCs based on π-conjugated polymers such as: poly(3-hexylthiophene) (P3HT) and poly [[4,8-bis [(2-ethyhexyl)oxy] benzo(1,2-b:4,5b) dithiophene 2, 6 diyl] [3fluoro2 [(2 ethylhexyl) carbonyl] thieno [3,4-b] thiophenediyl]] (PTB7) as electron donor materials. The donors were used in combination with [6,6]-phenyl-C61-butyric acid methyl ester (PCBM) as electron acceptor.

Different techniques were employed to improve the performance of BHJ-OSC devices. In this research the necessary efforts were made to optimize the composition of the photoactive layer in order to improve the power conversion efficiency (PCE) of the devices. To address the issue of environmental stability of the OSC devices we have conducted research on interfacial layer properties and morphology of the photoactive films. Experiments were carried out using both ternary and binary molecules blend photoactive layers in an effort to improve the photon absorption band of the medium. In most of the devices fabricated in these investigations a thin film of poly(ethylene -3-4-dioxy thiophene):poly styrene sulphonate, known as PEDOT:PSS, was formed by using spin coating which is used as a hole transport and

electron blocking layer (HTL). However, the acidic and hygroscopic nature of PEDOT:PSS has negative consequences for the performance and stability of BHJ-OSC devices. This problem was partially addressed using vanadium pentoxide (V_2O_5) thin films deposited by two electrochemical cells (TECC) as an alternative to PEDOT:PSS. We found encouraging results on the use of V_2O_5 to replace PEDOT:PSS as HTLs which effectively improved the performance and stability of the BHJ-OSC. The main cell parameters derived from the best-performed device with V_2O_5 HTL showed PCE, FF, V_{oc}, and J_{sc} are 2.43 %, 45 %, 550 mV, and 10 mAcm^{-2}, respectively. These values are higher than those parameters measured from PEDOT:PSS HTL devices using the same active layer. The lifetime measurements conducted on the various OSC devices provided us with information about the extent to which the devices were stable under ambient environment. We found OSCs with V_2O_5 as HTL exhibited more stability than PEDOT:PSS based devices by a factor of about ten.

The optical properties of transition metal oxide films such as V_2O_5 and ZnO/TiO_2 bilayer as a buffer layer in OSC devices showed high optical transmittance in the range from 400 nm to 700 nm. These films (V_2O_5 and ZnO/TiO_2 bilayer) exhibited a wide energy band gap of 2.4 eV and 3.4 eV, respectively.

In an effort to improve photon harvesting in OSC active layer, we have conducted experiment on both the binary and the ternary bulk-heterojunction active layer design prepared under ambient laboratory condition. The devices were composed of active layer using P3HT and PTB7 as donor and PCBM as acceptor materials. The devices have exhibited PCE ranging from (2 to 5)% depending on the type of the donor/acceptor blend active thin films and condition of buffer layers. The ternary blend showed generally better light harvesting compared to the binary counterpart.

The research also includes issues related to the deposition and characterization of some inor-

ganic thin films such as V_2O_5, ZnO, TiO_2 by using TECC for application in the OSCs. The thin films were characterized by employing several spectroscopic techniques such as double-beam UV-VIS spectrophotometer, scanning electron microscopy (SEM), energy-dispersive analysis X-ray (EDAX), transmission electron microscopy (TEM), Raman spectroscopy, photoluminces (PL), and X-ray diffractometer (XRD). The details of device preparations and characterization of the films are discussed extensively in the thesis.

PREFACE

The work described in this thesis was carried out from March 2013 to April 2016, under the supervision and direction of Professor Genene Tessema Mola, School of Chemistry and Physics , University of KwaZulu-Natal, Pietermaritzburg.

The thesis represent original work of the author and has not been otherwise been submitted in any form for any degree or diploma to any University. Where use has been made of the work of others it is duly acknowledged in the text.

Signature (Student):..... Date: 28^{th} of September 2016

Signature (Supervisor):..... Date: 28^{th} of September 2016

DECLARATION: PLAGIARISM

I, ELHADI ABDALLA ADAM ARBAB declare that:

(i) The research reported in this dissertation, except where otherwise indicated or acknowledged, is my original work.

(ii) This dissertation has not been submitted in full or in part for any degree or examination to any other university.

(iii) This dissertation does not contain other persons' data, pictures, graphs or other information, unless specifically acknowledged as being sourced from other persons.

(iv) This dissertation does not contain other persons writing, unless specifically acknowledged as being sourced from other researchers. Where other written sources have been quoted, then: a) Their words have been re-written but the general information attributed to them has been referenced.

b) Where their exact words have been used, their writing has been placed inside quotation marks, and referenced.

(v) Where I have used material for which publications followed, I have indicated in detail my role in the work.

(vi) This dissertation is primarily a collection of material, prepared by myself, published as journal articles or presented as a poster and oral presentations at conferences. In some cases, additional material has been included.

(vii) This dissertation does not contain text, graphics or tables copied and pasted from the Internet, unless specifically acknowledged, and the source being detailed in the dissertation and in the References sections.

Signed:.....

Date:.....

DECLARATION 2-PUBLICATIONS

Details of contribution to publications that form part and/or include research presented in this thesis (include publications in preparation, submitted, in journal and published give details of the contributions of each author to experimental work and writing of each publication)

1. Elhadi A.A. Arbab, and Genene T. Mola*, V_2O_5 thin films deposition for application in organic solar cells, Appl. Phys.A., 2016, 122, 405(p 8).

2. Genene T. Mola*, Elhadi A. A. Arbab, Bidini A. Taleatu, K. Kaviyarasu, A. Ishaq, and M. Maaza, Growth and characterization of V_2O_5 thin film on transparent electrode, Journal of Microscopy, 2016, pp. 1-8, DOI: 10.1111/jmi.12490.

3. Bidini A. Taleatu*, Elhadi A.A. Arbab and Genene T. Mola, Synthesis and some surface studies of laminated ZnO/TiO_2 transparent bilayer by two-step growth, Materials Science in Semiconductors Processing, 2016, 44, 85-90.

4. Elhadi A.A. Arbab, Bidini A. Taleatu and Genene Tessema Mola*, Ternary molecules blend organic bulk heterojunction solar cell, Materials Science in Semiconductors Processing, 2015, 40, 158-161.

5. Elhadi A.A. Arbab, Bidini Taleatu and Genene T. Mola*, Environmental stability of PTB7:PCBM bulk heterojunction solar cell, Journal of Modern Optics, 2014, 61(21), 1749-1753.

From all the above publications, my role included carried out all the experimental work and contributing to the writing of the manuscripts along the guidance of my supervisor. My supervisors were to edit, checking scientific content and my correction interpretation of data. Based on his expertise, has added some parts to the manuscripts.

Signed:.....

PUBLICATIONS I HAVE CONTRIBUTED BUT NOT INCLUDED IN THE THESIS

1. Bidini A. Taleatu*, Elhadi A.A. Arbab, and Genene T. Mola, Stable α-MnS thin film deposited by two-electrode cell: Synthesis, structural characterization and photoemission spectroscopic studies, Appl. Phys.A.,2015, 120, 959–965.

2. B. A. Taleatu*, E. Omotoso, E. A. A. Arbab, R. A. Lasisi, W. O. Makinde and G. T. Mola, Microstructural and optical properties of nanocrystalline MgS thin film as wide band gap barrier material, Appl. Phys. A, 2015, 118, 539-545.

3. Bidini A. Taleatu*, E. A.A. Arbab, E. Omotoso and G. T. Mola, Synthesis and microstructural studies of annealed Cu_2O/Cu_xS bilayer as transparent electrode material for photovoltaic and energy storage devices, Journal of Microscopy, 2014, 256 (1), 61–71.

4. Bizuneh Gebremichael, Elhadi A.A. Arbab, Genene Tessema Mola, Enhanced power conversion efficiency in a ternary structure polymer solar cell with additive at different composition of the donor, Manuscript submitted.

Signed:.....

Dedication

To my late mother

To my beloved father

To my wife Thurya

To my children

Rajeh, Raif, Reynad and Reydab

To my supervisor, Prof. Genene Tessema Mola

To those whom I hold dear in my heart

I dedicate this work.

Acknowledgements

Foremost, I would like to thank the Almighty Allah for everything, for his grace and for helping me to overcome all the challenges that I faced during the study.

I would like to express my sincere gratitude to my supervisor Prof. Genene Tessema Mola for the continuous support of my Ph.D. study and research, for his patience, motivation, enthusiasm, and immense knowledge. His guidance helped me throughout the time of research and writing of this thesis, as well as his financial support. I could not have imagined having a better advisor and mentor for my Ph.D. study.

My sincere thanks and appreciation also goes to Dr. Bidini A. Taleatu, for his encouragement, motivation, and enthusiasm.

I would like also to thank my family: especially my beloved wife, for their supporting me spiritually throughout my life.

I wish to extend special thanks to the Ministry of Higher Education & Scientific Research represented in Omdurman Islamic University, Khartoum, Sudan, for offering me the scholarship opportunities in its financial support.

I would like to thank also the University of KwaZulu-Natal (UKZN), College of Agriculture,

Engineering, and Science, School of Chemistry & Physics, Pietermaritzburg (PMB) campus, Scottsville, South Africa, for offering me the postgraduate scholarship opportunities and the equipment that I have used during my Ph.D. study.

Also, I thank my colleagues in the School of Chemistry & Physics, UKZN, PMB campus, in particular, Prof Mola's group for their support and motivation.

My gratitude also goes to members of staff at Microscopy and Microanalysis Unit (MMU) in the School of Life Sciences, UKZN.

In particular, I am grateful to Mr. Karl Penzhorn, Mr. Ravin Sivraman, and Mr. Shawn Bau, who made resources available for me when I needed them.

Last but not least, I would like to thank my friends, particularly my best friends Mr. Mugahid Tag-Eldin Abdelrahman and Mr. Hassan Abdalla Hassan for their support, encouragement and motivation.

List of Abbreviation and symbols

A	Acceptor
Al	Aluminum
Ag	Silver
AM	Air mass
BHJ-OSCs	Bulk heterojunction organic solar cells
C_{60}	Buckminsterfullerene
CIGS	Copper Indium Gallium Diselenide
CdS	Cadmium sulphide
CdTe	Cadmium telluride
CuPc	copper phthalocyanine
D	Donor
DMSCs	Small molecule solar cells
DSSCs	The dye-sensitized solar cells
e^-	Electron charge
ECD	Electrochemical deposition
EDAX or EDX	Energy-dispersive (analysis) X-ray
E_g	Band gap energy

EQE	External quantum efficiency
E_{opt}	Optical band gap energy
ETL	Electron transport layer
FESEM	Field Emission Scanning Electron Microscopy
FF	Fill factor
FLM	fluorescence light microscope
FTO or F:SnO_2	Fluorine doped tin oxide
FWHM	Full width at half maximum
h	Plank's constant
h^+	Hole charge
HCL	Hydrochloric acid
HTL	Hole transport layer
HOMO	Higher occupied molecular orbital
ITO	Indium tin oxide
J_{SC}	Short-circuit current density
J-V	Current density-voltage Curve
J_{max}	Maximum current density
LUMO	Lower unoccupied molecular orbital
LiF	Lithium fluoride
MoO_3	Molybdenum oxide
μ_e	electron mobility
μ_p	Hole mobility
NaOH	Sodium hydroxide
η_A	absorption efficiency

η_{CC}	charge collection efficiency
η_{CS}	charge separation efficiency
η_{ED}	exciton diffusion efficiency
η_{IQE}	Internal quantum efficiency
NHO_3	Nitric acid
NH_4VO_3	Ammonium metavanadate
NiO_x	Nickel oxide
NREL	National Renewable Energy Laboratory
OPV	Organic photovoltaic
OSCs	Organic solar cells
P3HT	Poly(3-hexylthiophene)
PCE	Power conversion efficiency
PCBM	[6,6]-phenyl-C61-butyric acid methyl ester
PCPDTBT	Poly[2,6-(4,4-bis-(2-ethylhexyl)-4H-cyclopenta [2,1-b;3,4-b'] dithiophene)-alt-4,7(2,1,3-benzothiadiazole])
PBDTTBT	poly(4,8-bis(2,5-dioctyl-2-thienyl)-benzo[1,2-b:4,5-b']dithiophene -alt-[4,7-bis(2-thienyl)-2,1,3-benzothiadiazole)-5,5'-diyl])
PEDOT:PSS	Poly(ethylene-3-4-dioxy thiophene):poly styrene sulphonate
PTC	Perylene tetracarboxylic
PL	Photoluminces
P_{max}	Maximum power
PPV	Poly(p-phenylene vinylene)
PSCs	Polymer solar cells

PTB7	Poly[[4,8-bis[(2-ethyhexyl)oxy]benzo(1,2-b:4,5b)dithiophene2,6diyl] [3fluoro2[(2ethylhexyl)carbonyl]thieno[3,4-b]thiophenediyl]]
PV	Photovoltaic
R2R	Roll-to-roll
SCLC	Space Charge Limited current
SEM	Scanning electron microscopy
R_s	series resistance
R_sh	shunt (parallel) resistance
TCOs	Transparent conducting oxides
TECC	Two electrochemical cell
TEM	Transmission electron microscopy
TiO_2	Titanium dioxide
$Ti(SO_4)_2$	Titanium(IV) Sulfate
TMO	Transition metal oxide
UV-Vis	Ultra violet-visible
V_2O_5	Vanadium pentoxide
V_{max}	Maximum voltage
V_{oc}	Open-circuit voltage
WF	Work function
WO_3	Tungsten oxide
XRD	X-ray diffractometer
ZnO	Zinc oxide

List of figures

List of tables

Contents

Chapter 1

INTRODUCTION

Global environmental degradation, climate change and global warming are often associated with the emission of carbon-dioxide into the atmosphere mainly by the use of fossil fuels. This has led to the quest for environmental friendly alternative energy sources. Moreover, fossil fuels are not sustainable in the long term which calls for alternative and renewable energy sources to address the issue of both environmental degradation and sustainability. The renewable energy source based on the conversion of solar energy to electricity via photovoltaic devices is one of the solutions which is sustainable and environmentally friendly and is also an inexhaustible source. The extensive use of solar energy in the world will contribute to the reduction of carbon dioxide emission and decreases our dependence on fossil fuel [1-5].

Although producing electricity from renewable resources is fundamentally dependent on their fabrication cost, the main challenge remains the reduction of the high overall cost of electricity production. Electricity generated by inorganic photovoltaic (PV) is still expensive compared to electricity produced by diesel, hydroelectric and nuclear power plants.

In order to address this issue, many research efforts have been dedicated to the development of alternative low cost thin film PV technologies such as organic photovoltaics (OPV). Although the OPV market is still at its infancy, production, integration and installation costs of this type of solar cells are expected to remain very low compared to the existing silicon based technologies. In particular, organic solar cell devices based on π-conjugated polymers have recently emerged as another substitute for the conventional inorganic solar cells due to their considerable potential in reducing the cost of device production, mechanical flexibility, light weight and the ease of thin film fabrication [6-15] (see Fig. 1.1a).

Organic materials are abundant in nature, environmentally safe and possess good optical as well as electrical properties [16-25]. Moreover, OSC devices can be fabricated by solution processing techniques that allow large-area device fabrication which is compatible with roll-to-roll (R2R) printing and coating approaches [6, 7, 12, 26, 27] (see Fig. 1.1b).

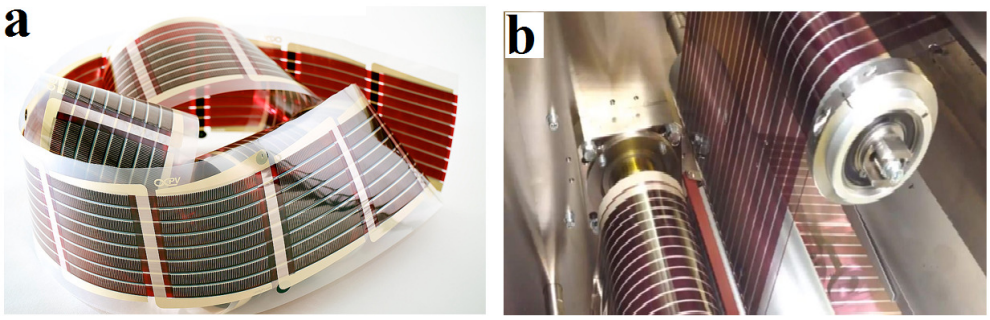

Figure 1.1: OSC devices a) flexible [28] b) roll-to-roll [29].

Despite the low charge mobility of organic semiconductors compared to inorganic semiconductor media, there has been rapid progress in improving the power conversion efficiency (PCE) of the OSC which currently stands over 10 % due to the synthesis of novel low energy band gap organic photoactive materials, introduction of suitable buffer layer materials and the modification of device architectures [30-34].

In spite of the tremendous progress in the PCE of organic solar cells environmental stability still remains a great challenge in harnessing solar energy using OSC (Fig. 1.2). This is due to the fact that organic materials are by nature more susceptible to degradation in the presence of oxygen and moisture. Fig. 1.2 represents the major challenges of the OSC devices such as improvement of the light harvesting, charge transport, devices environmental stability, open circuit voltage and device architecture, which should be roll-to-roll compatible. The environmental stability of OSCs has recently been partially addressed by employing new materials with enhanced optical and electronic properties, device engineering of photoactive layers such as inverted, tandem and ternary architectures as well as optimizing buffer layers, using stable metal oxide electrodes and encapsulation [35, 36].

Figure 1.2: The OSC devices major challenges [37].

1.1 Justifications

An increasing trend of global atmospheric temperature due to the high concentration of carbon dioxide in the atmosphere demands alternative green energy sources. Solar energy is one of the alternative green energy options that remains an untapped potential at present. However, the search for efficient mechanisms to convert solar energy into electricity has been the challenge ever since the realization of the concept of using solar energy. In the last few decades silicon based solar panels have been successfully used in the generation of electric power, but the cost of device fabrication is still expensive in spite of the recent declining trend. Organic solar cells emerged as a possible substitute for silicon based solar cells for the generation of low cost solar energy. Organic solar cells have attracted a lot of attention in recent years because of its ease of solution process ability, and possible large area fabrication on flexible substrate and light weight.

1.2 Aim of thesis

The aim of this Ph.D. research is to investigate the properties of organic molecules based solar cells fabricated under ambient environment. This can be achieved via optimizing the properties of the photoactive medium by blending various donor conjugated molecules as well as incorporating different charge transport buffer layers. Part of this research deals with the deposition and characterization of semiconductor oxide such as V_2O_5, ZnO and TiO_2 thin film on transparent and conductive electrodes for the purpose of using the layer as an effective charge transport medium. The investigation will also include the determination of device degradation in unprotected condition. This will provide information about the rate at which the devices degrade in ambient environment.

1.3 Objectives of thesis

The project focused on fabricated devices incorporating binary (PTB7:PCBM and P3HT:PCBM) and ternary (PTB7:P3HT:PCBM) blends as photoactive layers.

The specific objectives were to:

• Fabricate and characterize BHJ-OSC device under ambient laboratory condition as well as to improve the devices performance and stability.

• Enhance the PCE and life time of OSC devices by introducing transition metal oxide materials such as V_2O_5 as hole transport layer to replace PEDOT:PSS.

• Synthesize and characterize buffer layer for application in OSC such as V_2O_5 thin films and ZnO/TiO_2 bilayer by using low cost methods such as electrochemical deposition technique.

1.4 Outline of this thesis

This thesis contains eight chapters. Chapters one and two provide information about the introduction and general background of the study. Chapters three to seven discuss the research results in terms of published articles. Each of these chapters contains an abstract, introduction, experimental details, results and discussion as well as conclusion. These articles were submitted and published in different journals. Chapter eight is the conclusion of the work.

Chapter One (Introduction):

This chapter covers general information about the justification, aim, objectives and the outline of this thesis.

Chapter Two (Literature review):

This chapter describes the general background information of research, including the main types of the OSCs, basic processes in BHJ-OSCs and the factors limiting the performance of OSC devices with reviewed current-voltage characteristic, PCE parameters and the photoactive layer, electrodes, interfacial layer materials and their synthesis and characterization. It also covers the charge transport theory of the free carrier generation in OSCs.

Chapter Three (Article One):

In this chapter, we deal with synthesis and characterization of V_2O_5 thin films which is used as hole transport layer (HTL) in BHJ-OSC devices with resultant enhancement in PCE and stability, compared to devices with PEDOT:PSS as HTL under ambient environmental conditions.

Chapter Four (Article Two):

Chapter four discusses the growth of V_2O_5 thin film by using electrochemical deposition technique for OSCs application. The effect of annealing temperature treatment on the V_2O_5 thin films properties such as surface morphology, optical, photoluminescence properties and crystal structure were investigated.

Chapter Five (Article Three):

This chapter deals with the demonstration of layer deposition of transparent metal oxides structures from inorganic reagents that could be used as cathode buffer layers in OSC devices.

We also describe the preparation technique of a laminated ZnO/TiO_2 bilayer by two-steps growth on ITO coated glass such as electrochemical deposition and vacuum thermal evaporation.

Chapter Six (Article Four):

This chapter deals with fabrication and characterization of ternary blends BHJ-OSCs based on two electron donor materials (PTB7 and P3HT) incorporating to one electron acceptor material (PCBM). The optical, electrical and morphological properties of the ternary blend thin films were studied.

Chapter Seven (Article Five):

In this chapter, we reported fabrication, characterization and the stability of the BHJ-OSC devices in ambient laboratory conditions using PTB7:PCBM binary blends as photoactive layer.

Chapter Eight (Conclusion and Future work):

This final chapter gives an account of the summary and conclusion of the study carried out with recommendations and possible future works.

Bibliography

[1] A. Gupta, S. Praveen, A. Kumar, P. Shree, S. Mishra and C.M.Joseph, International Journal of Electrical and Electronics Engineering (IJEEE) 1(4) (2012) 2231-5284.

[2] S. H. Eoma, H. Park, S.H. Mujawar, S. C. Yoon, S-S Kim, S-I Na, S-J Kang, D. Khim, D-Y Kim, S-H Lee, Organic Electronics 11 (2010) 1516–1522.

[3] W. P. Chu, Y. S. Tsai, F. S. Juang, T. S. Li and C. H. Chung, PIERS ONLINE, 3(6) (2007) 825.

[4] W. Zhou, H. Yang, Z. Fang, Applied Energy 84 (2007) 1187–1198.

[5] N. Grossiord, J. M. Kroon, R. Andriessen, P. W.M. Blom, Organic Electronics 13 (2012) 432-456.

[6] G. A. dos R. Benatto, B. Roth, M. Corazza, R. R. Søndergaard, S. A. Gevorgyan, M. Jørgensen and F. C. Krebs, Nanoscale 8 (2016) 318–326.

[7] S-H. Park, S-J. Lee, J. H. Lee, J. Kal, J. Hahn and H-K. Kim, Organic Electronics 30 (2016) 112-121.

[8] I. A. Sahito, K.C. Sun, A. A. Arbab, M. B. Qadir, Y. S. Choi and S.H.Jeon, Journal of Power Sources 319 (2016) 90-98.

[9] S. H.n Kim, H. J. Son, S. H. Park, J. S. Hahn, D. H. Kim, Solar Energy Materials & Solar Cells, 144 (2016) 187–193.

[10] B. Zimmermann, H.F.Schleiermacher, M.Niggemann, U.Wurfel, Solar Energy Materials & Solar Cells 95 (2011) 1587–1589.

[11] M. Kaltenbrunner, M. S. White, E. D. Głowacki, T. Sekitani, T. Someya, N. S. Sariciftci & S.Bauer, Nature Communications (2012) DOI: 10.1038.

[12] F. C. Krebs, Solar Energy Materials & Solar Cells 93 (2009) 465–475.

[13] S-I. Na, S-S. Kim, J. Jo, and D-Y. Kim, Adv. Mater. 20 (2008) 4061–4067.

[14] C. Lungenschmieda, G. Dennlera, H. Neugebauera, S. N. Sariciftcia, M. Glatthaarb, T. Meyerc and A. Meyer, Solar Energy Materials & Solar Cells 91 (2007) 379–384.

[15] K-W. Seo, Y.-J. Noh, S-I. Na and H-K. Kim, Solar Energy Materials & Solar Cells 155 (2016) 51–59.

[16] K-S. Liao, S. D. Yambem, A. Haldar, N. J. Alley and S. A. Curran, Energies 3 (2010) 1212-1250.

[17] E. Kymakis, N. Kornilios and E. Koudoumas, J. Phys. D: Appl. Phys. 41 (2008) 165110 (5pp).

[18] D. Gao, M. G. Helander, Z-B. Wang, D. P.Puzzo, M. T. Greiner, and Z-H. Lu,emph, Adv. Mater. 22 (2010) 5404–5408

[19] E. Bundgaard, F. C. Krebs, Solar Energy Material and Solar Cells 91 (2013) 954–985.

[20] S. Shaheen, K. Brown, A. Miedaner, C. Curtis, P. Parilla, B. Gregg, and D. Ginley,NREL/CP (2007) 520-597.

[21] W-H. Baek, H. Yang, T-S. Yoon, C.J. Kang, Hyun Ho Lee, Yong-Sang Kim, Solar Energy Materials and Solar Cells 93 (2009) 1263–1267.

[22] V. Sadhu, N.A. Nismy, A. A. D. T. Adikaari, S. J. Henley, M. Shkunov and S. Ravi P. Silva, Nanotechnology 22 (2011) 265607 (5pp).

[23] H. J. Park, H. Kim, J. Y. Lee, T. Leec and L. J. Guo, Energy Environ. Sci., 6 (2013) 2203–2210.

[24] G. Zhao, Y. He, and Y. Li, Adv. Mater. 22 (2010) 4355–4358.

[25] K. Kawano, J. Sakai, M. Yahiro, and C. Adachi, Solar Energy Materials and solar cells 93 (2009) 514–518.

[26] J. Luc, Bredas, J. E. Norton, J. Cornil, and V. Coropeanu, Accounts of Chemical Research, 42(11) (2009) 1691-1699.

[27] T. M. Eggenhuisen, Y. Galagan, A. F. K. V. Biezemans, T. M. W. L. Slaats, W. P. Voorthuijzen, S. Kommeren, S. Shanmugam, J. P. Teunissen, A. Hadipour, W. J. H. Verhees, S. C. Veenstra, M. J. J. Coenen, J. Gilot, R. Andriessen and W. A. Groen, J. Mater. Chem. A, 3, 2015, 7255-7262.

[28] www.herox.com/news/282-printed-organic-solar-cells-and-led.

[29] www.ise.fraunhofer.de/en/press-and-media/press-releases/press-releases-2014/new-world-record-for-solar-cell-efficiency-at-46-percent.

[30] C.C. Chen, W.H. Chang, K. Yoshimura, K. Ohya, J. You, J. Gao, Z. Hong and Y. Yang, Adv. Mater. 26 (2014) 5670–5677.

[31] Y. Liu, J. Zhao, Z. Li, C. Mu, W. Ma, H. Hu, K. Jiang, H. Lin, H. Ade and H. Yan, Nat. Commun. 4 (2014) 6293.

[32] L. Nian, W. Zhang, N. Zhu, L. Liu, Z. Xie, H. Wu, F. Wurthner and Y. Ma, J. Am. Chem. Soc. 137 (2015) 6995–6998.

[33] I. Constantinou, T-H. Lai, D. Zhao, E. D. Klump, J. J. Deininger, C. K. Lo, J. R. Reynolds, and F. So, Appl. Mater. Interfaces 7 (2015) 4826-4832.

[34] N. Li and C.J. Brabec, Energy Environ. Sci. 8 (2015) 2902–2909.

[35] H. Benten, D. Mori, H. Ohkita and S. Ito, J. Mater. Chem. A. 4 (2016) 5340–5365.

[36] E. A.A. Arbab, B. Taleatu and G. T. Mola, Journal of Modern Optics 61(21) (2014) 1749–1753.

[37] N. K. Elumalai1, C. Vijila, R. Jose, A. Uddin and S. Ramakrishna, Mater. Renew. Sustain. Energy (2015) 4:11 pp25.

Chapter 2

LITERATURE REVIEW

2.1 INTRODUCTION

The photovoltaic effect was discovered in 1839 by French physicist A.E. Becquuel [1]. In 1954, the first crystalline silicon photovoltaic (PV) device was established at Bell laboratories. These devices, based on Si thin films, represent the first generation of PV which gained rapid improvement in power conversion efficiency from about 6% to 10% [2]. Afterwards, the devices based on CdS/CdTe, Cu(In,Ga)Se_2 CIGS) and multijunction a-Si/a-SiGe were fabricated and formed the second generation of PV technology. These generations have relatively reduced the fabrication cost by using R2R processing on flexible stainless steel with $\sim$ 20% efficiency [3]. In 1977, in an attempt to further reduce the fabrication cost, polyacetylene was doped to the level of metallic conduction and since then π-conjugated polymers are seen as an alternative for inorganic semiconductors [4]. The search for inexpensive photoactive materials that are low temperature solution processable and compatible for large scale throughput led to the discovery of the third generation of PV which is based

on organic materials [5]. Recently, organic solar cells (OSCs) have achieved efficiency above 10% threshold [6].

The commercialization of OSC devices has been slowed due to low power conversion efficiencies and short lifetime. However, there has been steady progress in the field. Fig. 2.1 shows the improvement of solar cell devices efficiency as reviewed by the National Renewable Energy Laboratory (NREL) USA. As shown in Fig. 2.1, crystalline silicon materials (blue colour) have displayed more stable and high efficiency devices of 25% compared to OSC (red colour) with device efficiency slightly above 10%. However, the fabrication cost and environmental waste in the fabrication of Si solar cell is still high. OSCs serve as a potential inexpensive alternative in terms of cost of materials and fabrication process, recording a dramatic improvement in efficiency[7, 8].

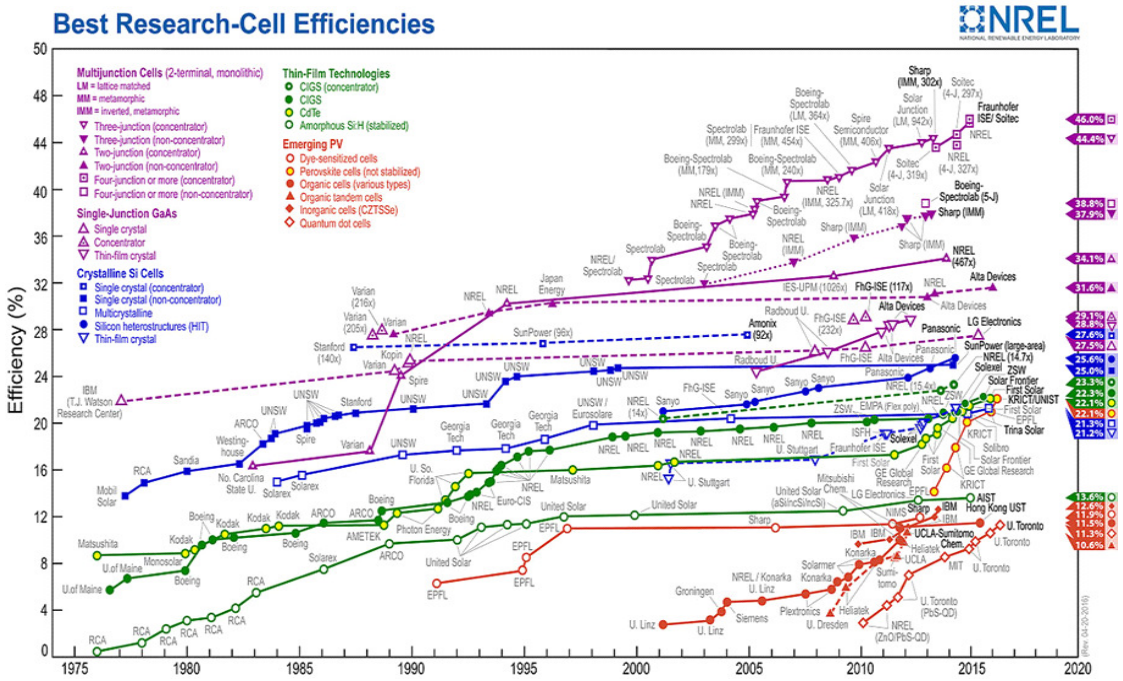

Figure 2.1: Report progress of power conversion efficiency of solar cell devices reviewed by NREL [Accessed 25 May 2016] [9].

Organic semiconductors are carbon-based materials possessing semiconductor characteristics. OSCs can be divided mainly into three different categories depending on the molecules viz: small molecules, dye-sensitized and polymer based OSCs. This classification is based on difference in methods of their synthesis, purification and device fabrication processes.

I- Small molecule solar cells (SMSCs):

These are fabricated by using thermal evaporation deposition in a high vacuum condition. The vacuum-based deposition technique is a costly throughput production process, therefore the solution processing has been currently employed to fabricate SMSCs [10].

II- The dye-sensitized solar cells (DSSCs):

The dye-sensitized solar cell (DSSC) technology separates the two requirements as the charge generation is done at the semiconductor-dye interface and the charge transport is done by the semiconductor and the electrolyte. In a dye-sensitized solar cell, a photon absorbed by a dye molecule gives rise to electron injection into the conduction band of nanocrystalline oxide semiconductors such as TiO_2 or ZnO [11]. The spectral properties optimization of DSSC can be done by modifying the dye alone, while the carrier's transport properties can be improved by optimizing the semiconductor and the electrolyte composition [12-15].

III- Organic solar cells (OSCs):

Organic solar cells can be solution processed which enables the roll to roll (R2R) production with low cost deposition techniques such as spin coating [16], inkjet printing [17] and spray deposition [18]. Organic semiconductors are composed of organic molecules which are formed by a π-conjugated system. The π-bond system can have different bonding configurations according to the electron wave function overlap of neighbouring atoms.

In organic semiconductors, the Highest Occupied Molecular Orbital (HOMO) and the Lowest Unoccupied Molecular Orbital (LUMO) characterize the hybridization between bonding and anti-bonding of the π-conjugated electrons. When an electron is excited from the HOMO to

the LUMO of an organic semiconductor, the molecule itself is excited into a higher energy state [19-21].

Depending on the device's photoactive layer architecture, the OSCs can be divided into three basic types: single layer, bilayer, and bulk heterojunction.

2.1.1 Single layer OSCs:

Single layer organic photovoltaic cells are the simplest device structure and are comprised of only one photoactive material sandwiched between the TCO's bottom electrode (high work function) such as ITO and a metallic top electrode (low work function) such as Al (Fig. 2.2a). Single layer organic solar was established in 1994 by R. N. Mark et al. using a photoactive layer of poly(p-phenylene vinylene) (PPV), but the cells performed poorly with a low power conversion efficiency which is less than 0.1% [22]. The properties of this cell are strongly dependent on the nature of the electrodes. A disadvantage is that the electric field resulting from the difference between the two conductive electrodes is not sufficient to dissociate the exciton, thus the electrons recombine with the holes without reaching the electrode [23, 24].

2.1.2 Bilayer OSCs:

Bilayer cells contain two materials with varying electron affinity and ionization energy layers in between the transparent and back electrodes (Fig 2.2b), therefore electrostatic forces are generated at the interface between the two layers. The materials are chosen to make the differences large enough that these local electric fields are strong, which dissociates excitons much more efficiently compared to a single layer OSCs [25].

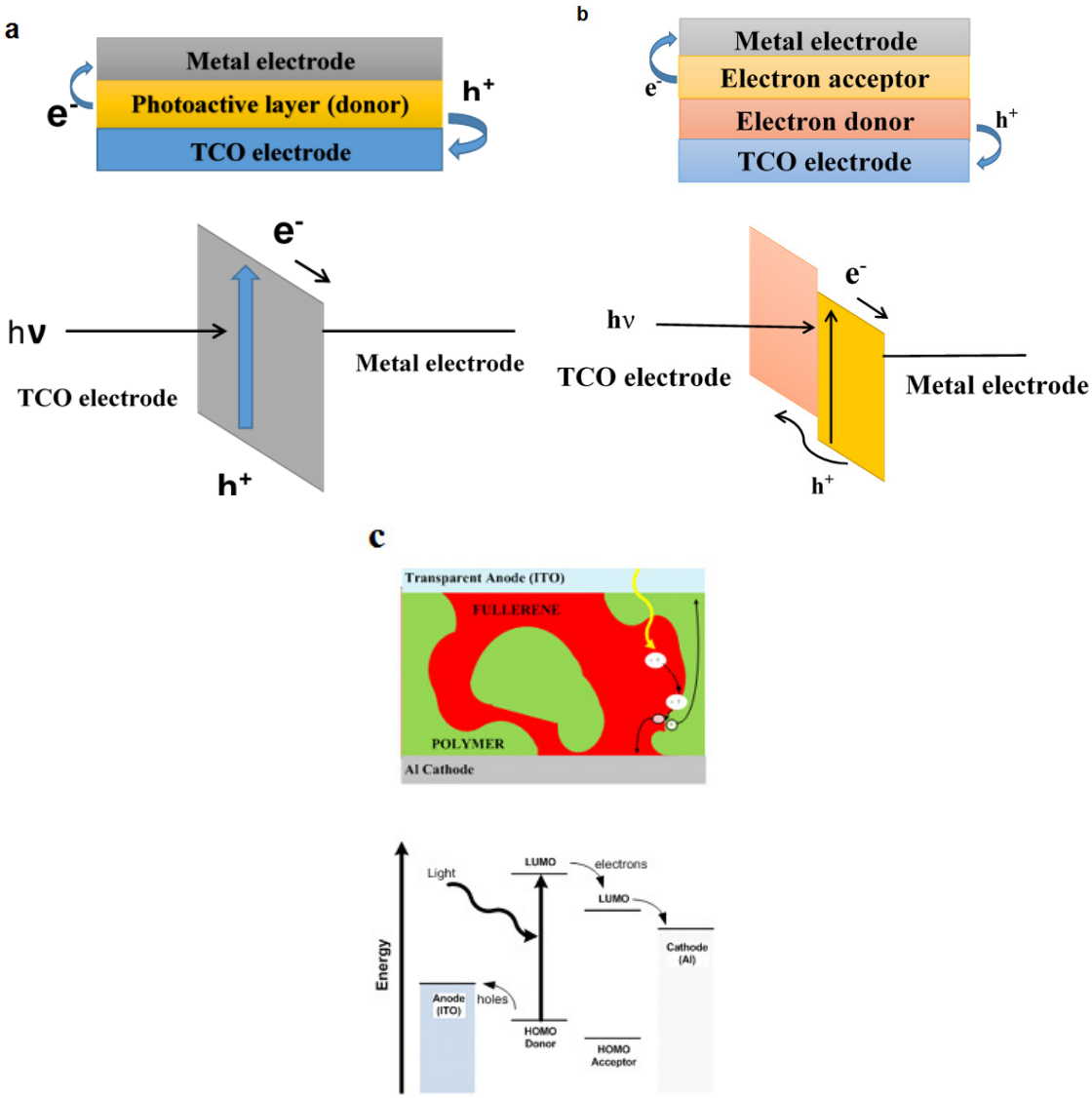

Figure 2.2: Architectures and energy levels of the photoactive layer OSC devices: a) single layer, b) bilayer, and c) BHJ [30].

The electron acceptor layer materials have higher electron affinity and ionization potential than the electron donor layer materials. This structure is also called a planar donor (D) - acceptor (A) heterojunction [24, 26, 27]. Planar D-A heterojunction OSCs structure was established for the first time in 1986 by C. W. Tang from Kodak, and the device photoactive layer comprised of copper phthalocyanine (CuPc) as electron donor and perylene tetracar-

boxylic derivative (PTC) as electron acceptor and the reported PCE was $\sim$ 1% [28]. The photoactive layer is coated between ITO for collection of holes and silver (Ag) to collect the electrons. In 2003 Peumans et al. reported PCE of 3.5% by using fullerene C_{60} as an alternative to PTC derivative as electron acceptor with the same device structure as above [24, 29].

2.1.3 Bulk heterojunction OSCs:

Bulk heterojunctions are designed in such a way that the photoactive layer is composed of the blends of donor and acceptor molecules. These molecules are desolved in organic solvent after being coated on the substrate. The molecules then form an interpenetrating nanoscale structure which enhances the dissociation of excitons in the medium (Fig. 2.2c). The photoactive layer blend forms domains of nanostructured morphology giving room for excitons with short lifetimes and diffusion length to reach an interface and dissociate into separate charge carriers [30].

Most bulk heterojunction solar cells use two components, namely binary BHJ-OSCs, although three-component cells denoted as ternary BHJ-OSCs have been explored. The ternary BHJ-OSCs are based on two donors and one acceptor (D1:D2:A) or one donor and two acceptors (D:A1:A2)] (Fig. 2.4a) [31, 32]. The additional donor or acceptor polymer in this structure helps to extend the photon absorption band to a high wavelength, thereby increasing the light harvesting [33-37].

These ternary cells operate through one of three distinct mechanisms: charge transfer, energy transfer or parallel-linkage as shown in Fig. 2.3, which are fundamentally different from each other. Each of them has its own advantage and limitations [38].

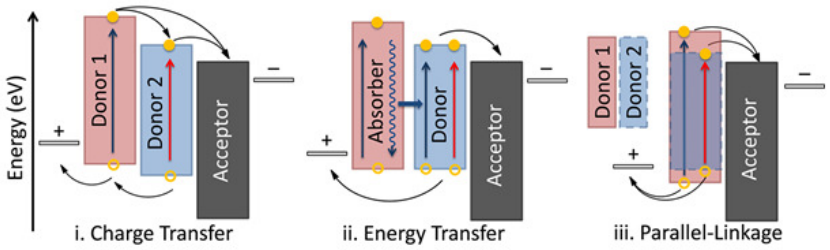

Figure 2.3: Three distinctly different mechanisms that can potentially improve the performance of ternary OSCs: i) charge transfer, ii) energy transfer, and iii) parallel-linkage [38]

In an attempt to further extend photon harvesting to cover a larger part of the spectrum, double-junction cell (tandem) solar cells offers the distinct advantage that photon energy is used more efficiently, because the voltage at which charges are collected in each sub-cell is closer to the energy of the photons absorbed in that cell (Fig. 2.4b). Moreover, the performance of the tandem cells is higher than single-junction cells (binary and ternary) BHJ-OSC devices [39-43].

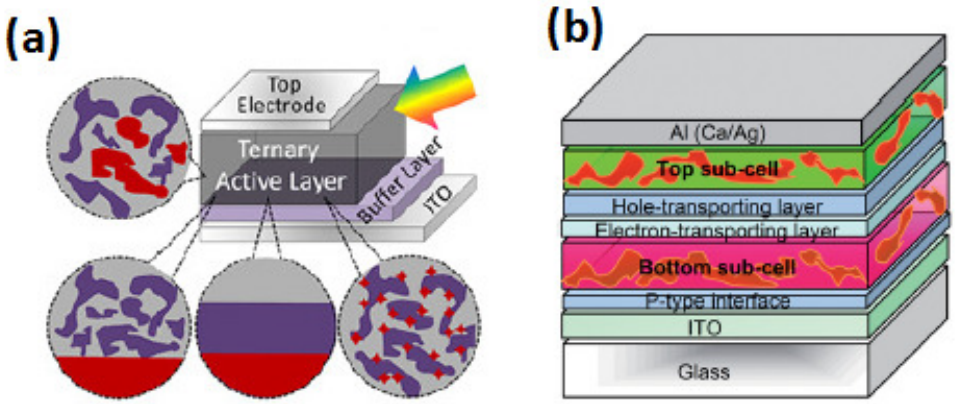

Figure 2.4: The BHJ-OSC device architecture a) Ternary blend [38] b) tandem structure [44].

2.2 Charge carrier transport theory

The solar cells based on organic materials have a low charge carrier mobility in the range of 10^{-7} to 10^{-3} lower by 10 orders of magnitude than silicon semiconductor [45]. This low charge mobility is attributed to the complex structure of organic molecules and the nature of photon induced charge generation and transportation mechanisms in the organic medium. The main charge transport mechanism in organic medium is, however, hopping from one site to another which depends on space and applied electric field. The methods employed to understand the charge transport in inorganic semiconductors can, in principle, be applied to the organic medium too. In general, the current derived from OSC devices is caused by drift and diffusion of charge carriers and is also dependent on the device thickness. The high absorption coefficient of the organic materials ($\geq 10^5 cm^{-1}$) allows for the usage of a very thin film as photoactive layer which in turn minimizes undesired electrical resistance such as series resistance which has a significant impact on charge carrier transport through the photoactive layer [46, 47]. Regardless of device operation principle and the effect of charge traps in the medium, the mechanism of charge carrier transport can be described by the drift-diffusion current density equations [47-49]:

$$J_{total} = J_{drift} + J_{diffusion} \tag{2.1}$$

$$J_n = q\mu n\xi + qD_n \bigtriangledown n \tag{2.2}$$

$$J_p = q\mu p\xi + qD_p \bigtriangledown p \tag{2.3}$$

$$J_{cond.} = J_n + J_p \tag{2.4}$$

where n and p are the concentrations of electrons and holes in the conductor, q is the elementary charge, ξ is the applied electric field. The diffusion constants for the two types

of charge carriers are denoted D_n and D_p for electrons and holes respectively. The electron (hole) mobilities are given by the letters μ_n and μ_p. Using the Poisson's and continuity equations, the one dimensional current densities are ξ can be expressed as:

$$\frac{d\xi}{dx} = \frac{q}{\varepsilon}(\rho - n) \tag{2.5}$$

For the one-dimensional case and using the Einstein diffusion equation, Eqs (2.2) and (2.3) become [48]:

$$D_{n,p} = (\frac{K_B T}{q})\mu_{n,p} \tag{2.6}$$

where K_B is the Boltzmann's constant and T is temperature in degrees Kelvin.

$$J_n = q\mu n(x)\xi(x) + qD_n\frac{dn}{dx} = q\mu_n(n(x)\xi(x) + \frac{KT}{q}\frac{dn}{dx}) \tag{2.7}$$

$$J_p = q\mu p(x)\xi(x) + qD_p\frac{dp}{dx} = q\mu_p(p(x)\xi(x) + \frac{KT}{q}\frac{dp}{dx}) \tag{2.8}$$

where x is the x-direction of the flow of charges.

2.3 Space charge limited current (SCLC)

The space charge limited current in the device is observed when the current reaches a steady state condition, where the traps in the medium are filled and the current is mainly dependent on the bulk properties of the medium. In bulk heterojunction solar cells a better understanding of charge carrier transport phenomenon across two different electrodes is critical to improve the performance of the OSC devices. BHJ devices have unbalanced charge-carrier mobility, with the hole mobility being at least an order of magnitude lower than that of the electron mobility. This results in build-up of space charge, leading to a decrease in the

fill factor (FF) as well as power conversion efficiency of the device. For the fabrication of efficient BHJ-OSCs the photoactive film needs to be thin enough (less than 200 nm) to avoid recombination of the charge carriers [45].

Space charge limited current (SCLC) regime is a region dominated by charge carriers injected from the electrode contacts and the current density-voltage characteristics becomes quadratic ($J \propto V^2$). In the SCLC region of the J-V curve, the current density can be described using electric field and temperature dependent mobility equation which obeys the Poole–Frenkel law [50]:

$$\mu = \mu_o \exp(\gamma\sqrt{\xi}) \tag{2.9}$$

where μ is charge carrier mobility, μo is the zero field mobility and γ is the field activation factor.

Under the condition of SCLC, in the absence of traps in the medium, the drift current controls the total current density flow and the diffusion part is neglected, therefore the Poisson's and continuity equation becomes:

$$J = e\mu_n n(x)\xi(x) \tag{2.10}$$

$$\frac{d\xi}{dx} = \frac{q}{\varepsilon} n(x) = \frac{J}{\varepsilon\varepsilon_0\mu_n\xi(x)} \tag{2.11}$$

Analytical expression of SCLC can be derived for a constant mobility and drift dominated transport. Under the assumption of negligible trap density, solving the current density equation together with the Poisson equation gives as:

$$J = \frac{9}{8}\varepsilon\varepsilon_0\mu_n\frac{V^2}{L^3} \tag{2.12}$$

where ε and ε_0 are the relative dielectric permittivity of photoactive medium and free space, respectively, L is the thickness of photoactive thin films layer and this equation is known as Mott-Gurney law [45, 50, 51].

2.4 Working Principles of BHJ-OSCs

The photoactive medium of bulk heterojunction design of organic solar cells is composed of donor polymer and acceptor organic molecules blend. The nature of the molecular blend determines the effectiveness of the medium for photon harvesting. The molecules in the photoactive layer create the so-called donor/acceptor (D/A) interfacial layers at the molecular level which significantly contributes to the efficient dissociation of charges. In OSCs, the creation of free charge carriers is the result of a number of necessary processes to achieve a high performance device (Fig. 2.5). These are:

1) Photon absorption and Exciton generation.
2) Exciton diffusion and dissociation.
3) Charge separation and charge transport.
4) Charge collection by the electrodes.

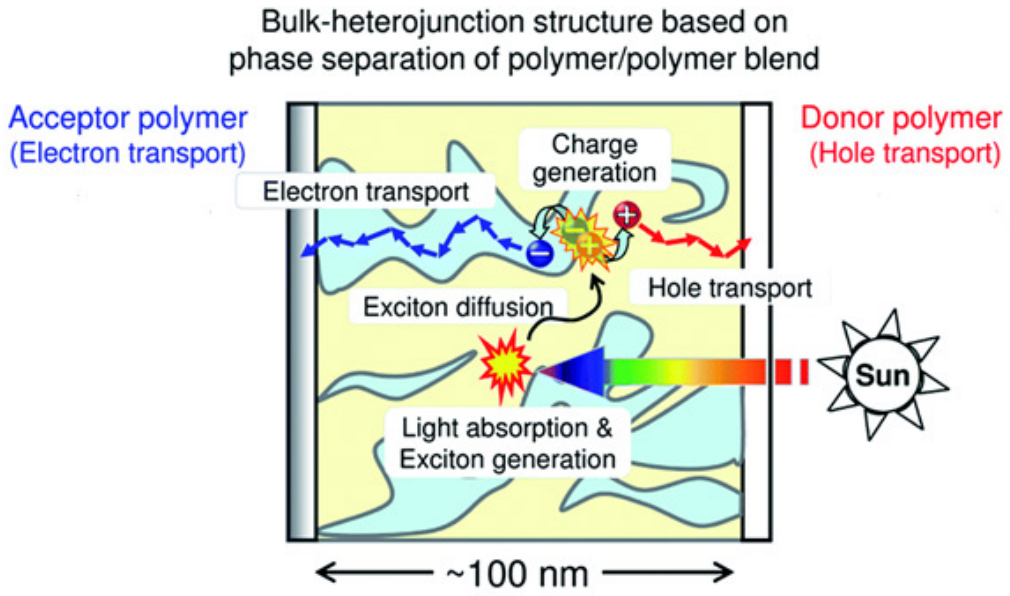

Figure 2.5: Operating principles of BHJ-OSCs [67].

Organic materials usually have low dielectric constant ($\varepsilon = 3-4$) and weak non-covalent electronic interactions among the molecules, resulting in strong attractive Coulomb electrostatic interaction between electron and hole [52].

2.4.1 Light absorption and exciton formation:

To obtain a highly efficient collection of photons in organic photoactive layers the absorption bandwidth of the molecules should be matched with the solar emission spectrum [53]. In addition, the layer should have sufficient layer thickness to absorb most of the incident photons [54, 55]. By lowering the band gap of the polymer material it is possible to harvest more incident photons [56, 57]. Low charge mobilities in organic photoactive materials limit the film's thickness to less than 250 nm. Also, additional losses in photons absorption might originate from optical interference which modifies the light absorption profile in thin multilayer films [52]. The photoactive layer of OSCs absorbs an incident photon through TCO electrode, so the photon should have minimum energy to excite electron from the highest occupied molecular orbital (HOMO) level to the lowest unoccupied molecular orbital (LUMO) of the donor molecules. As a result, the electron in LUMO and the associated hole in HOMO level are attracted by strong electrostatic Coulomb force which creates a quasi-particle called exciton [58-61].

When the energy of the incident light is larger than the band gap of the organic molecules in the photoactive layer ($h\nu \geqslant E_g$), the excess energy ($h\nu - E_g$) is lost due to thermalization processes and non-optical absorption of the solar spectrum which has restricted this process and therefore affected the open circuit voltage (V_{oc}) of the device [62].

2.4.2 Exciton diffusion and dissociation:

The formed exciton must diffuse and dissociate at the D/A interface with support of the extra energies of the absorbed photons [61, 63]. This is restricted by the short diffusion length (L_{exc}) of the exciton in conjugated polymers ($\sim$ 10 nm), resulting in charge recombination before being able to diffuse to the D/A interface. The diffusion length is proportional to the square root of the exciton life time τ_{exc} and the diffusion coefficient D_{exc}, which is given by:

$$L_{exc} = \sqrt{\tau_{exc} D_{exc}} \tag{2.13}$$

Moreover, the higher the exciton diffusion length, the higher the probability of exciton dissociation at D/A interface with lesser probability of recombination and trapping [52, 53, 62].

2.4.3 Charge separation

In order to be sure of the charge separation, the exciton binding energy (E_{exc}) is mostly greater than the difference between ionization potential of the donor (I_D) and electron affinity of the acceptor (χ_A); this condition can be expressed as[53, 60]:

$$E_{exc} > I_D - \chi_A \tag{2.14}$$

Exciton separation provides additional energy to overcome the Coulomb binding energy which depends on the energy between LUMO levels of donor and acceptor at D/A interface, as well as the HOMO levels difference between donor and acceptor [61, 63].

2.4.4 Charge transport and collection:

As a result of exciton dissociation, the holes are transported through the back of the donor polymer chain while the electrons are transported via the acceptor domain. However, if the carriers' separation and transport efficiency are higher it reduces the chances for charge recombination [57, 64]. The drift velocity (V) of the charge carriers acquired under the influence of an electric field (E) is given by the relation:

$$V = \mu_i E \tag{2.15}$$

where μ_i is charge mobility. The mobility in organic materials is relatively small because of the charge carrier localization and formation of polaron [65, 66].

The charge carriers move to the electrodes, therefore the holes and electrons are collected at the anode and cathode electrodes, respectively. This process is limited by the so-called non-geminate recombination losses which may occur during charge transport to electrodes [53, 65].

2.5 Characterization of OSC device

The characterization of OSCs is often determined by measuring current density-voltage characteristics of the devices, the so-called J-V curve, which provides the necessary information about the solar cell. Experimentally, it is possible to extract most of the important parameters of the device from the J-V curve, namely short-circuit current density (J_{sc}), open-circuit voltage (V_{oc}), fill factor (FF) and power conversion efficiency (PCE) (Fig. 2.6).

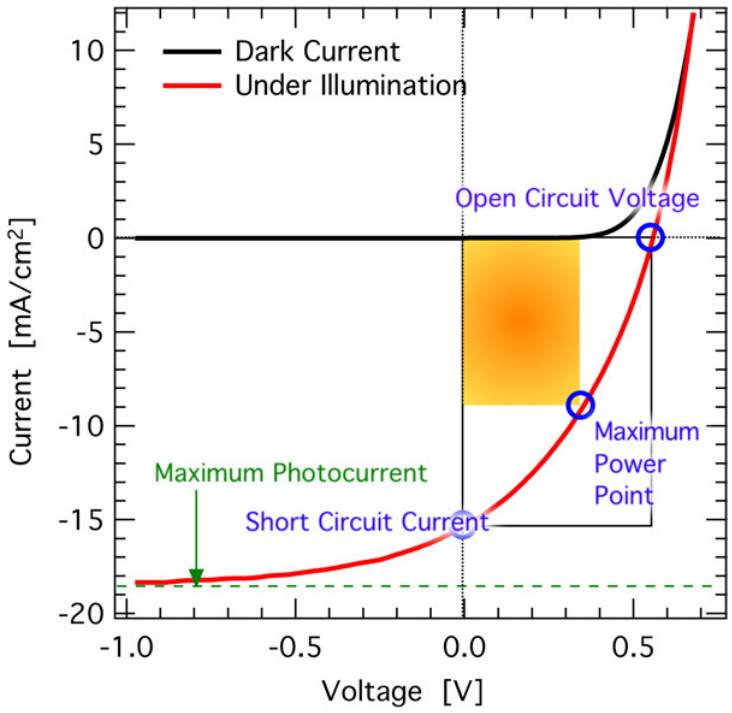

Figure 2.6: J-V characteristic of OSCs [52].

2.5.1 Short-circuit current density (J_{sc}):

The short-circuit current density (J_{sc}) is the photo-generated current of the solar cell measured at zero applied voltage or zero load resistance. The J_{sc} relies on a number of factors such as the effective area of the photoactive layer (A), the incident light intensity and the spectrum of the incident light of power density which is 100 mW/cm^2 under AM1.5 solar irradiance. Fig. 2.7 shows the emission of the solar spectrum that is used to characterize the performance of solar cells under standardized conditions such as AM1.5.

The optical and electrical properties of the photoactive layer material and the carriers collection probability of the solar cell depends on the surface passivation and the minority carrier lifetime in the base [68, 69].

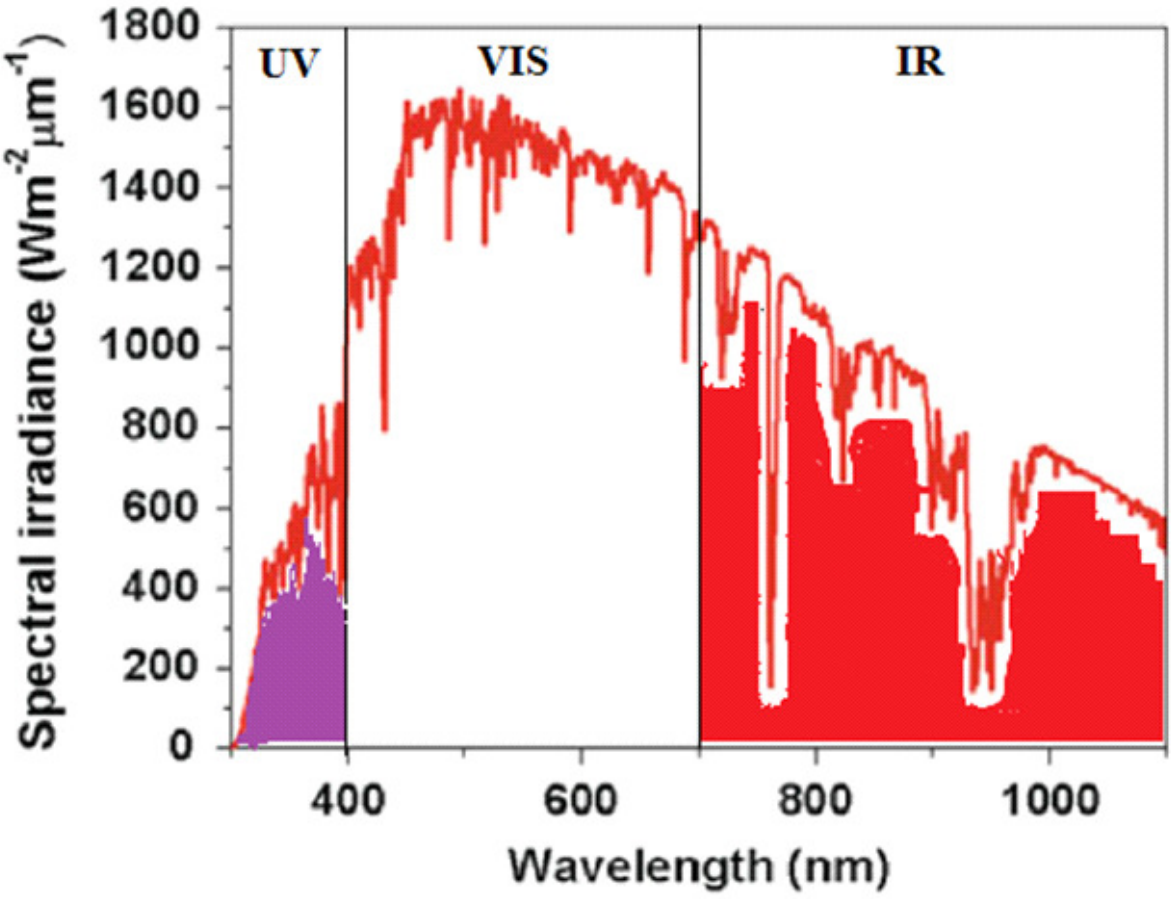

Figure 2.7: The emission of the solar spectrum [70].

The dark current is mainly caused by thermal generation and charge injection by electrodes and flows in the device in the opposite direction. It is reverse current and can be expressed as [71]:

$$J_{dark} = J_s[(\exp[\frac{qV}{K_BT}) - 1] \tag{2.16}$$

The general equation for the total current density can be expressed by Schockley solar cell

equation [72]

$$J(V) = J_{ph} - J_s[(\exp[\frac{qV}{K_BT}) - 1] \tag{2.17}$$

where J_{ph} is the photogenerated current density. J_s is the saturation current density, and V is the applied voltage in the dark. In an ideal solar cell, J_{ph} is equal to the J_{sc} measured in mA/cm^2 and is given by:

$$J_{sc} = \frac{I_{sc}}{A} \tag{2.18}$$

where I_{sc} is the short circuit current in Ampere and A is an affective area of the cell. Also, J_{sc} can be expressed by:

$$J_{sc} = q \int b_s(E) QE(E) dE \tag{2.19}$$

where $QE(E)$ is the quantum efficiency of cell and is defined by the probability that an incident photon of energy E will deliver one electron to the external circuit, which depends on the absorption coefficient of the solar cell material and $b_s(E)$ is the incident spectral photon flux density [69].

2.5.2 Open-circuit voltage (V_{oc}):

The Open-circuit voltage is the maximum voltage created in the solar cell when no current is flowing in the device due to infinite load resistance is given by:

$$V_{oc} = \frac{nK_BT}{q} \ln(\frac{J_{ph}}{J_s} + 1) \tag{2.20}$$

The V_{oc} can be also determined from carrier concentration by relation:

$$V_{oc} = \frac{K_BT}{q} \ln(\frac{(N_A + \Delta n)\Delta n}{n_i^2}) \tag{2.21}$$

where $\frac{K_B T}{q}$ is the thermal voltage, N_A is the doping concentration, and n_i is the intrinsic carrier concentration [69]. The V_{oc} mainly depends on the band gap of the molecules involved in the active layer as well as the work function of the electrodes. In organic solar cells based on BHJ the V_{oc} is determined by the energy difference between the HOMO level of the donor and the LUMO level of acceptor assuming electrodes making ohmic contact with active layer. Therefore, V_{oc} can be expressed as [39, 73]:

$$V_{oc} = \frac{1}{q}(E_{HOMO-donor} - E_{LUMO-acceptor}) - \Delta V \tag{2.22}$$

where ΔV is an experimental constant that is concerned to the dark J-V curve of the diode. The ΔV is determined by [52]:

$$\Delta_{HOMO} < \Delta V < \Delta_{LUMO} \tag{2.23}$$

where,

$$\Delta_{HOMO} = HOMOofacceptor - HOMOofdonor \tag{2.24}$$

whereas,

$$\Delta_{LUMO} = LUMOofacceptor - LUMOofdonor \tag{2.25}$$

2.5.3 Fill factor (FF):

The FF is defined as the ratio of the maximum power output of a solar cell to the product of the V_{oc} and J_{sc}, is given by:

$$FF = \frac{P_{max}}{V_{oc} \times J_{sc}} = \frac{J_{max} \times V_{max}}{V_{oc} \times J_{sc}} \tag{2.26}$$

The FF is also defined as the measure of the squareness from the J-V curve of the solar cell [32, 53, 69]. The FF relies on the cell technology and on the active layer morphology [53].

2.5.4 Power conversion efficiency (PCE, η):

The PCE is the most commonly used parameter to compare the performance of one solar cell to another. The PCE is defined as the percentage ratio between the output power from the solar cell to input power from the sun, which can be expressed by [52, 71]:

$$PCE = \eta = \frac{P_{electrical}}{P_{light}} = \frac{P_{max}}{P_{in}} = \frac{FFV_{oc} \times J_{sc}}{P_{in}} \tag{2.27}$$

where the input power for efficiency calculation is $100 mW/cm^2$ at AM 1.5.

2.6 J-V curve and the equivalent circuit of the solar cells:

For equivalent circuit of ideal solar cells, there are many important concepts which should be studied and understood such as:

2.6.1 External quantum efficiency (EQE):

The EQE of device is defined by the ratio of the collected electrons $(n_e(\lambda))$ to the number of incident photons (IPCE)$(n_{ph}(\lambda))$ at a particular wave length of the incident photon. The EQE as a function of wave length can be given by [62]

$$EQE(\lambda) = \frac{n_e(\lambda)}{n_{ph}(\lambda)} = \frac{J_{sc}(\lambda)}{P_{in}(\lambda)} \times \frac{hc}{e\lambda} = 1240 \frac{J_{sc}(\lambda)}{\lambda \times P_{in}(\lambda)} \tag{2.28}$$

The EQE is also given by:

$$EQE(\lambda) = \eta_A \eta_{IQE} \times = \eta_A \times \eta_{ED} \times \eta_{CS} \times \eta_{CC} \tag{2.29}$$

where η_{IQE} is internal quantum efficiency, η_A is absorption efficiency of the cell, η_{ED} is exciton diffusion efficiency, η_{CS} is charge separation efficiency and η_{CC} is charge collection efficiency. The η_{IQE} defines as the ratio between the number of the charge carriers collected at an electrode and the number of photons absorbed in the device. η_{IQE} can be expressed as:

$$\eta_{IQE} = \frac{\eta_{EQE}}{1 - T - R} \tag{2.30}$$

where T and R are transmissivity and reflectivity, respectively [53, 62, 74].

2.6.2 The parasitic resistances:

In real cells, the current is lost through the contact resistance as well as through the leakage currents around the side of the device. Therefore the series resistance R_s and shunt resistance (R_{sh}) are introduced into the equivalent circuit (Fig. 2.8) to take into account the possible resistances in real devices. The R_s is derived from the bulk resistances of photoactive layer and electrode, whereas the R_{sh} originates from the leakage current induced by the panel in the cell, or the current leakage from the edge of the device. This includes the influence of the local shunts between the two electrodes. The parallel resistance relies on charge carrier losses owing to short circuit pathways and carrier recombination. In an ideal solar cell the series resistance is near to zero ($R_s = 0$) and the shunt resistance is equal to an infinite value ($R_{sh} = \infty$)[52, 53].

From the equivalent circuit model (Fig. 2.8) and including R_s and R_{sh}, the net current density in dark can be derived from J-V characteristics of a solar cell and expressed by using Shockley equation:

$$J(V) = J_s[(\exp[\frac{q(V - JR_s)}{nK_BT}) - 1] + \frac{V - JR_s}{R_{sh}} \tag{2.31}$$

and, under illumination the net current density is given by:

$$J(V) = J_s[(\exp[\frac{q(V - JR_s)}{nK_BT}) - 1] + \frac{V - JR_s}{R_{sh}} - J_{ph} \tag{2.32}$$

where n is the diode ideally factor [11, 52, 69, 71, 74, 75].

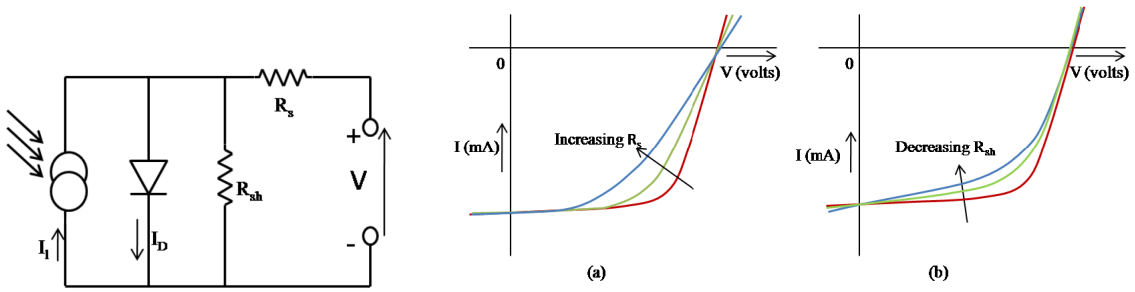

Figure 2.8: Equivalent circuit of the solar cell[30].

For an experimental case where parasitic resistances R_s and R_{sh} become important, the current in Eq. (2.31) becomes:

$$J(V) = J_s(V - JAR_S)[(\exp[\frac{q(V - JAR_S)}{nK_BT}]) - 1] + \frac{V - JAR_s}{AR_{sh}} \tag{2.33}$$

whereas Eq. (2.32) becomes:

$$J(V) = J_s(V - JAR_S)[(\exp[\frac{q(V - JAR_S)}{nK_BT}]) - 1] + \frac{V - JAR_s}{AR_{sh}} - J_{ph} \tag{2.34}$$

If the R_s is very small and R_{sh} is large, the net current density may be equal to zero. In this case, V_{oc} in Eq. (2.20) can be derived from Eq. (2.34):

$$J_s(V_{oc})[(\exp[\frac{q(V_{oc})}{nK_BT}]) - 1] + \frac{V_{oc}}{AR_{sh}} - J_{ph} = 0 \tag{2.35}$$

where $(V - JAR_S)$ is equal to V_{oc} [74].

2.6.3 The properties of the J-V curve taken under dark:

Fig. 2.9 shows the J-V curve. The forward bias characteristic in dark can be divided into three regions, where the first region (I) is straight line at negative and positive voltage with a

slope determined by the $1/R_{sh}$ which is the ohmic conduction. The current density depends linearly on voltage ($J \propto V$) due to leakage current (shunt) through R_{sh} until the current through diode is sufficiently large. The next region (II) is an exponential line (injection), where the current depends exponentially on the voltage ($lnJ \propto V$) and depends on the current injected by electrodes. In the third region (III), the J-V curve is a second straight line at high voltages with the slope controlled by $1/R_s$. If R_s is large, then the increase in current density with increasing voltage will lead to less squareness of J-V curve (lower FF) since $J \propto V^2$. However, in the reverse bias condition, there is only one region [52, 57, 71, 75-77].

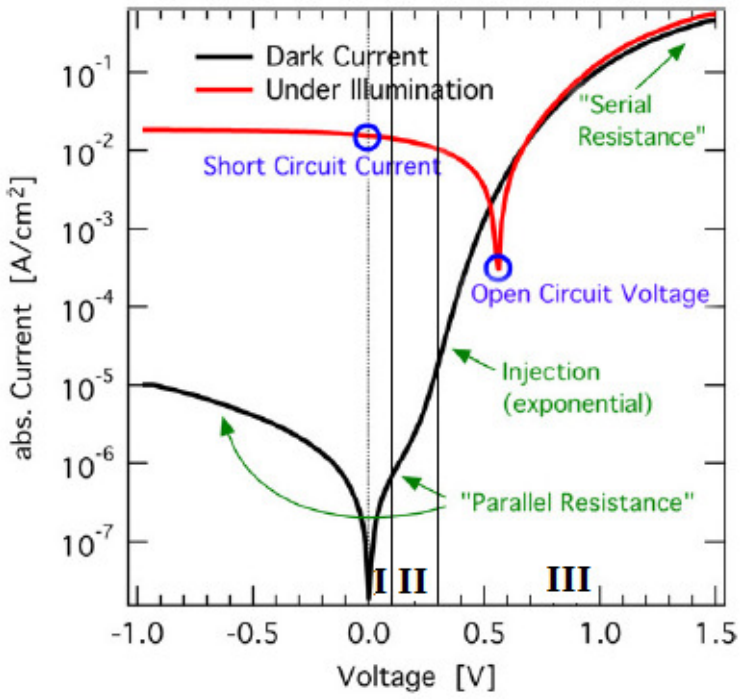

Figure 2.9: J-V curve region [52].

2.6.4 PCE limiting factors

As indicated in the earlier discussions, the improvement of power conversion efficiency of BHJ–OSC devices has been achieved through the enhancement of J_{sc}, V_{oc}, and FF. This means PCE is strongly correlated to material properties, device structure and interfacial materials effects [78].

The photocurrent density of BHJ-OSC is affected by numerous factors including generation, exciton separation rate and the mobility of free charge carriers in the photoactive medium. The exciton separation rate in BHJ films is quite effective due to the existence of several dissociation sites (D/A interfaces) within the reach of exciton diffusion length. The method of blending conjugated polymers such as P3HT (2.0 eV) and PTB7 (1.8 eV) as donor with high electron affinity molecules, such as fullerene C_{70} ($PC_{71}BM$) and $C60$ (PCBM) derivatives, has become the most efficient and rapid exciton dissociation method resulting in solar cells with relatively high power conversion efficiencies. This is due to the fact that the interpenetrating networks between the polymer and fullerene derivatives give rise to ultra-fast (less than 100 fs) electron transfer between the donor and acceptor molecules [70]. However, the efficiency of BHJ-OSC can be limited by the exciton generation rate and collection efficiency of free charge carriers. In the case of the BHJ-OSC containing P3HT as donor material which harvests photons in solar emission spectrum of less than 650 nm in the visible range, it can, however, only absorb $\sim 25\%$ of the incident photons due to the high optical band gap energy of P3HT [70]. Several other conjugated polymers with low optical band gap of about 1.1 eV can absorb $\sim 80\%$ of the light, resulting in an improved solar cells power conversion efficiency [70]. However, in order to increase the optical absorption of the photoactive medium it is necessary to optimize the thickness of the film without compromising the charge transport process.

The mobility of charge carriers in most conjugated polymers is quite low compared to inorganic counterpart. Consequently, in thick films most of the photo-generated carriers disappear through recombination processes or form space charges that limit the flow of current [77, 79, 80]. The low optical band gap polymer usage to ensure good harvesting of photons extends to the red and near infrared portion of the solar spectrum [80].
The second factor that limits efficiency is the V_{oc}, which itself is affected by several factors including interfacial layer work functions, shunt losses, interfacial dipoles and morphology of the photoactive layer [77]. The third important factor that limits efficiency is the fill factor which is related to the properties of the device properties which can be influenced by the choice of electrodes, interfacial layers and the device preparation conditions. As such, high series resistance is also one of the limiting factors as observed in BHJ-OSC devices caused by device preparation conditions [77, 79, 80].

The other challenge of organic solar cells is environmental stability and lifetime which is dependent on the chemical composition of the organic materials and ambient moisture conditions. These might affect the optical and electric properties of materials to generate electricity from ambient electromagnetic radiation (Fig. 2.10). An instability of BHJ-OSC devices can be attributed to chemical and physical degradation of photoactive layer and electrodes which is due to the presence of oxygen and humidity in the polymer matrix [81, 82].

2.7 Photoactive layer materials

The most common types of organic molecules often used in the preparation of bulk - heterojunction (BHJ) OSCs are π-conjugated polymers such as Poly(3-hexylthiophene) (P3HT)

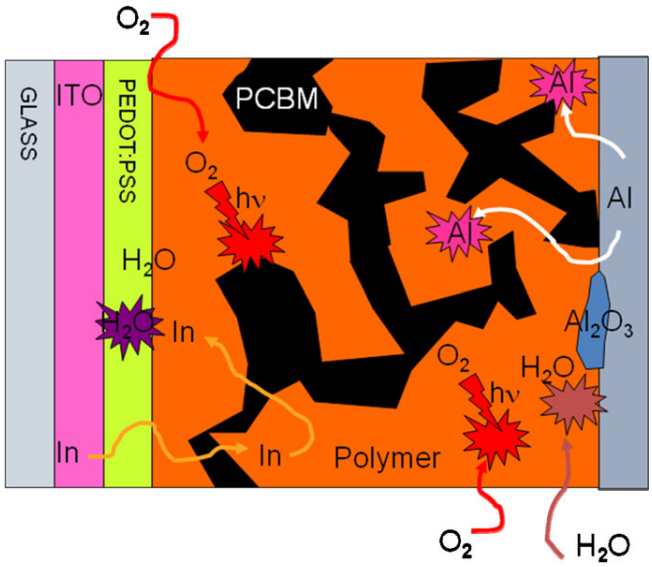

Figure 2.10: Degradation process in the BHJ-OSCs [82].

(HOMO and LUMO levels at -5.2 and -3.2 eV), PTB7 (HOMO level of -5.15 eV and a LUMO level of -3.31 eV), PCPDTBT (HOMO level of -5.3 eV and a LUMO level of -3.6 eV) and PBDTTBT (HOMO level of -5.5 eV and a LUMO level of -3.7 eV), with fullerene derivatives such as [6,6]-phenyl–C_{61}–butyric acid methyl ester ($PC_{61}BM$) or [6,6]-phenyl–C_{71}–butyric acid methyl ester ($PC_{71}BM$). PCPDTBT has deeper HOMO compared to others and therefore leads to higher V_{OC} of $\sim$ 1 V [70, 75]. Figure 2.11 shows some donor and acceptor materials structure. In BHJ-OSC devices, suitable phase segregation allows the formation of donor and acceptor interfaces in the medium.

2.8 Electrodes buffer layer materials

The interfacial materials incorporated as buffer layers at the photoactive layer and electrodes interfaces are very important for the improvement of the performance and stability of the

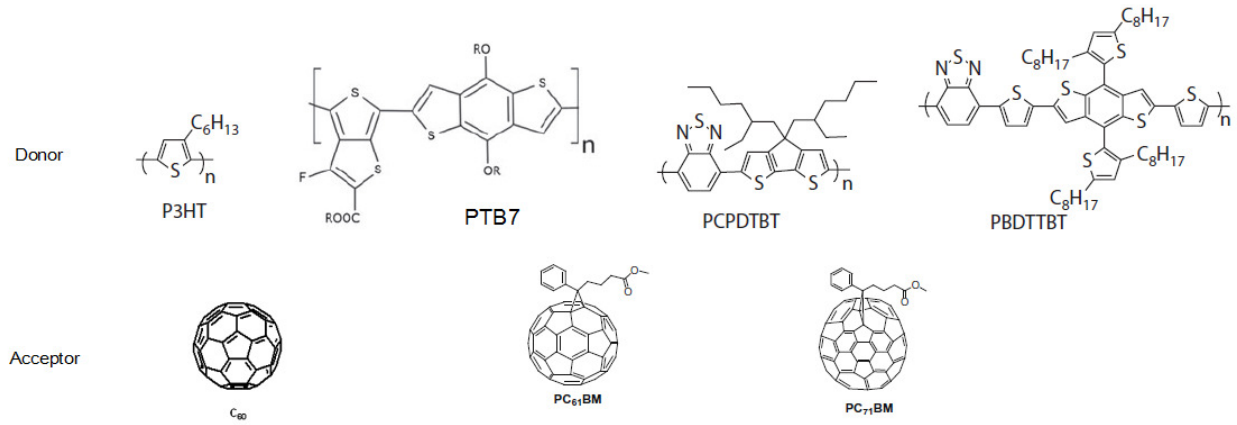

Figure 2.11: Some BHJ-OSCs photoactive layer materials structure.

OSC devices due to their potential to serve as electron transporting layer and hole blocking layer which allows for the selective transporting of one type of charge carrier and blocking the other one from reaching the electrode (Fig. 2.12). In addition, the buffer layers can play the role of an insulating layer capable of prohibiting the chemical reaction between the photoactive layer and electrodes, as well as the diffusion of the metal atoms into the photoactive layer during the thermal evaporation deposition of the back electrode which causes high electric resistance of the OSC devices thereby restricting their performance and stability.

On the other hand, buffer layers are also used to reduce roughness and to modify the work function of the transparent electrode [75, 83].

2.8.1 Anodic buffer layer materials

Transparent conducting oxides (TCOs) such as indium tin oxide (ITO) and fluorine doped tin oxide (FTO or F:SnO_2) are commonly used as transparent electrodes (anode) in opto-

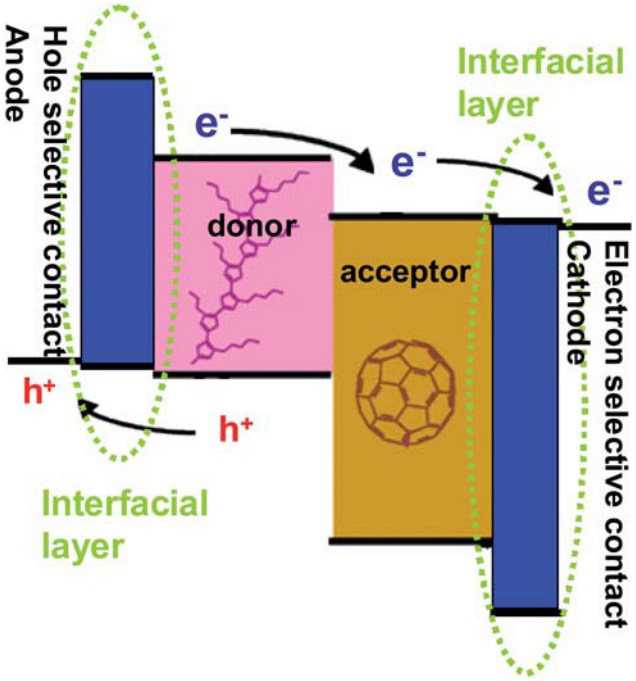

Figure 2.12: Schematic illustration of photogenerated charge carriers by photoactive layer, extracted by interfacial (buffer) layers, transported to be collected at the electrodes [95].

electronic devices due to their attractive unique properties such as high optical transparency and high electrical conductivity. FTO exhibits a similar sheet resistance, and is slightly less transparent and much rougher compared to ITO. Additionally FTO has thermal stability which enables it to conserve its optoelectronic properties above 600^0C, at which the properties of ITO degrade [84].

Poly(ethylene -3-4-dioxy thiophene):polystyrene sulphonate (PEDOT:PSS) is the most common hole transport layer (p-type) in OSC devices, which has many advantages such as high work function which matches the HOMO level of the most used donor polymers, high transparency in the visible range higher than 80%, good electrochemical and thermal stability, and high electrical conductivity polymer[85]. Moreover, it smooths the surface and has the ability to reduce or increase the work function of ITO surface roughness for efficient collec-

tion of holes and protects the photoactive layer from oxidative effect [86, 87]. PEDOT:PSS is also used in transparent electrode as an alternative to the ITO on flexible substrates. The conductivity of the PEDOT:PSS ranges from $10^{-3}Scm^{-1}$ up to $10^{3}Scm^{-1}$ depending on the solvent and it can be improved by post-treatments [86].

Despite these advantages, PEDOT:PSS can etch ITO electrodes due to its acidic nature [88, 89]. But Monein Elshobaki et al. (year) have reported that PEDOT:PSS can etch only a few nanometers of ITO which does not seriously affect the charge carrier transport and collection in OSC devices [90]. Besides that, the hygroscopic nature of PEDOT:PSS [16, 91, 92] facilitates etching the ITO layer, however, boosting sheet resistance which limits the stability of OSC devices [82, 88]. It has also been reported that PEDOT:PSS is high hydrophilic, thereby causing inhomogeneous film morphology and worsening electrical properties and stability [91, 93]. Several strategies have been devoted to reduce the acidic nature of PEDO:PSS by doping PEDO:PSS with high work function TMOs such as WO_3, V_2O_5 [91, 93] and MoO_3 [94]. Alternatively, transition metal oxides (TMOs) such as vanadium, tungsten, nickel and molybdenum oxide (V_2O_5, WO_3, NiO_x and MoO_3) are now mostly being used to replace PEDOT:PSS as buffer layers for OSC devices, which facilitates better charge carriers extraction in OSCs [94-97].

2.8.2 Cathodic buffer layer materials

In conventional structure BHJ-OSC devices, an energy level offset between the work function of cathode electrode such as AL (-4.3 eV) and LUMO level of the acceptor material such as PCBM (-4.3 eV) could result in charge carrier recombination due to carrier aggregation from undesirable electrons extraction. Therefore, the need to introduce a buffer layer such as Ca, Ba, LiF, ZnO and TiO_2 between the back electrode and photoactive layer is very important

[75]. Lithium fluoride (LiF) is commonly used as electron transport layers (ETLs) in OSC devices which acts as an excellent barrier to limit oxygen and moisture diffusion into organic photoactive layer, prevents the cathode electrode such as Al from being oxidized, and also enhances the devices FF and stabilizes high V_{oc}. Due to its insulating nature, the LiF buffer layer must be thin (0.5-1 nm) because a thicker layer of LiF creates a dipole layer that also lowers the electrode work function [75, 98-100].

Other alkali metal compounds such as NaF, KF, and C_s have also been used as cathode buffer layers [95]. Moreover, the use of metal oxides as ETLs has become more popular in recent years due to their excellent properties as explained below:

Zinc oxide (ZnO) is often used as the electron transport layer in OSC devices due to its attractive properties such as direct wide band gap (3.37 eV) and Fermi level of 4.3 eV which matched with LUMO of PCBM. In addition, ZnO is a non-toxic semiconductor material with good electrical, chemical, physical and magnetic properties. The crystal structures of ZnO are zinc blend and rock salt [75, 77, 95].

Titanium dioxide (TiO_2) is also widely used as an electron transport layer in OSC devices. TiO_2 has a large band gap in the range of 3.02 eV, 3.2 eV and 2.96 eV for the crystalline, anatase, rutile and brookite structures, respectively. ZnO and TiO_2 are also used as a hole-blocking layer, oxygen barrier and optical spacer which improves absorption inside a thin device by modifying the optical field [77, 95].

2.9 General processing techniques

Solution processing by roll to roll (R2R) technology to fabricate organic solar cells on large area flexible substrate with low cost production and high throughput is the main objective of organic solar cell research. However, in the laboratory scale various deposition techniques have been employed in the device fabrication processes of OSC to deposit the photoactive layer, buffer layers and electrodes, respectively. The following sections discuss the different methods of deposition:

2.9.1 Spin coating

Spin coating is a simple technique that uses solution in the deposition of films on the substrate. The thickness of the films on spin coating can be easily controlled by several parameters such as the concentration of solution and solvent, drying rate, spin time and spin speed which are independent of each other. The drying of host solvent from the wet film by evaporation depends on the duration of spin. The thickness of the film is exponentially proportional to spin time and spin speed. Many reports on OSCs have used spin coating technique to deposit photoactive thin film layer and some electrode buffer layers on device substrates. BHJ photoactive films and buffer layers have been processed from solution mainly through the spin coating method which is quite easy and cheap [101].

2.9.2 Thermal evaporation deposition

The thermal evaporation deposition involves the heating of materials in vacuum which is used to deposit a thin film of metal or small molecules organic materials. The substrate is

placed several centimeters away from the source so that evaporated material may be directly deposited onto the substrate. This method is useful for depositing many layers of different materials without chemical interaction between different layers. The control of materials evaporation depends on several parameters such as vacuum chamber pressure, materials purity and evaporation rate. In particular, the pressure of the vacuum chamber must be high enough ($10^{-6} - 10^{-7}$ mbar), because if pressure is insufficient, the hot vaporized material particles may interact with the remaining oxygen molecules and thereby form metal oxide. Also, the hot vaporized material can create holes in the film due to shadowing, which causes an increase in the device series-resistance and short circuit. In addition, the materials that deposit on the wall of the chamber can contaminate later depositions. There are sometimes problems with film-thickness uniformity over large-area substrates.

2.9.3 Electrochemical deposition

Electrochemical deposition (ECD) technique is one of the low temperature solution processing methods under non-vacuum conditions which is an inexpensive technique involving relatively simple instruments that consume considerably less energy than thermal evaporation technique. In this technique, electrochemical reactions occur at the electrode electrolyte interface and charges are transported through the deposits which can be controlled by varying parameters such as applied potential, deposition time, physical and chemical nature of the substrate surface and concentration of the suspension [95, 102]. In ECD technique, electric field has been generally used for the growth of electrically conductive materials, such as metals, semiconductors, and conductive polymers which offers several advantages such as a simple control of the microstructure, surface morphology and homogeneity of the deposited oxide films via easy adjustment of deposition parameters. The investigation of other meth-

ods is an important issue since the properties of the films are dependent on the deposition method. ECD cells are divided into two types depending on the number of electrodes which are: three electrodes cells and two electrodes cells. Fig. 2.13a shows a three electrodes ECD cell which involves the use of a working electrode (cathode), a counter electrode (anode), and a reference electrode. A conductive substrate is used as the working electrode, an inert material is employed as the counter electrode, and the reference electrode exists to measure and control the potential difference between the anode and cathode. The reference electrode allows the process to be performed potentiostatically, meaning the potential of the substrate can be controlled [103]. Fig. 2.13b shows ECD cell containing two electrodes, counter electrode (graphite piece) and working electrode (conductive substrate) [95, 103, 105].

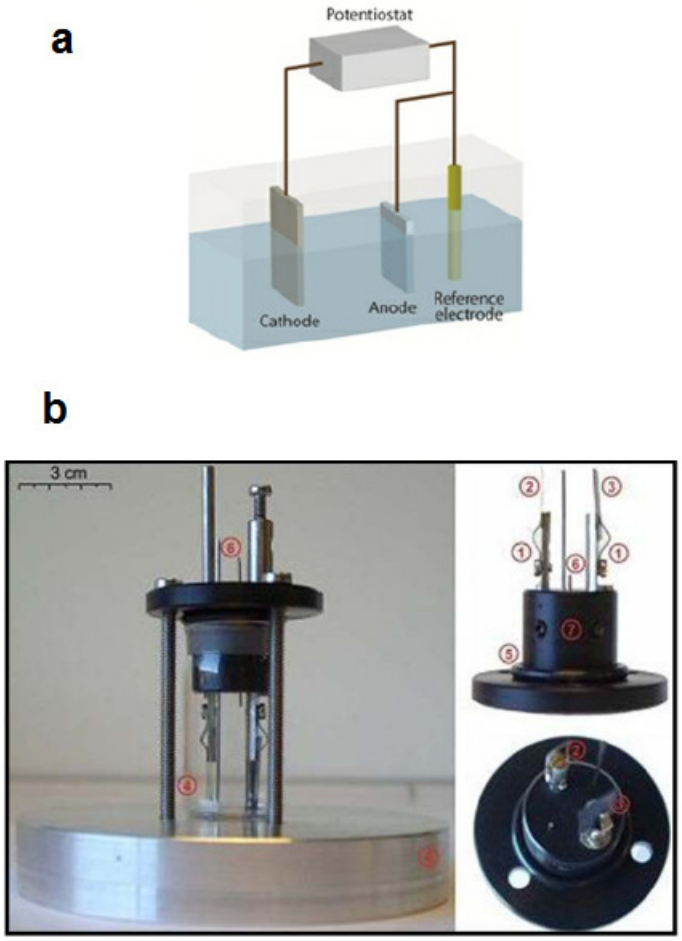

Figure 2.13: Electrodeposition cell a) three electrodes [102] b) two electrodes. (1) electrode holders with clamps made from stainless steel (2) working electrode (3) counter electrode (4) glass container (5) rubber gasket. (6) inlet tubes and holes for gases and liquids. (7) screws for adjusting electrode older height. (8) aluminium stand. [103].

Bibliography

[1] A. R. Jha, Solar Cell Technology and applications, Talor & Francis Groups, New York (2010).

[2] P. Hersch and K., Zweibel SERI/ISP-290-1448, Basic Photovoltaic Principles Methods, Solar Information Module-6213 Washington (1982).

[3] A. Goetzberger and V. U. Hoffmann, Photovoltaic solar energy generation, Springer (2005) Berlin.

[4] C. K. Chiang, C. R. Fincher, Y. W. Park, A. J. Heeger, H. Shirakawa, E. J. Jouis, S. C.Gau and A. G. MacDiarmid, Phys. Rev. Lett. 39 (1977) 1098.

[5] F. Liua, Y. Gua, X. Shena, S. Ferdousa, H-W. Wanga and T. P. Russell, Progress in Polymer Science 38 (2013) 1990– 2052.

[6] Y. Zhang, J. Griffin, N.W. Scarratt, T. Wang, and D. G. Lidzey, Prog. Photovolt: Res. Appl. 24 (2016) 275–282.

[7] Y. Zhang, J. Griffin, N. W. Scarratt, T. Wang and D. G. Lidzey,Prog. Photovolt: Res. Appl. 24 (2016) 275–282.

[8] X. Liu, H. Chen and S. Tan, Renewable and Sustainable Energy Reviews 52 (2015) 1527-1538.

[9] https://en.wikipedia.org/wiki/Photovoltaics (2016).

[10] Y. Liu, C-C. Chen, Z. Hong, J. Gao1, Y. (M.) Yang, H. Zhou, L. Dou, G. Li & Y. Yang, SCIENTIFIC REPORTS (2013) 3:3356 DOI:10.1038/srep03356.

[11] H. Huang and J. Huang, Organic hybrid solar cell, Springer, (2014) New York.

[12] M. K. Nazeeruddin, E. Baranoff, M. Gratzel, Solar Energy 85 (2011) 1172–1178.

[13] M. R. Narayan, Renewable and Sustainable Energy Reviews 16 (2012) 208–215.

[14] N. A. Ludin, A. M. A-A. Mahmoud, A-B. Mohamad, A. A. H.Kadhum, K. Sopian and N. S. A-Karim, Renewable and Sustainable Energy Reviews 31 (2014) 386–396.

[15] H. Hug, M. Bader, P. Mair and T. Glatzel, Applied Energy 115 (2014) 216–225.

[16] E. A. A. Arbab, G. T. Mola, Appl. Phys. A (2016) 122:405 pp8.

[17] T. M. Eggenhuisen, Y. Galagan, A. F. K. V. Biezemans, T. M. W. L. Slaats, W. P. Voorthuijzen, S. Kommeren, S. Shanmugam, J. P. Teunissen, A. Hadipour, W. J. H. Verhees, S. C. Veenstra, M. J. J. Coenen, J. Gilot, R. Andriessen and W. A. Groen, J. Matter. Chem. A, 3 (2015) 7255-7262.

[18] J. G. Tait, B. J. Worfolk, S. A. Maloney, T. C. Hauger, A. L. Elias and J. M. Buriak, K. D.Harris, Solar Energy Materials & Solar Cells 110 (2013) 98–106.

[19] H. Spanggaard, F. C. Krebs, Solar Energy Materials & Solar Cells 83 (2004) 125–146.

[20] G. A. dos R. Benatto, B. Roth, M. Corazza, R. R. Søndergaard, S. A. Gevorgyan, M. Jørgensen and F. C. Krebs, Nanoscale 8 (2016) 318–326.

[21] S-H. Park, S-J. Lee, J. H. Lee, J. Kal, J. Hahn, H-K. Kim, Organic Electronics 30 (2016) 112-121.

[22] R. N. Marks, J. Halls, D. Bradley, R. Friend and A. Holmes, J. physics: Condens. Matter 6(1379) (1994).

[23] J-M. Nunzi, C. R. Physique 3 (2002) 523–542.

[24] S. S. Sun and N. S. Sariciftici, Organic Photovoltaic: Machanism, Materials and devices, Taylor & Francis Group, LLC, (2005) USA.

[25] D. Leman, M. A. Kelly, S. Ness, S. Engmann, A. Herzing, C. Snyder, H. W. Ro, R. J. Kline, D. M. DeLongchamp, and L. J. Richter, Macromolecules 48 (2015) 383-392.

[26] P. Kumar and S. Chand, Prog. Photovolt: Res. Appl. 20 (2012) 377–415.

[27] K. H. Lee, P. E. Schwenn, A. R. G. Smith, H. Cavaye, P. E. Shaw, M. James, K. B. Krueger, I. R. Gentle, P. Meredith and P. L. Burn, Adv. Mater. 23 (2011) 766–770.

[28] C. W. Tang, Appl. Phys. Lett. 48 (1986) 183-185.

[29] A. Y. P. Peumans and S. R. Forrest, J. Appl. Phys. 93 (2003).

[30] K-S. Liao, Soniya D. Yambem, Amrita Haldar, Nigel J. Alley, and Seamus A. Curran, Energies 3 (2010) 1212-1250.

[31] P. P. Khlyabich, A. E. Rudenko, R. A. Street, and B. C. Thompson, ACS Appl. Mater. Interfaces 6 (2014) 9913-9919.

[32] T. Ameri, P. Khoram, J. Min, and C. J. Brabec, Adv. Mater. 25 (2013) 4245–4266.

[33] Y. Ohori, S. Fujii, H. Kataura, and Y. Nishioka, Jpn. J. Appl. Phys. 54 (2015) 04DK09.

[34] E. A.A. Arbab, B. A. Taleatu, G. T. Mola, Materials Science in Semiconductor Processing 40 (2015) 158–161.

[35] J. Zhang, Y. Zhang, J. Fang, K. Lu, Z. Wang, W. Ma, and Z. Wei, J. Am. Chem. Soc. 137 (2015) 8176-8183.

[36] L. Ye, H-H. Xu, H. Yu, W-Y. Xu, H. Li, H. Wang, N. Zhao, and J-B. Xu, J. Phys. Chem. C 118 (2014) 20094-20099.

[37] M. Zhang, F. Zhang, Q. An, Q. Sun, J. Wang, L. Li, W. Wang, J. Zhang, Solar Energy Materials & Solar Cells 141 (2015) 154–161.

[38] L. Yang, L. Yan and W. You, J. Phys. Chem. Lett. 4 (2013) 1802-1810.

[39] T. Ameri, G. Dennler, C. Lungenschmied and C. J. Brabec, Energy Environ. Sci., 2 (2009) 347–363.

[40] J. You, C.C. Chen, Z. Hong, K. Yoshimura, K. Ohya, R. Xu,S. Ye, J. Gao, G. Li, and Y. Yang, Adv. Mater., 25 (2013) 3973-3978.

[41] Z. M. Beiley and M. D. McGehee, Energy Environ. Sci., 5 (2012) 9173–9179.

[42] J. Jo, J-R. Pouliot, D. Wynands, S. D. Collins, J. Y. Kim, T. L. Nguyen, H. Y. Woo, Y. Sun, M. Leclerc, and A. J. Heeger, Adv. Mater. 25 (2013) 4783–4788.

[43] K. Zhang, K. Gao, R. Xia, Z. Wu, C. Sun, J. Cao, L. Qian, W. Li, S. Liu, F. Huang, X. Peng, L. Ding, H-L. Yip, and Y. Cao, Adv. Mater. (2016) DOI: 10.1002/adma.201506270.

[44] T. Ameri, N. Lia and C. J. Brabec, Prog. Photovolt: Res. Appl. 24 (2016) 275–282.

[45] V. Coropceanu, J. Cornil, D. A. da S. Filho, Y. Olivier, R. Silbey, and J-L. Bredas, Chem. Rev. 107 (2007) 926-952.

[46] A. Guerrero, N. F. Montcada, J. Ajuria, I. Etxebarria, R. Pacios, G. G-Belmonte and E. Palomares, J. Mater. Chem. A 1 (2013) 12345-12354.

[47] K.G. Jespersen, F. Zhang, A. Gadisa, V. Sundsträm, A. Yartsev, and O. Inganäs, Org. Electron. 7, 235-242 (2006).

[48] S. M. Sze and K. K. Ng, Physics of semiconductor devices, John Wiley & Sons 3rd edition (2007) New Jersey.

[49] J. T. Bell and G. T. Mola, Physica B: Condensed Matter, 437 (2014) 63-66.

[50] S. S. M. Tuladhar, D. Poplavskyy, S. A. Choulis, J. R. Durrant, D. C. Bradley and J. Nelson, Adv. Funct. Mater. 15 (2005) 1171-1182.

[51] C. V. Kumar, L. Cabbau, E. N. Koukaras, A. Viterisi, G. D. Sharma and E. Palomares, J. Mater. A. 3 (2015) 4892-4902.

[52] C. Deibel, V. Dyakonov, Rep. Prog. Phys. 73 (2010) 096401(39pp).

[53] B. Ratier, J. M. Nunzi, M. Aldissi, T. M. Kraft and E. Buncel, Polym. Int. 61 (2012) 342-354.

[54] J. Y. Kim, S. H. Kim, H-H. Lee, K. Lee, W. Ma, X. Gong and A. J. Heeger, Adv. Mater. 18 (2006) 572–576.

[55] D. Lee, J. Kim, S. Noh, and C. Lee, IEEE (2010).

[56] J. Nelson, Materialstoday 14(10) (2011) 462–469.

[57] K. Vandewal, A. Gadisa, W. D. Oosterbaan, S. Bertho, F. Banishoeib, I. V. Severen, L. Lutsen, T. J. Cleij, D. Vanderzande, and J. V. Manca, Adv. Funct. Mater. 18 (2008) 2064–2070.

[58] F. Padinger, R. S. Rittberger, and N. S. Sariciftci, Adv. Funct. Mater. 13(1) (2003) 85–88.

[59] J. H. Park, J. S. Kim, J. H. Lee, W. H. Lee, and K. Cho, J. Phys. Chem. C. 113 (2009) 17579–17584.

[60] A. L. Ayzner, C. J. Tassone, S. H. Tolbert, and B. J. Schwartz, J. Phys. Chem. C. 113 (2009) 20050–20060.

[61] S. V. D. Prasad, V. Krishnanaik, K. R. Babu, International Journal of Science and Modern Engineering (IJISME) 1(9) (2013) 2319-6386.

[62] L. Z. Gang, Z. X. Yan, L. Xin, G. Z. Qiang, M. B. Xiu and H. Wei, Sci. Chem. 55(4) (2012) 553-578.

[63] P. W. M. Blom, V. D. Mihailetchi, L. J. A. Koster, and D. E. Markov, Adv. Mater. 19 (2007) 1551–1566.

[64] V. Sadhu, N. A. Nismy, A. A. D. T. Adikaari, S. J. Henley, M. Shkunov and S. R. P. Silva, Nanotechnology 22 (2011) 265607(5pp).

[65] J. L. Bredas, J. E. Norton, J. Cornil, and V. Coropeanu, Accounts of Chemical Research 42(11) (2009) 1691-1699.

[66] S. R. Cowan, N. Banerji, W. L. Leong, and A. J. Heeger, Adv. Funct. Mater. 22 (2012) 1116–1128.

[67] H. Benten, D. Mori, H. Ohkita and S. Ito, J. Mater. Chem. A 4 (2016) 5340–5365.

[68] A. Ibrahim, M. R. I. Ramadan, S. Aboul-Enein, A. A-A. ElSebaii and S.M. El-Broullesy, International Journal of Renewable Energy Research, IJRER, 1(3) (2011) 553-559.

[69] J. Nelson, The physics of solar cells, Imperial college press, UK (2003).

[70] W. C. H. Choy, Organic Solar Cells: Materials and Device Physics, Springer (2013) London.

[71] B. Qi and J. Wang, Phys. Chem. Chem. Phys. 15 (2013) 8972-8982.

[72] T. Markvart and L. Castafier, Solar Cells: Materials, Manufacture and Operation, Amsterdam, The Netherlands (2006).

[73] G. Li, R. Zhu and Y. Yang, Nature Photonics 16 (2012) 153-161.

[74] A. Gaur and P. Kumar, Pro. Photovolt: Rws. Appl.(2013).

[75] Q. Qiao and K. Iniewski, Organic Solar Cell: Materials, Devices, Interfaces and Modeling, CRC Press, Tylor & Francis group, New York, (2015).

[76] J. D. Servaites, M. A. Ratner and T. J. Marks, Energy Environ. Sci. 4 (2011) 4410–4422.

[77] J. You C-C. Chen, L. Dou, S. Murase, H-S Duan, S. A. Hawks, T. Xu, H. J. Son, L. Yu, G. Li and Y. Yang , Adv. Mater. 24 (2012) 5267-5272.

[78] S. H. Park, A. Roy, S. Beaupure, N. Coates, J. S. Moon, D. Moses, M. Leclerc, K. Lee and A. J. Heeger, Nature Photonics, 3 (2009) 297-302.

[79] C. J. Brabec, M. Heeney, I. McCulloch and J. Nelson, Chem. Soc. Rev. 40 (2011) 1185-1199.

[80] R. A. J. Janssen and J. Nelson, Adv. Mater. 25 (2013) 1847-1858.

[81] J. Li, S. Kim, S. Edington, J. Nedy, S. Cho, K. Lee, A. J. Heeger, M. C. Gupta, J. T. Y. Jr, Solar Energy Materials & Solar Cells 95 (2011) 1123–1130.

[82] M. Jørgensen, K. Norrman, F. C. Krebs, Solar Energy Materials and Solar Cell 92 (2008) 686-714.

[83] N. K. Elumalai, C. Vijila, R. Jose, A. Uddin and S. Ramakrishna, Mater Renew Sustain Energy 4 (2015) (11pp).

[84] Y. H. Kim, C. Sachse, M. L. Machala, C. May, L. M-Meskamp, and K. Leo, Adv. Funct. Mater. 21 (2011) 1076–1081.

[85] D. J. Lipomi, J. A. Lee, M, Vosgueritchain, B. C. Tee, J. A. Bolander and Z. Bao, Chem. Mater., 24 (2012) 373-382.

[86] M, Vosgueritchain, D. J. Lipomi and Z. Bao, Adv. Funct. Mater. 22 (2012) 421-428.

[87] W. S. Yip and K. Woon, Optoelectronics and advanced materials-Papid Communications, 4(7) (2010) 1037-1039.

[88] L. Lu, T. Xu, I. H. Jung and L. Yu, J. Phys. Chem. C 118 (2014) 22834-22839.

[89] F. Ongul, Optical Materials, 50 (2015) 244-249.

[90] M. Elshobaki, J. Anderegg and S. Chaudhary, ACS Appl. Mater. Interfaces 6 (2014) 12196-12202.

[91] H. Choi, B. S. Kim, M. J. Ko, D-K. Lee, H. Kim, S. H. Kim and K. Kim, Organic Electronics, 13 (2012), 959-968.

[92] S-P. Cho, J-S. Yeo, D-Y. Kim, S-I. Na, S-S. Kim, Solar Energy Materials & Solar Cells 132 (2015) 196–203.

[93] S. J. Lee, H. P. Kim, A. R. M. Yusoff, and J. Jang, Sol. Energy Mater. Sol. Cells 120 (2014) 238-243.

[94] Y. Zhao, J. Chen, W. Chen, and D. Ma, J. Appl. Phys. 111 (2012) 043716.

[95] R. Steim, F. R. Kogler and C. J. Brabec, J. Mater. Chem. 20 (2010) 2499-2512.

[96] X. Bao, Q. Zhu, T. Wang, J. Guo, C. Yang, D. Yu, N. Wang, W. Chen, and R. Yang, ACS Appl. Mater. Interfaces, 7 (2015) 7613-7618.

[97] K. Zilberberg, J. Meyerb and T. Ried, J. Mater. Chem. C, 1 (2013) 4796-4815.

[98] C. J. Brabec, S. E. Shaheen, C. Winder, N. S. Sarcificiftci and P. Denk, Appl. Phys. Lett. 80 (2002) 1288-1290.

[99] D. Gao, M. G. Helander, Z-B. Wang, D. P. Puzzo, M. T. Greiner and Z-H. Lu, Adv. Nater. 22 (2010) 5404-5408.

[100] T. Yanagidate, S. Fujii, M. Ohzeki, Y. Yanag, Y. Arai, et al., JPN. Appl. Phys. 53 (2014) 02BE05.

[101] S. Beke, Thin Solid Films, 519 (2011) 1761-1771.

[102] https://www.polyu.edu.hk/abct/en/staff-singledemo376a2.html?id=72.

[103] B. A. Taleatu, A. Y. Fasasi, G. DiSanto, S. Bernstorff, A. Goldoni, M. Fanetti, L. Floreano, P. Borghetti, L. Casalis, B. Sanavio and C. Castellarin-Cudia, AIP ADVANCES 1 (2011) 032147.

[104] D. Rehnlund, M. Valvo, K. Edstrom, and L. Nyholm, Journal of The Electrochemical Society 161 (10) (2014) D515-D521.

[105] B. A. Taleatu, E. A.A. Arbab, G. T. Mola, Materials Science in Semiconductor Processing 44 (2016) 85–90.

Chapter 3

V_2O_5 THIN FILM DEPOSITION FOR APPLICATION IN ORGANIC SOLAR CELLS

Appl. Phys. A (2016)122:405
DOI 10.1007/s00339-016-9966-1

Applied Physics A
Materials Science & Processing

V_2O_5 thin film deposition for application in organic solar cells

Elhadi A. A. Arbab[1] · Genene Tessema Mola[1]

Received: 22 December 2015 / Accepted: 1 March 2016

Abstract Vanadium pentoxide V_2O_5 films were fabricated by way of electrochemical deposition technique for application as hole transport buffer layer in organic solar cell. A thin and uniform V_2O_5 films were successfully deposited on indium tin oxide-coated glass substrate. The characterization of surface morphology and optical properties of the deposition suggest that the films are suitable for photovoltaic application. Organic solar cell fabricated using V_2O_5 as hole transport buffer layer showed better devices performance and environmental stability than those devices fabricated with PEDOT:PSS. In an ambient device preparation condition, the power conversion efficiency increases by nearly 80 % compared with PEDOT:PSS-based devices. The devices lifetime using V_2O_5 buffer layer has improved by a factor of 10 over those devices with PEDOT:PSS.

3.1 Abstract

Vanadium pentoxide (V_2O_5) films were fabricated by way of electro-chemical deposition technique for application as hole transport buffer layer in organic solar cell. A thin and uniform V_2O_5 films were successfully deposited on indium tin oxide (ITO) coated glass substrate. The characterization of surface morphology and optical properties of the deposition suggest that the films are suitable for photovoltaic application. Organic solar cell fabricated using V_2O_5 as hole transport buffer layer (HTL) showed better devices performance and environmental stability than those devices fabricated with PEDOT:PSS. In an ambient device preparation condition, the power conversion efficiency increases by nearly 80% compared with PEDOT:PSS based devices. The devices life time using V_2O_5 buffer layer has improved by a factor of 10 over those devices with PEDOT:PSS.

Keywords: Hole transport; electrodeposition; optical properties; OSCs

3.2 Introduction

Bulk heterojunction organic solar cells (OSC) have achieved remarkable progress in improving the power conversion efficiency (PCE) in the past ten years. The PCE of organic solar cell is currently reached the required mass production rate close to 10% [1-6], but the environmental stability is still remain the major challenge [7-12]. Despite such problems the OSC offers a number of advantages over the traditional inorganic molecules based solar cells. Among others the roll-to-roll solution processing techniques in the fabrication of organic solar cell is expected to reduce the cost of the devices. The mechanical flexibility of the polymer film is an added advantage that allows the integration of OSC devices in non-planer surfaces. The standard OSC device structure, composed of a sequence of layers of materials

as ITO/PEDOT:PSS/Active layer/LiF/Al, uses thin film buffer layers for various reasons. For example, PEDOT:PSS is the most common hole transport layer in OSC which facilitates the collection and transportation of holes from the active layer to the ITO electrode. However, the acidic and hygroscopic nature of PEDOT:PSS are among some of the factors that negatively contributes to performance and stability of OSC. Therefore, a suitable choice of an interfacial buffer layer can prevent the photoactive medium from exposure to moisture and oxygen which are the major factors for device degradation. Besides, poor film uniformity and surface morphology would also further deteriorate the environmental stability of the OSC devices [13-25]. Hence, it was long overdue to find an alternative and suitable charge transport materials to replace PEDOT:PSS. Transition metal oxides (TMOs) are found to be a suitable candidates for possible substitute for PEDOT:PSS interfacial layer such as V_2O_5, MoO_3, NiO, and WO_3. These semiconductor metal oxides have favorable electronic and optical properties; such as high optical transmittance, low barrier height at ITO/photoactive layer/ interface due to their high work functions. Moreover, their high level of technological compatibility in organic electronics and possibility for low temperature deposition using solution processing method makes them an ideal alternative [1-16, 25-28]. The V_2O_5 particularly interesting in this study because of its potential application in OSC to be used as hole transport and electron blocking layer [26, 28]. Several deposition methods have been employed to synthesis and grow V_2O_5 thin film on various substrates. The most common one is a vacuum deposition method which is relatively expensive and unsuitable for large area deposition. Recently, the focus of attentions was diverted into solution processing methods to fabricate V_2O_5 buffer layer which is low cost and produces the same level of deposition quality as vacuum techniques [13, 15-19, 26, 27]. We are employing here electro-chemical deposition which has numerous advantages over vacuum deposition such as the ease of film preparation, low processing costs, low temperature growth, environmentally

friendly, nontoxic and can be expanded into industrial scale. In electro-chemical deposition, the film microstructure, surface morphology and homogeneity of the deposited film can be easily controlled via simple adjustment of deposition parameters. In the present work, two electrodes electrodeposition cell was used which allows flexibility in the choice of both counter and working electrodes compared to common three electrodes electrodeposition cell.

3.3 Experimental Details

ITO coated glass substrate (sheet resistance of 15Ω/sq) were purchased from Ossila Ltd and used in the deposition of V_2O_5. Initially, the ITO substrates were partially etched with acid solution at the concentration of (HCl:H_2O : HNO_3 at 48:48:4 ratio by volume). The substrates were thoroughly cleaned using ultrasonic cleaner in deionized water, acetone and isopropanol (IPA) for 10 min, respectively. The substrates are then dried in a furnace at 120^oC for 15 min before the V_2O_5 film deposition. Cream powder ammonium metavanadate (NH_4VO_3) (99.7%, Sigma Aldrich) was used to synthesis vanadium pentoxide (V_2O_5) film.

3.3.1 Preparation of V_2O_5 Film

We adopted the synthesis and electrodeposition method developed and reported in the literatures [29-31]. In a typical synthesis, 0.585g of cream powder ammonium metavanadate (NH_4VO_3) at 0.05M concentration was used to prepare a solution. The electrolyte was dissolved in 100 ml de-ionized water (DI water) and continuously stirred at 70^oC for overnight. The resulting transparent yellowish solution was kept in room temperature for 5 days to obtain a dense solution in order to enhance film crystallization. In the current experiment,

the graphite piece and ITO-coated glass electrodes were used as a counter and working electrodes, respectively. The electrodeposition was performed by applying a potential difference of 2.5 volt for 5min. The resulting films were rinsed in a fresh DI water after deposition and then thermally annealed in the furnace under ambient condition at 300^{o}C, 350^{o}C, 400^{o}C, 450^{o}C and 500^{o}C for an hour. Surface morphology of the films were investigated by Zeiss EVO LS 15 ultra plus FESEM (Field Emission Scanning Electron Microscopy) fitted with Oxford EDAX (Energy Dispersive Analysis of X-ray) detector (INCA Point ID software for quant optimization). Optical absorption across ultraviolet to infrared spectrum was measured using double beam UV/VIS spectrophotometer, respectively. In order to improve the quality of (V_2O_5) film and reduce residual impurities we employed three types cleaning procedures such as, as deposited, 5 minutes ultrasonic cleaning in DI water and 5 minutes ultrasonic cleaning in DI water, acetone and IPA, respectively. Finally, the substrates were dried in the furnace at 150^{o}C for 15 min in air.

3.3.2 Preparation of OSC devices

Several OSC devices were fabricated based on standard device structure ITO/ V_2O_5 / P3HT:PCBM/LiF:Al in ambient laboratory condition (Fig 3.1a). The photoactive layer of the solar cells was composed of poly (3-hexythiophene) (P3HT) and [6-6] phenl-C61-butuyric acid methyl ester (PCBM) blend at 1:1 ratio by weight. The solution of the polymers blend was prepared in chloroform solvent at concentration of 20mg/ml and sonicated for 3hrs at 40°C to enhance the miscibility of the molecules. The active layers were then spin coated on top of V_2O_5 at the rate of 1200 rpm for 50 sec and dried in the furnace at 70^{o}C, for 5 min under nitrogen atmosphere. The samples were then loaded into the vacuum chamber (Edward Auto 306 deposition unit) at a base pressure of 10^{-6} mbar. Finally, a thin buffer layers

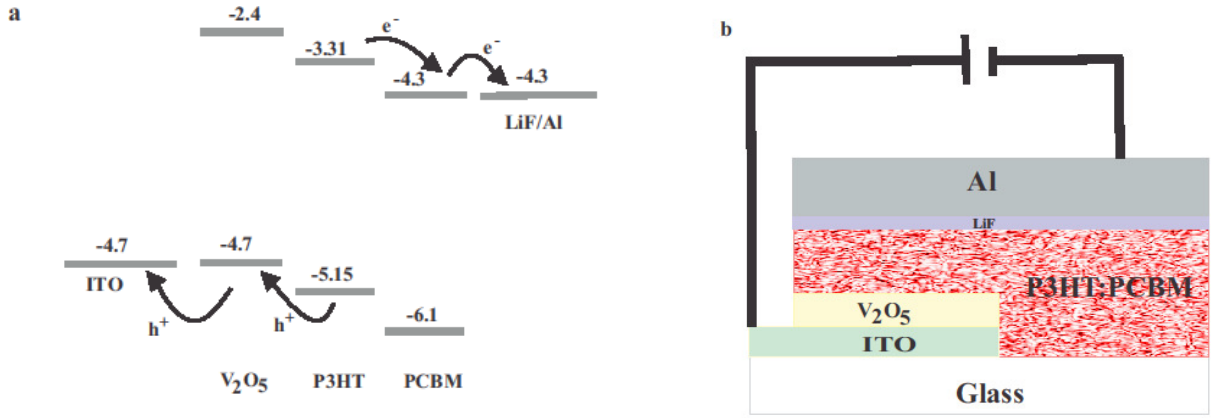

Figure 3.1: Schematic diagram for a) energy level of organic solar cells based V_2O_5 HTL and b) device structure of OSCs.

of lithium fluoride and aluminium electrode were deposited on top of the active layer with thickness 0.4nm and 50nm, respectively. The electrical characterization of the devices was carried out using computer interfaced Keithley HP2400 source-meter and a solar simulator (model SS50AAA) at AM1.5 operating at an integrated power intensity of 100 mW/cm^2. The resulting diodes had effective area was 0.04 cm^2. According to the information provided in Fig (5.1a) the valence band of V_2O_5 (-4.7 eV) is higher than the HOMO of P3HT (-5.15 eV) which is favorable for hole transport at the interface ITO/ V_2O_5/P3HT [27, 33]. Moreover, the existence of large energy band offset between the LUMO of P3HT (-3.2eV) and conduction band of V_2O_5 (-2.4eV) suggest that V_2O_5 buffer layer is indeed an electron blocking layer which prevents electrons from entering into the ITO electrode. As a result, the V_2O_5 film as an interfacial layer can prevent the recombination of the charge carriers at the interface between active layer and ITO electrode.

3.4 Results and Discussion:

3.4.1 Characterizations of V_2O_5 Films

After electro-chemical deposition of V_2O_5 on ITO coated glass substrates we studied the optical and microstructural properties of the films. The thickness of the films as determined by SEM and ellipsometery measurements ranges from (45-65)nm and the deposition parameters are kept the same. The crystalline structure of V_2O_5 thin films were analyzed using X-ray diffractometer with CuK_α radiation ($\lambda = 0.15406$ nm). Fig. 3.2 shows the XRD pattern of V_2O_5 thin film deposited on ITO coated glass substrate after annealing at different temperatures for 1h. The diffraction peaks are indexed as (101), (301), (400), (211) and (002) planes of V_2O_5 which are located at $2\theta = 21.4°$, $30.4°$, $30.4°$ and $45.2°$, respectively. All the diffraction peaks in the pattern corresponding to the orthorhombic crystal structure of V_2O_5. It is evident that the crystallinity of the films increase with temperature and reached maximum at 450°C as attested by enhanced intensities (Fig. 3.2). Some of the weak diffraction peaks appeared at lower angles in XRD spectra of the 500°C and 450°C annealed samples are associated with (200) and (001) planes of V_2O_5 crystal located at $2\theta = 18{,}7°$ and $20.5°$, respectively. The peaks marked by $(*)$ are due to the presence of ITO on the glass substrate. The results confirmed the formation of V_2O_5 crystal on the glass substrate which are in agreement with literature [34-36]. The optical transmittance spectra provided in Fig 3.3a are taken from the samples which are undergone to various post-deposition heat treatment in an ambient environment. Generally, the spectra clearly show high optical transmittance which is suitable for the preparation of organic solar cell. Those samples annealed at 400°C, 450°C, 500°C exhibited high transmittance in the region from 400 nm to 700 nm. The samples treated below 400°C were found to be less transparent in the same region of wavelengths.

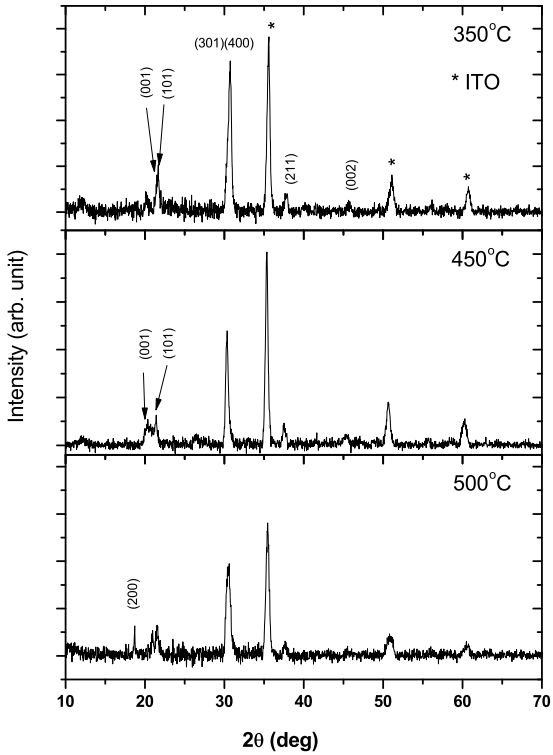

Figure 3.2: The XRD spectra of V_2O_5 films deposited on ITO coated glass substrate

Based on the experimental evidences, from XRD and optical absorption measurements, the optimum temperature for better transmittance and crystal quality of V_2O_5 film was found to be 450°C. Further investigation was also conducted on the effect of deposition residual impurities on V_2O_5 films prepared using identical deposition parameters followed by annealing at 450°C. The samples were then undergone in three types of cleaning procedures; **Type 1)** as deposited **Type 2)** 5 min ultra sonication in DI water

Type 3) 5 min ultra sonication in DI water, acetone and isopropanol, respectively (standard).

The measured optical transmittance spectra taken from the samples show generally similar absorption pattern (see Fig. 3.3b) except those samples cleaned under standard procedure

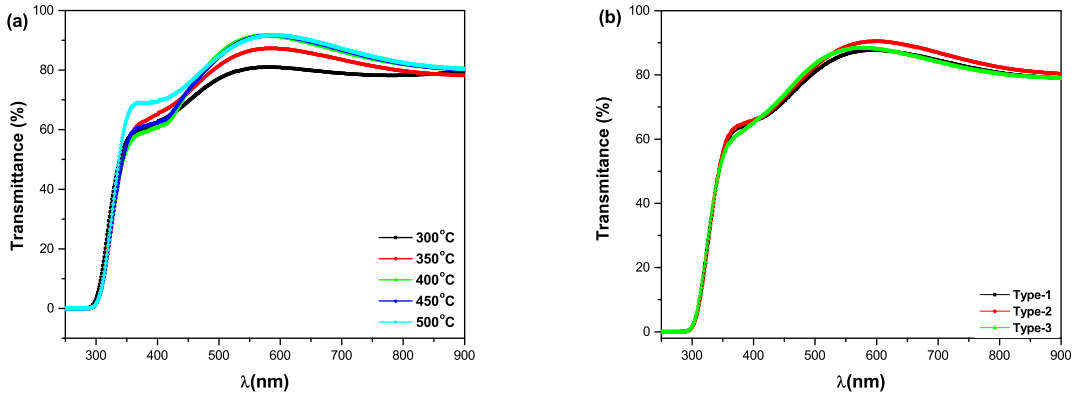

Figure 3.3: Optical transmittance spectra of V_2O_5 films a) annealed at various temperatures after electrodeposition b) absorbance taken from samples without and with cleaning after annealed at 450°C.

(type 3) which slightly show better transmittance in the wavelength range from 550 nm to 700 nm. Moreover, the scanning electron microscopic (SEM) images taken from the surface of the samples distinctly show the effect of cleaning on the microstructure and crystal grain size distributions of V_2O_5 films (see Fig. 3.4). The top panel of Fig. 3.4a is the image taken directly after the deposition of the film (Type 1) which consists of V_2O_5 film covered with some form of artifacts. In this image, it is evident about the existence of larger grain size of

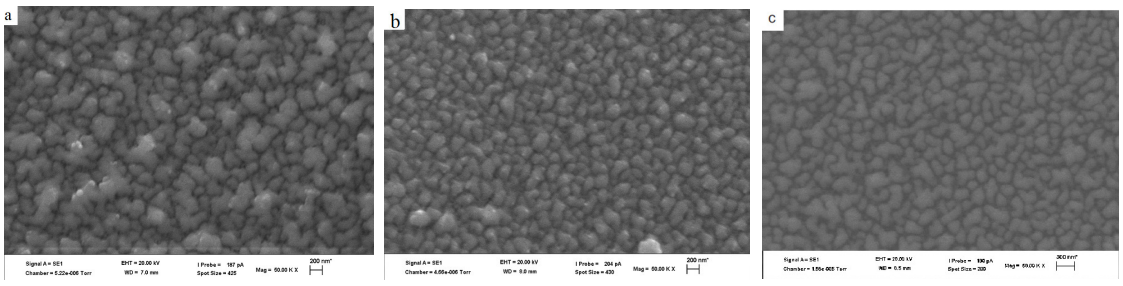

Figure 3.4: SEM images taken from V_2O_5 films after post-deposition annealing followed by a) without cleaning b) cleaning with DI water for 5min c) cleaning with DI water, acetone and IPA for 5min.

V_2O_5 molecule. The artifacts largely disappeared from the surface when the sample is cleaned with DI water (Type 2) but still some defect like structure are evident on the surface (Fig. 3.4b). Finally, we found no defect on the surface of the film as depicted on the bottom panel (Fig. 3.4c) for (type 3) cleaning procedure. In all cases, the films exhibited uniform and densely distributed microstructure of poly-crystalline grain of V_2O_5. The elemental analysis of the EDAX data confirmed the formation of V_2O_5 on top of ITO coated glass substrate.

3.4.2 Characterizations of OSC devices

The photoactive layers of the solar cells, composed of P3HT and PCBM blend, were spin coated on several V_2O_5 film coated substrates which were undergone through various post-deposition heat treatments. The OSC devices fabricated on V_2O_5 were compared with samples produced on PEDOT:PSS hole transport layer (HTL). The current-voltage (J-V) characteristics given in Fig. 3.5 are taken from OSC devices whose hole transport layers were annealed at various temperatures as indicated in the panel. Devices with V_2O_5 as a hole transport layer are generally performs better than those produced on PEDOT:PSS(Fig. 3.5). The best device performance was recorded from samples whose V_2O_5 film was annealed at 450°C (Table 3.1). The maximum device parameters from this experiment, using V_2O_5 as hole transport layer, are PCE = 2.43%, FF = 45%, $J_{sc} = 10\text{mA/cm}^2$ and V_{oc}= 550 millivolts. These values are well above the parameters measured from devices produced on PEDOT:PSS layer (Table 3.1). It is to be noted that only those V_2O_5 film depositions annealed at 400°C and 450°C outperformed those on PEDOT:PSS layer. The rest of post-deposition annealing temperatures did not yield the desired film property. For example, the power conversion efficiency grew by 50% when the 450°C annealed V_2O_5 film was used as hole transport layer compared to PEDOT:PSS (Table 3.1). The reason for such high improvement in PCE is

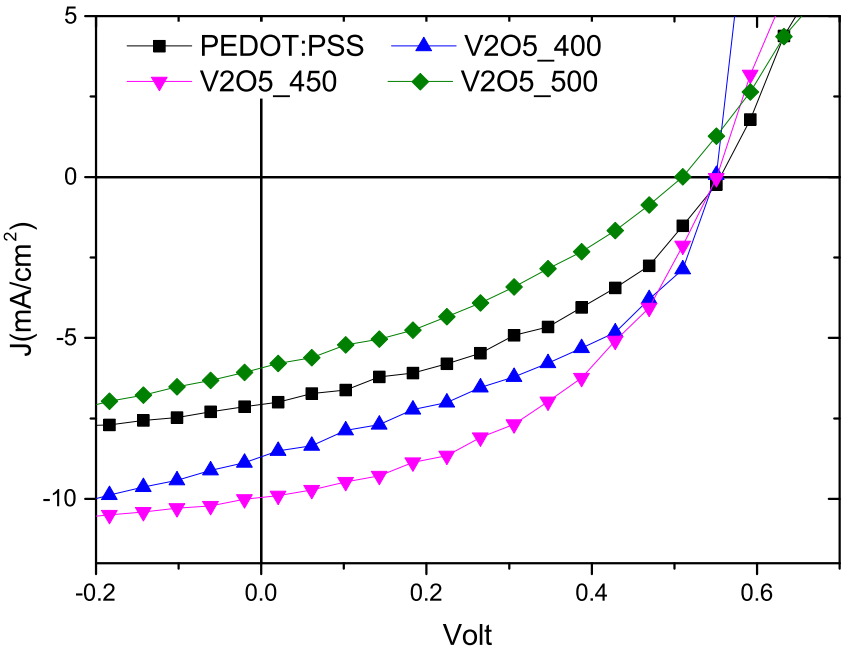

Figure 3.5: The J-V characteristics of the devices under illumination with V_2O_5 hole transport layers which were annealed at various temperatures as indicated in the panel.

mainly due to enhanced short circuit current collected from device with V_2O_5 layer. According to the results, it appeared to us that V_2O_5 buffer layer prevents the leakage currents by creating high shunt resistance and lower series resistance at the interface, at least for 400°C and 450°C annealed films(Table 3.1). The open circuit voltage measured from the sample whose V_2O_5 film was annealed at 500°C was lower than all other devices. This could be attributed to the oxygen deficiency of the V_2O_5 film due to high temperature and resulting in the formation undesirable layer that could change the work function of the ITO electrode.

3.4.2.1 Effect of post-deposition cleaning

The purpose of post-deposition cleaning is to reduce the deposition residual impurities without harming the film properties and to improve device performance. The effect of cleaning V_2O_5 films was discussed in terms of changes in optical and structural properties in the pre-

Table 3.1: Performance of solar cells fabricated at various V_2O_5 processing temperatures without post-deposition cleaning.

HTL material	Annealing temp. (^{o}C)	V_{oc} volt	J_{sc} mA/cm^2	FF %	PCE %	R_s ohms	R_{sh} ohms
$PEDOT$:PSS	150	0.56	7.12	40.4	1.62	305	2710
V_2O_5	300	0.54	9.03	24.4	1.19	602	1187
V_2O_5	350	0.59	6.22	38.7	1.43	528	2712
V_2O_5	400	0.55	8.74	43.4	2.09	195	4155
V_2O_5	450	0.55	9.95	44.3	2.43	156	5400
V_2O_5	500	0.51	5.94	34.1	1.05	875	4538

vious sections. Devices were produced on several substrates which were undergone in one of the three cleaning procedure. The electrical properties of OSC devices provided in Fig. 3.6 clearly shows the difference in device performances. We found significant improvement in device performance after cleaning the substrate with DI water after V_2O_5 deposition. The power conversion efficiency was enhanced by 11% compared to samples produced without cleaning (Table 3.2). However, cleaning the vanadium pentoxide film using (type 3) procedure has significantly reduced the device performance in most of the samples. One of the device parameter that suffered by the effect is the open circuit voltage which is recorded to the value of 270 milivolts (Table 3.2). The low device performance in type 3 could be the result of the interaction between V_2O_5 film and ITO electrodes facilitated by the presence of organic solvents. Such interactions could lead to the formation of interfacial defect layer between the ITO and V_2O_5 buffer layer which reduces the magnitude of V_{OC}. The presence of such interfacial layer would modify the work function of the electrode as well as can cause high series resistance in the medium. Besides, the measured low short circuit current (J_{SC}

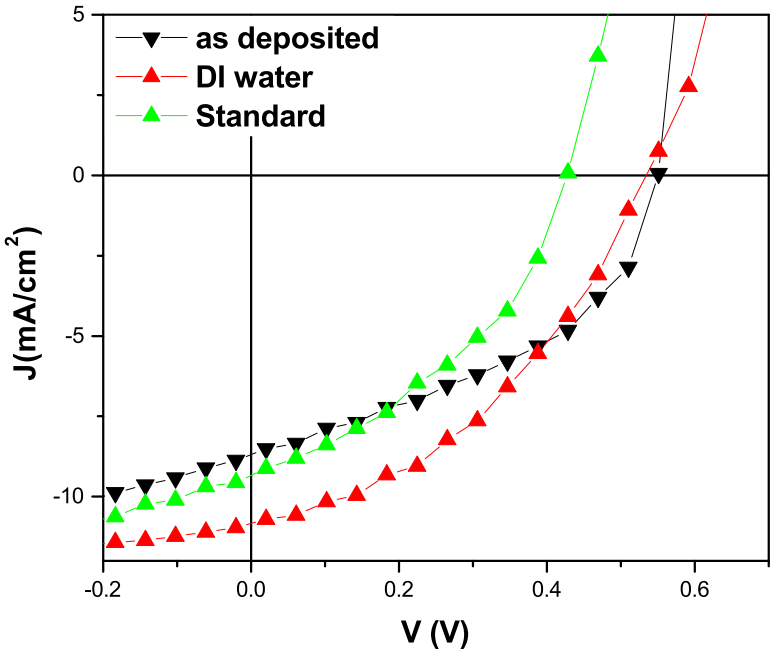

Figure 3.6: J-V characteristics of OSCs devices under illumination whose V_2O_5 films were annealed at 450°C and followed by three types of cleaning procedures.

$= 5.53\ mA/cm^2$ is another indication of the presence of high series resistance in the interfacial layer. Our results suggest that cleaning the hole transport layer (V_2O_5) with organic solvents after deposition would result in poor device performance. However, the films which were annealed at 350°C after deposition appeared to be more stable in organic solvents than 450°C and the result will be communicated in the near future.

3.4.2.2 Environmental stability of OSC devices

The environmental stability of devices produced with V_2O_5 and PEDOT:PSS hole transport layers were compared under exposure to ambient environment. The laboratory condition such as temperature and humidity level were 21°C and 54%, respectively. The current-voltage characteristics of the devices were measured in a regular time interval and then the samples were kept in the N_2 atmosphere until the next measurement. According to the

Table 3.2: Device performances following three types of cleaning procedures after V_2O_5 deposition.

V $_2O_5$ film annealed at 450°C				
Cleaning Procedure	V_{oc} volt	J_{sc} mA/cm^2	FF %	PCE %
Type 1	0.55	9.95	44.3	2.4
Type 2	0.58	10.12	45.6	2,7
Type 3	0.27	5.53	39.7	0.6

results depicted in Fig. 5.7(a) and (b) the solar cell parameters decreases very quickly in devices with PEDOT:PSS layer than V_2O_5. In the first one hour of device life time the

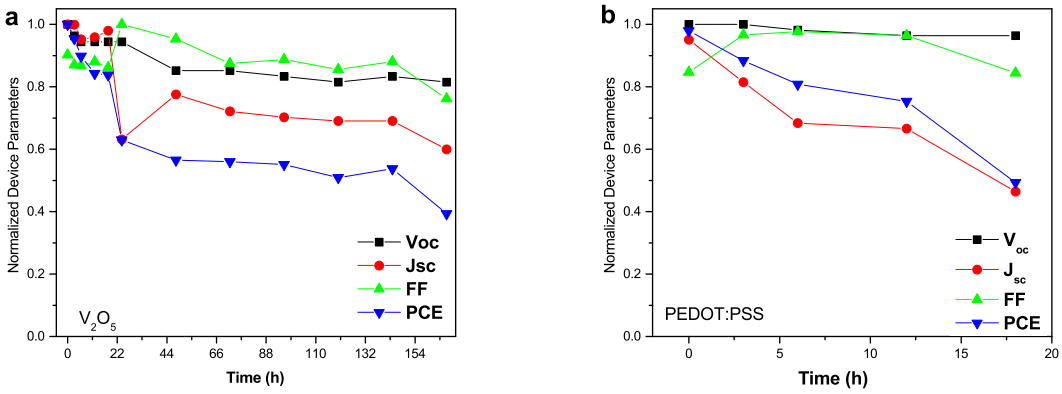

Figure 3.7: Normalized device parameters of OSCs using a)V_2O_5 HTL b) PEDOT:PSS HTL.

parameters of the two groups of solar cells do not change very much. Noticeable change of parameters have been recorded from devices with V_2O_5 HTL only after 15 hours. However, in the case of PEDOT:PSS based devices most of the device parameters monotonically decreases beginning from the first hour of existence. The power conversion efficiency of these devices decreases by 50% in 16 hours while devices with V_2O_5 HTL take nearly 130 hours.

Therefore, V_2O_5 buffer layer is not only effective hole transport layer but also protects the active layer from degradation. The faster degradation of the PEDOT:PSS-based devices is presumably due to the acidic nature of the molecule as well as it's tendency to absorb moisture from the environment [14, 22]. The PEDOT:PSS film is known for its susceptibility to the formation of the so called pinholes which results in short circuiting and prone to hold defects. However, the V_2O_5 films as depicted in Fig. 3.4 are found to be more uniform and less likely to have pinhole like structure. Furthermore, it has been reported that V_2O_5 thin films is more hydrophobic than the PEDOT: PSS which contribute to better device performance [14, 22].

3.5 Conclusions

We have successfully fabricated vanadium pentoxide (V_2O_5) layer through electro-chemical deposition for efficient and stable hole transport layer in the preparation of organic solar cell. The behavior of the film is found to be dependent on post-deposition heat treatment as well as cleaning procedure used. The optimum annealing temperature for better crystal growth of V_2O_5 film was found to be 450°C. The OSCs fabricated on V_2O_5 buffer layer were found to be more stable and effective in extraction and transportation of charge carriers from active layer to ITO electrode than PEDOT:PSS. Moreover, the devices produced using (V_2O_5) exhibited longer life time in an ambient environment. From the current investigations, we noted several advantages of V_2O_5 layer over PEDOT:PSS which include the ease of film preparation at room temperature, low production cost, high optical transmittance over a wide range of solar spectrum, and suitable energy level alignment for hole transport compared to PEDOT:PSS. Because of such attractive behavior of V_2O_5 the film preparation can be

scaled up for mass production of organic solar cell. The investigation need to be expanded into the deposition of the film on flexible substrate. Therefore, the V_2O_5 layer has promising potential to be used as hole transport layer to replace the PEDOT:PSS in the fabrication of OSC devices.

Acknowledgments

This work is partially supported by National Research Foundation (NRF)(Grant numbers 92786 and 85589), South Africa. The authors are also thankful to members of staffs at Microscopy and Microanalysis Unit (MMU) in the School of Life Sciences, UKZN.

Bibliography

[1] C.C. Chen , W.H. Chang , K. Yoshimura , K. Ohya , J. You ,J. Gao , Z. Hong , and Y. Yang, Adv.Mater. 26,(2014), 5670-5677.

[2] Y. Liu, J. Zhao, Z. Li, C. Mu, W. Ma, H. Hu, K. Jiang, H. Lin, H. Ade and H.Yan, Nature Commun.,4,(2014),6293.

[3] J. You, L. Dou, K. Yoshimura, T. Kato, K. Ohya, T. Moriarty, K. Emery, C.C. Chen, J. Gao, G. Li and Y. Yang, Nature Commun.,4,(2013), 1446-1455.

[4] L. Nian, W. Zhang, N. Zhu, L. Liu, Z. Xie, H. Wu, F.Wurthner,and Y. Ma, J. Am. Chem. Soc. 137,(2015), 6995-6998.

[5] J. You, C.C. Chen, Z. Hong, K. Yoshimura, K. Ohya, R. Xu,S. Ye, J. Gao, G. Li, and Y. Yang, Adv. Mater., 25, (2013), 3973-3978.

[6] N. Li and C. J. Brabeca, Energy Environ. Sci., 8, (2015), 2902–2909.

[7] M. Jørgensen, K. Norrman, S. A. Gevorgyan, T. Tromholt, B. Andreasen, and F. C. Krebs, Adv. Mater., 24,(2012), 580-612.

[8] J. Kesters, P. Verstappen, J. Raymakers, W. Vanormelingen, J. Drijkoningen, J. D. Haen, J. Manca, L. Lutsen, D. Vanderzande, and W. Maes, Chem. Mater., 27, (2015), 1332-1341.

[9] M.L. Jin, J. K. Choi, D. W. Kim, J.M. Park, C. J. An, H, J, Kim, B. J. Kim, Y. Diao, H.T. Jung, Organic Electronics, 15, (2014), 680-684.

[10] E A. Arbab, B. Taleatu and G. T. Mola, Journal of Modern Optics, 61(21), 2014), 1749-1753.

[11] M. Jørgensen, K. Norrman, F. C. Krebs, Solar Energy Materials and Solar Cells, 92, (2008), 686-714.

[12] K. Norrman, M. V. Madsen, S. A. Gevorgyan, and F. C. Krebs, J. Am. Chem. Soc., 132, (2010), 16883-16892.

[13] L. Lu, T. Xu, I. H. Jung, and L. Yu, J. Phys. Chem. C, 118, (2014), 22834-22839.

[14] S. P. Cho, J. S. Yeo, D. Y. Kim, S. Na, S. S. Kim, Solar Energy Materials and Solar Cells, 132, (2015),196-203.

[15] X. Bao, Q. Zhu, T. Wang, J. Guo, C. Yang, D. Yu, N. Wang, W. Chen, and R. Yang, ACS Appl. Mater. Interfaces, 7, (2015), 7613-7618.

[16] K. Zilberberg, J. Meyerb and T. Ried, J. Mater. Chem. C, 1, (2013), 4796-4815.

[17] C. Gong, H. B. Yang, Q. L. Song and C. M. Li, Organic Electronics, 13, (2012),7-12.

[18] I. Hancox, L. A. Rochford, D. Clare, M. Walker, J. J. Mudd, P. Sullivan, S. Schumann, C. F. McConville, and T. S. Jones, J.Phys.Chem.C., 117, (2013), 49-57.

[19] H.Q. Wang, N. Li, N. S. Guldal and C. J. Brabec, Organic Electronics 13 (2012) 3014-3021.

[20] T. Stubhan, T. Ameri, M. Salinas, J. Krantz, F. Machui and et al., Appl. Phys. Lett., 98, (2011), 253308.

[21] J. M. Yun , J. S. Yeo , J. Kim , H. G. Jeong , D. Y Kim , Y.J. Noh , S.S. Kim , B.C. Ku , and S.I. Na, Adv. Mater., 23, (2011), 4923-4928.

[22] Y. Kwon, Y. Kim , H. Lee, C. Lee, J. Kwak,Organic Electronics, 15, (2014) 1083-1087.

[23] J. Kettle, H. Waters, M. Horie and S. W. Chang,J. Phys. D: Appl. Phys., 45, (2012) 125102(7pp).

[24] W. K. Lin, S. H. Su, Y. F. Lin, J. R. Wang, J. L. Huang, and M. Yokoyama, International Conference on Solid State Devices and Materials, Nagoya, (2011), 751-752.

[25] S. J. Lee, H. p. Kim, A. R. M. Yusoff, and J. Jang, Sol. Energy Mater. Sol. Cells, 120, (2014), 238-243.

[26] G. T. Escobar, J. Pampel, J. M. Caicedo and M. L. Cantu, Energy Environ. Sci., 6, (2013),3088-3098.

[27] J. Wua, Y. Zhanga, P. Xua, W. Guoa, L. Shena and S. Ruan, Synthetic Metals, 170 (2013), 7-10.

[28] J. Meyer, S. Hamwi,, M. Kröger, W. Kowalsky, T. Riedl, and A. Kahn, Adv. Mater., 24, (2012), 5408-5427.

[29] B. A. Taleatu, E. A. A. Arbab, E. Omotoso, and G. T. Mola,Journal of Microscopy, 256, (2014),61-71.

[30] B. A. Taleatu, E. Omotoso, E. A. A. Arbab, R. A. Lasisi, W.O. Makinde and G. T. Mola, Appl. Phys. A, 118, (2015),539-545.

[31] B. A. Taleatu, E. A. A. Arbab, and G. T. Mola, Appl. Phys. A, 118, (2015),539-545.

[32] V. Shrotriya, G. Li, Y. Yao, C. W. CHu and Y. Y. Yang, Applied Physics Litters, 88, (2006),073508.

[33] E. A. A. Arbab, B. A. Taleatu, and G. T. Mola, Materials Science in Semiconductor Processing, 40, (2015),158-161.

[34] F. Ongul, Optical Materials, 50, (2015), 244-249.

[35] M. Abbasi, S.M. Rozati, R. Irani and S. Beke, Materials Science in Semiconductor Processing, 29, (2015), 132-138.

[36] J-K. Lee, G-P. Kim, I. K. Song and S-H. Baeck, Electrochemistry Communications, 11, (2009), 1571-1574.

Chapter 4

Growth and characterization of V_2O_5 thin film on conductive electrode

Journal of Microscopy

Journal of Microscopy, Vol. 00, Issue 0 2016, pp. 1–8 doi: 10.1111/jmi.12490
Received 10 June 2016; accepted 7 September 2016

Growth and characterization of V_2O_5 thin film on conductive electrode

GENENE T. MOLA*, ELHADI A. A. ARBAB*, BIDINI A. TALEATU*,†, K. KAVIYARASU‡,§, ISHAQ AHMAD‖ & M. MAAZA‡,§

*School of Chemistry & Physics, University of KwaZulu-Natal, Pietermaritzburg Campus, Private Bag X01, Scottsville, 3209, South Africa

†Department of Physics & Engineering Physics, Obafemi Awolowo University, Ile-Ife, Nigeria

‡UNESCO-UNISA Africa Chair in Nanosciences/Nanotechnology Laboratories, College of Graduate Studies, University of South Africa (UNISA), Muckleneuk Ridge, PO Box 392, Pretoria, South Africa

§Nanosciences African network (NANOAFNET), Materials Research Group (MRG), iThemba LABS-National Research Foundation (NRF), 1 Old Faure Road, 7129, PO Box 722, Somerset West, Western, Cape Province, South Africa

‖National Center for Physics, Quaid-i-Azam University, Islamabad, 44000, Pakistan

4.1 Abstract

Vanadium pentoxide (V_2O_5) thin films were grown at room temperature on ITO coated glass substrates by electrochemical deposition. The resulting films were annealed at 300°C, 400°C and 500°C for 1h in ambient environment. The effect of heat treatment on the films properties such as surface morphology, crystal structure, optical absorption and photoluminescence were investigated. The X-ray diffraction study showed that the films are well crystallized with temperatures. Strong reflection from plane (400) indicated the film's preferred growth orientation. The V_2O_5 films are found to be highly transparent across the visible spectrum and the measured photoluminescence quenching suggested the film's potential application in OPV device fabrication.

Keywords: V_2O_5 **thin films; electrochemical deposition; optical band gap; PL**

4.2 Introduction

Solution processing of the functional buffer layer is desired for large scale and high throughput production of organic photovoltaics (OPVs). The effectiveness of photo-generated charges collection in OPV is largely depend on the properties of the interface between the photoactive layer and electrodes because of the built-in potential across the region (Lee et al., 2014). As much as the built in potentials are useful for the functioning of OPV devices, in some cases, it is counter productive to charge transport process across the interface because of the insurmountable barrier heights. It became customary to introduce a thin layer of suitable materials often called buffer layers in an effort to lessen the barrier caused by built in potential across electrode/active layer interfaces as well as to improve devices stability (Zhao et

al., 2010; Sun et al., 2011; Lim et al., 2012; Tan et al., 2012; Voroshazi et al., 2011; Litzov & Brabec, 2013; Bao et al.,2015;Liu et al.,2016). The generation of free charges in bulk-heterojunction design of organic photovoltaics begins with the absorption of a photon via active layer which excite an electron from HOMO to LUMO level of donor molecule and create a quasi particle called exciton. The resulting exciton diffuse towards an interfacial region between the donor and the acceptor molecules. The formed exciton is then dissociated at the interface to create a free charge carriers which can be transported to the opposite electrodes (Lee et al., 2014). Hence, the performance of OPV devices heavily dependent on the efficiency of charge extraction from the photo-active medium by reducing lose of the free charge carriers (Bao et al., 2015). The most common buffer layer that facilitate hole-extraction in OPV is Poly (3, 4-ethylene dioxythiophene): poly (styrene sulfonate) (PEDOT:PSS). However, the acidic and hygroscopic nature of PEDOT:PSS can cause etching to indium tin oxide (ITO) film from the substrate which eventually degrade the photoactive film and contributing to poor device stability (Escobar et al., 2013; Lee et al., 2014; Bao et al., 2015; Cho et al., 2015). The transition metal oxides (TMOs) thin films have a significant role to play in manufacturing of OPV devices as buffer layers owing to their suitable characteristics such as optical and electrical properties as well as energy band gap and high work function (Lee et al., 2014, Escobar et al., 2013, Wu et al., 2013, Arbab & Mola, 2016). Among these oxides, vanadium pentoxide has drawn significant interest in the past decades due to their various application potentials in the area of electrochromics, microelectronic, gas sensing, optical switching, and optoelectronic devices. It can also be used as cathode materials in Li batteries (Lee et al., 2009; Meyer et al., 2012).

A solution processed V_2O_5 layer have been recently employed as buffer layer to improve the efficiency and stability of OPVs (Arbab & Mola, 2016). Vanadium pentoxide is one of the most promising buffer layer material because of its non-toxicity and stability in ambient

environment. Other properties such as high optical transmittance in the visible light region, lowering energy barrier at the interface of ITO/photoactive layer and high level of technological compatibility in organic electronics as well as the ease of processing at low temperature make it suitable in the area of nanotechnology (Escobar et al., 2013; Bao et al., 2015). Many deposition methods have been reported for the synthesis and growth of V_2O_5 thin films. Some of these are electron beam evaporation, magnetron sputtering, pulsed laser deposition, chemical vapor deposition, spray pyrolysis, thermal evaporation, sol-gel, and spin coating (Bouzidi et al., 2002; Ramana et al., 2005; Escobare et al., 2013; Wu et al., 2013; Abbasi et al., 2015). Among these techniques, electrochemical deposition offers numerous advantages such as simplicity, low processing costs, low temperature growth, environmental friendliness, non-toxicity and the ease of control of the microstructure, surface morphology and homogeneity of the deposited oxide films via simple adjustment of deposition parameters (Lee et al., 2009; Taleatu et al., 2011; Vernardou et al., 2013). Several authors have prepared V_2O_5 thin films by electrochemical deposition predominantly for electrochromics, microelectronics, gas sensing, optical switching and as cathode materials in Li batteries applications (Lee et al., 2009; Vernardou et al., 2013). Little has been reported on the application V_2O_5 as a buffer layer in OPV. In this article solution processed V_2O_5 film deposition is presented and discussed in terms of results obtained from several spectroscopic measurements.

4.3 Experimental Details

4.3.1 Substrate Cleaning

ITO coated glass with surface resistance ($15\Omega sq^{-1}$) were purchased from (Ossila Ltd.,Sheffield, UK) and used as received in the deposition of vanadium pentoxide layers. Prior to the deposition, the ITO substrates were thoroughly washed with detergent followed by successive cleaning in ultrasonic bath containing acetone and isopropanol (IPA) for 15 minutes each. The cleaned substrates were then dried in an open furnace at a temperature of 150°C for 30 minutes in order to remove the water contents in the film.

4.3.2 Materials and method

In electrodeposition, the applied electric field is generally driving factor for the growth of electrically conductive materials such as metals, semiconductors and polymers on conductive substrates from electrolyte solution. The reactions occur through the electrolytes and solid deposits (films) are formed on the working electrode. In this study, a two-electrode electrochemical cell was used for the growth of vanadium oxide thin films (Taleatu et al., 2011; Taleatu et al., 2015). The cell allows flexibility in the choice of both counter and working electrodes compared to the common three-electrode type. In preparing the solution electrolyte, 0.585 g of cream powder ammonium meta vanadate (NH_4VO_3) (99.7%, Sigma Aldrich) was dissolved in 100 ml of DI water under continuous stirring at 70°C overnight to yield a concentration of 0.05 M. The pH of the solution was adjusted to 9.2 at 20°C using NaOH (1.0 M). The resulting transparent yellow solution was kept at room temperature for 5 days to ensure stability. Stability of precursor enhances film crystallization and dura-

bility. During deposition, graphite piece and ITO-coated glass substrate were used as the counter (anode) and working electrodes (cathode), respectively. The growth was carried out potentio-statically at 2.5 volt for 5 min. After deposition, the resulting films were rinsed in DI water and then dried immediately in open furnace at 150°C for 30 minutes to remove residual water content and impurities. The samples were then annealed in air at 300°C, 400°C and 500°C for 1 hour, separately.

The characterization of the films were carried out using several spectroscopic methods such as surface morphology of the films was investigated by Zeiss EVO LS 15 ultra plus Field Emission Scanning Electron Microscopy (FESEM) fitted with Oxford Energy Dispersive Analysis of X-ray detector (EDAX). Crystal structure of the films was studied using x-ray diffractometer with Cu Kα radiation ($\lambda = 0.15406nm$). Optical absorption across ultraviolet/visible spectra region was studied using a double beam UV/VIS spectrophotometer.

4.4 Results and Discussion:

4.4.1 X-ray diffraction study

Figure 4.1 shows the XRD patterns of the electro-deposited V_2O_5 thin films after annealing at various temperatures. Diffraction peaks at 2θ= 21.4°, 30.4°, 38.2° and 45.6° correspond respectively to reflections from planes (101), (400), (211) and (002) indicating the formation of orthorhombic crystal structure of V_2O_5 (Wu et al., 2013). Other peaks are due to the ITO coated glass substrate. In all XRD spectra, it is evident that the peaks are enhanced with annealing temperature as sign of improvement in the crystallinity of the films. At 500°C, two new peaks at 2θ = 18.7° and 20.5° are apparent corresponding to planes (200) and

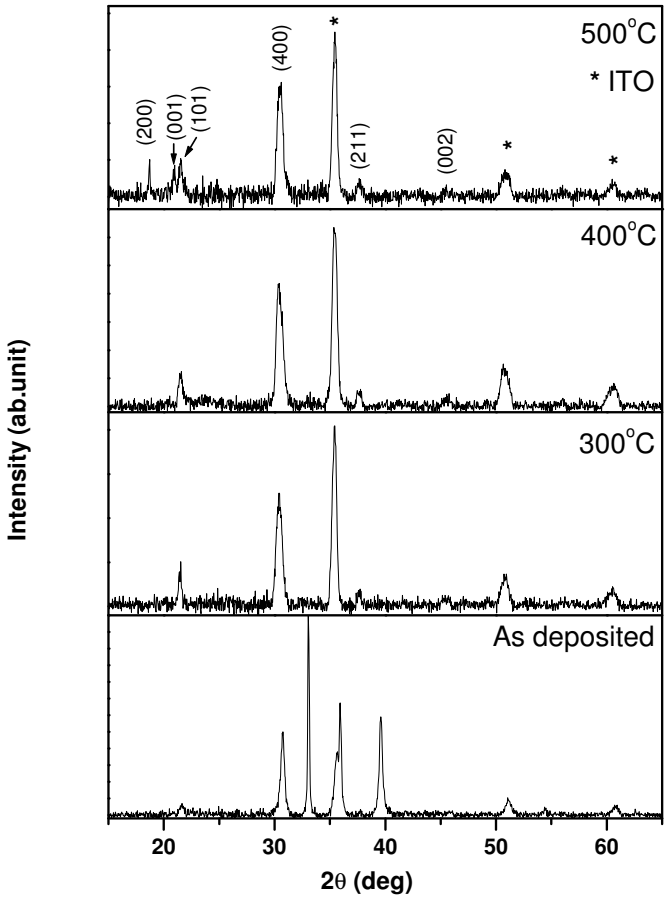

Figure 4.1: XRD patterns of electro deposited V_2O_5 thin films. The films were annealed in air at (300-500)°C for 1h.

(001) associated with different structures. However, there is no obvious difference in peaks pattern of the samples annealed at 300°C and 400°C, respectively. These new peaks could be attributed to the structure of the elements beneath V_2O_5 layer. As-deposited sample was decorated with two other prominent peaks at $2\theta = 33.8°$ and 39.6° which are associated with adsorbed impurity residing on the surface of the sample. The peaks eventually disappear from the spectrum at higher annealing temperatures. The crystallite grain size (D) of the

films were estimated using Scherrer's formula stated in Eq. 4.1:

$$D = \frac{0.94\lambda}{\beta cos\theta} \tag{4.1}$$

Where λ is wavelength of x-ray beam, β is full width at half maximum (FWHM) of the most intense peak and θ is Bragg's reflection angle. From Table 4.1, it can be seen that the estimated crystallite size increased with annealing temperature. This implies that the film became more crystalline as a result of post-deposition heat treatment. This is in agreement with the report by Ramana et al. 2005 who have reported that V_2O_5 film was completely amorphous as deposited and later found well defined nano-crystal structures after annealing the samples with 200°C and 500°C. According to their results, film's grain size increased from 50 to 300 nm with annealing. In this investigation, crystallite size estimated with respect to peak width broadening using Eq. (1) increased from the As-grown film to the one annealed at 500°C (see Table 4.1). A closer look at diffraction angles of the prominent peaks show that there is a shift from 30.76° to 30.41° when the samples were annealed at 300°C and 400°C, respectively. This is a clear indication of enhanced crystallite size.

Table 4.1: Crystallite sizes of electrodeposited V_2O_5 thin films.

Annealing temperature (^oC)	2θ (deg)	FWHM (hkl) index (400)(deg)	Crystallite size D (nm)
As-deposited	30.76	0.688	11.98
300	30.14	0.621	13.25
400	30.41	0.519	15.88
500	30.48	0.427	19.28

4.4.2 Raman spectral analysis

In view of the fact that Raman spectroscopy has a higher sensitivity than XRD for thin film-substrate characterization, we have used it to study the crystal phase of V_2O_5 thin film. The Raman spectra of the pure V_2O_5 thin film in the 300–4500 cm^{-1} region were recorded by Ocean optics, high-performance Raman microscope spectrometer, using a 532.2 nm diode laser. The spectra revealed distinct peaks at different temperature (Fig. 2). Two peaks located at 302 cm^{-1} (Bg) and 479 cm^{-1} (Ag) are assigned to the bending vibration of the V=O bonds. Peaks at 599 and 650 cm^{-1} can be attributed to the doubly coordinated oxygen (V2-O) stretching mode, whereas terminal oxygen (V=O) stretching mode has become evident. Thus, the Raman scattering profiles gave further evidence that V_2O_5 phase is the major crystalline structure in all three targets. In this connection, morphological structure of the V_2O_5 thin film were related to calcinated temperature at 300°C, 400°C and 450°C, which revealed V_2O_5 phase as confirmed by XRD pattern. It can be observed that the intensity of Raman signals increased with higher annealing temperature (450°C) and it is favourable for Raman efficiency. The first sharp primary peak appears at 302 cm^{-1} but does not exist in pure ITO film. When V_2O_5 was added, D band (650 cm^{-1}), G band (1204 cm^{-1}) and 2D band (1863 cm^{-1}) appeared in the Raman spectra. The area under the Raman peak changed with the vanadium percentage and increased with higher concentration, probably due to vanadium-induced surface roughness to identify the AFM and PL images. According the peaks at 1187 cm^{-1} and 1341 cm^{-1}1 are assigned to the V-O stretching mode of tetrahedral and indistinct sharp peak, respectively. Although the broad band at 650 cm^{-1} is due to the V-O-V stretching mode. Bands below 479 cm^{-1} are from the bending modes of V-O. Vibrational mode of the molecule causes the Raman shift and gives useful information about the structure in the form of different type of lattice vibrations. The analysis of Raman

structure and optical properties of the thin films has revealed the influence of deposition parameters on the properties of vanadium oxides which revealed that As-deposited films were amorphous, whereas annealed films had V_2O_5 crystal form.

4.4.3 Surface morphology

Figure 4.3 shows microstructure of the V_2O_5 films obtained by FESEM. All the images were taken at the same magnification. The impact of annealing temperature on surface distribution and grain structure was evaluated under ambient environmental condition. The FESEM images in Figure 4.3 revealed uniform distribution of V_2O_5 particles and formation of polycrystals by grain agglomeration. The substrates surfaces are completely covered by the films particles as depicted in Figure 4.3(a). When the samples were annealed at higher temperature a clear indication of the formation of both small-sized grains and the agglomerates (polycrystals) emerged (Fig. 4.3b). Although large grain size nano-particles are formed at 300°C the crystallization process was not complete. However, at 400°C annealing temperature the film becomes more clearer and almost all film particles were incorporated in some grain boundaries (Fig. 4.3c). The surface morphology in Figure 4.3(c) showed that the deposited film is highly crystalline and particle shapes are distinct. Such transition into crystal structure confirms the prediction made by computer simulation on structural properties and phase stability of complex fluids as a function of the deposition parameters (Abramoet al.,2010; Abramoet al.,2011; Pellicane & Pandaram, 2014). Raj et al. (2013) indicated that larger film particles can be formed with annealing temperature, as confirmed by XRD measurements as well, which provides sufficient thermal energy to activate crystallization. At 500°C, however the crystal grain boundaries become blurred again (see Fig. 4.3(d)) indicating the dissolution of the crystal. It therefore possible to suggest that the optimum annealing

temperature for best crystal quality of V_2O_5 films is (400-450) °C. At a temperature above the recommended range could cause substantial lose of oxygen concentration as well as some important constituents from the film and hence deteriorating the crystal structure. In fact, high temperature promotes rapid diffusion of V_2O_5 into the substrate layers which can alter the properties of the transparent electrode. Furhtermore, the observed 'new' two peaks, in a sample annealed at 500°C in XRD studies, can be attributed to some emerging substrate structures beneath V_2O_5 layer. Elemental composition analysis of the films using EDAX in all the samples confirmed the presence of substantial amount of vanadium and oxygen on the deposited films. No other impurity contaminations were found on the films according to EDAX analysis.

4.4.4 Optical Properties

Optical properties of V_2O_5 films were studied using UV-Vis optical absorption and transmission measurement provided in Figure 4.4. According to the transmission data given in Figure 4.4 the film is almost transparent to the visible and infrared region where the intensity of solar radiation is high. All films produced transmitted above 85% of the visible spectrum (Fig. 4.4). Maximum transmittance of about 90% was recorded in the region of λ= 500 - 750 nm in samples annealed at over 400°C. This suggests that film transmission can be enhanced with annealing temperature which reduces the stress and density associated with defects in the deposited films (Meyer et al., 2012; Wu et al., 2013. The complete absorption in the UV region is due to the glass substrate. The optical energy band gap (E_{opt}) of the films was calculated using the relation below (Cho et al., 2015).

$$\alpha h\nu = A(h\nu - E_{opt})^n \tag{4.2}$$

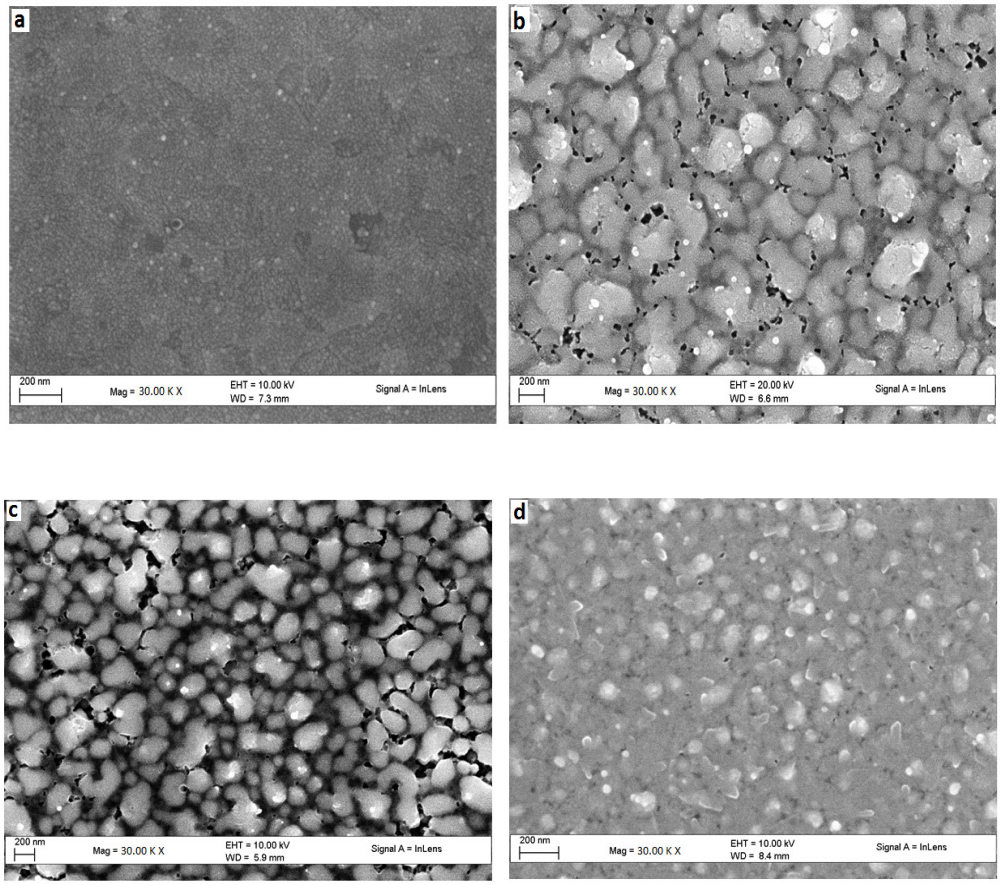

Figure 4.2: Surface morphology of the V_2O_5 films (a) As deposited, and annealed at (b) 300^oC (c) 400^oC (d) 500^oC.

where α is absorption coefficient, hν is the photon energy, A is the absorption constant, relying on the charge carriers mobility and n is related to the lowest allowed electronic transition which is 0.5 and 2 for direct and indirect band transition, respectively. Optical absorption coefficient (α) can be determined using the relation below assuming film's reflectance is very negligible (Meyer et al., 2012; Cho et al., 2015).

$$\ln T = -\alpha t \tag{4.3}$$

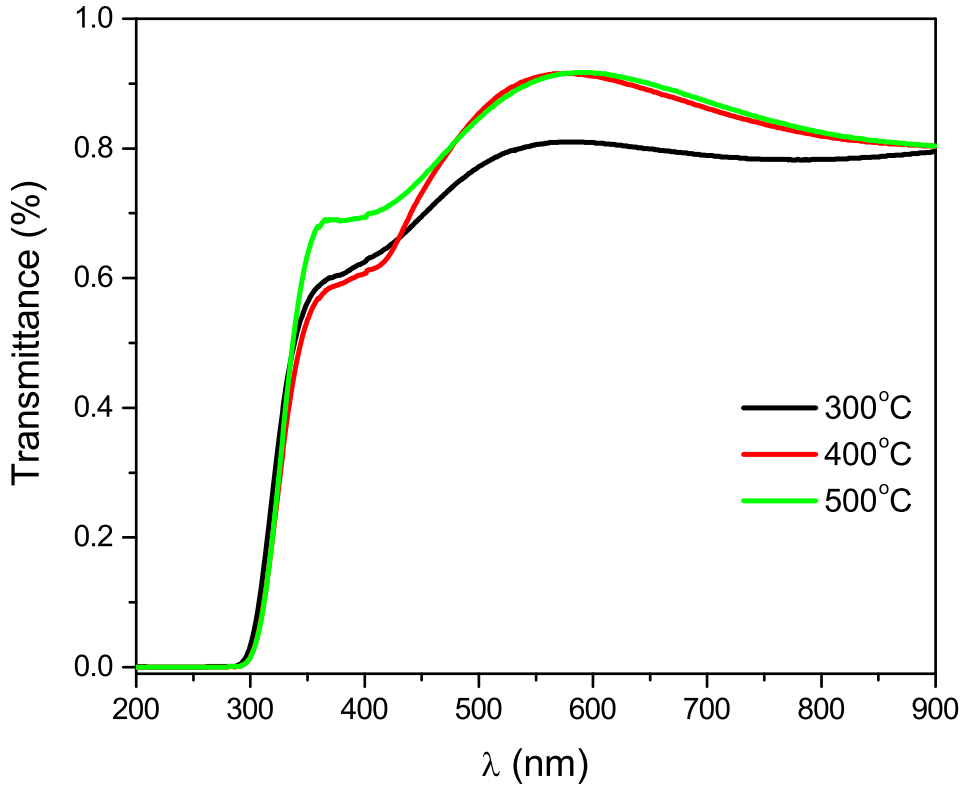

Figure 4.3: Optical spectra of V_2O_5 thin films after annealing at various temperatures (A) absorbance and (B) transmittance.

where T is optical transmittance and t is thickness of the film. E_{opt} is determined by extrapolating linear region of the Tauc's plot to energy axis where $(\alpha h\nu)^2 = 0$. All the films have direct allowed energy transition. Estimated values of E_{opt} are 2.44, 2.62 and 2.47 eV for the films annealed at 300°C, 400°C and 500°C, respectively (Fig. 4.5). These values are in agreement with some previous reports (Escobar et al., 2013; Cho et al., 2015).

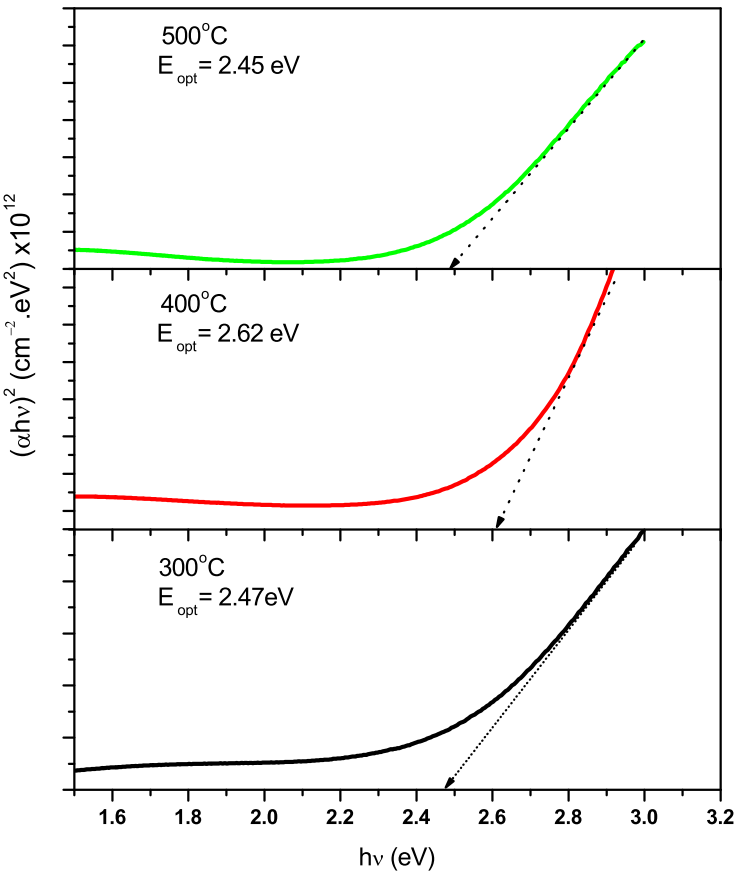

Figure 4.4: Tauc's plots showing energy band gaps of the V_2O_5 films annealed at different temperatures.

4.4.5 Photoluminescence (PL)

Photoluminescent emission has been widely used to investigate photon-induced charge transfer processes in semiconductors. It also provides information about the content of impurity-related defects on the surface of thin films semiconductor. The V_2O_5 nanorods film was reported to have strong PL emission on the visible region, which was attributed to the existence of oxygen-related defects (Yin Hu et al., 2009). We have conducted photoluminescence measurement on the samples using 290 nm laser-induced excitation and found strong

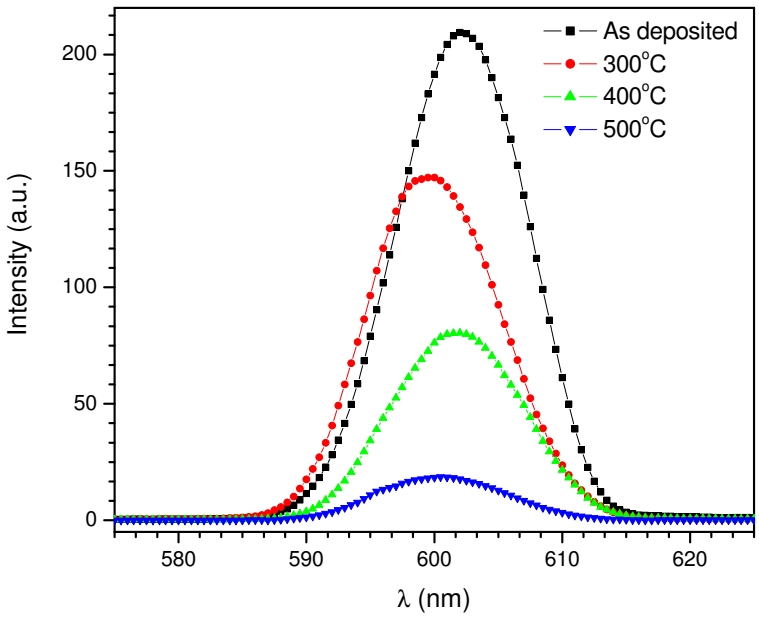

Figure 4.5: Photoluminescence spectra of V_2O_5 films deposited and annealed at different temperature.

PL emission in the visible region ranging from 580 to 620 nm (Fig. 4.6). Maximum peaks were exhibited at $\lambda = 602$ nm for As-deposited and samples annealed at 400°C whereas for those samples annealed at 300°C and 500°C the peak maxima were shifted at 600 nm and 601 nm, respectively. The intensities of the photoluminescence significantly decreases with temperature due to increasing crystal size of the V_2O_5 nanoparticle which reduces the formation and concentration of surface oxygen vacancies and defects. Moreover, according to RBS result discussed in the next section found that substantial amount of V_2O_5 diffused into indium tin oxide layer and hence the quenching of the PL spectra could be attributed to the efficient charge dissociation processes in the medium that reduces the PL intensities. Inspite of oxygen deficiency observed using SEM images on the surface of 500°C annealed sample the observed low PL intensities could be attributed to low concentration of defects on the surface and effective separation of photon-induced charges.

4.4.6 Rutherford Back Scattering (RBS)

Rutherford Backscattering spectrometry (RBS) was employed to study the thickness and elemental concentration with depth of V_2O_5 thin films using well-collimated beams of 2 MeV $He2^+$ with 14 nA beam current with surface barrier detector at 1700 using 5MV Tandem Pelletron Accelerator at National Centre for Physics. XRUMP and SIMNRA software were used to analyze the data. The RBS spectra given in Figure 4.7 clearly shows the RBS

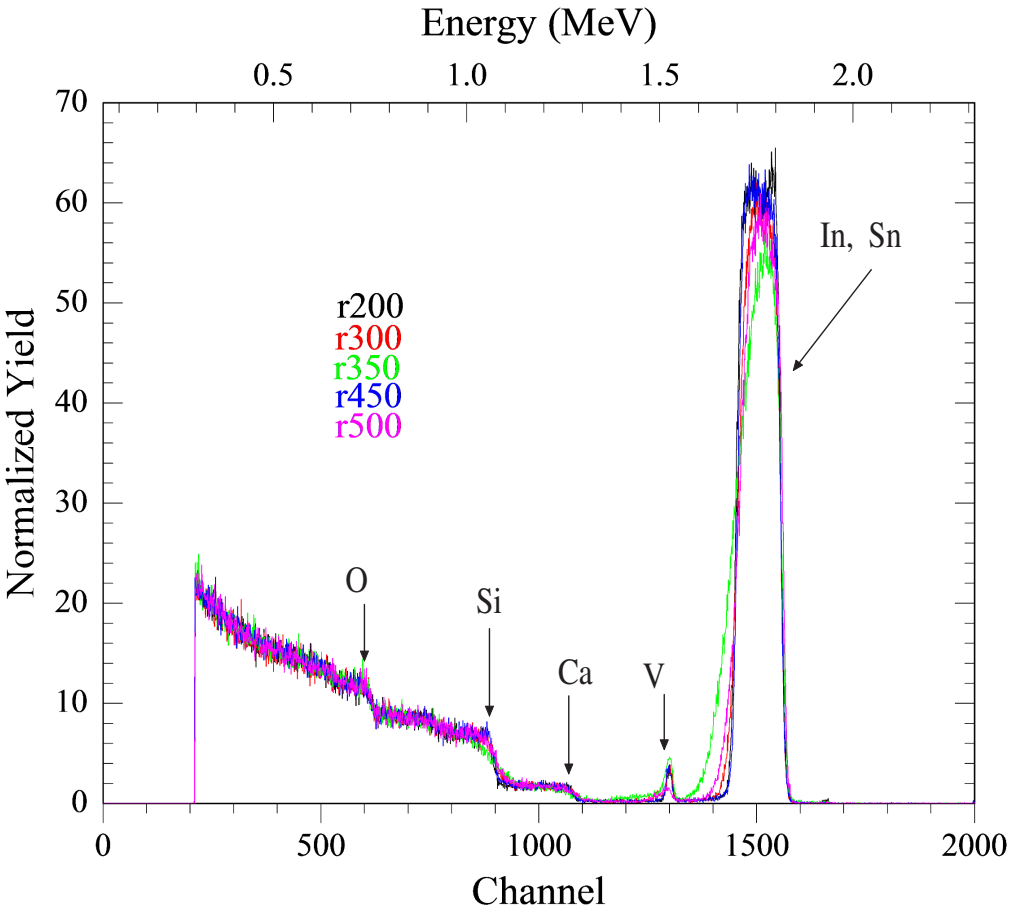

Figure 4.6: RBS spectra of V_2O_5 films annealed at different temperature.

spectra of V_2O_5 thin films on ITO. Concentrations of vanadium at different depths of the V_2O_5 thin films were analyze using XRUMP and SIMNRA software. The Low energy tail (Fig. 4.7) indicated by arrows (diffusion of V) demonstrated that V_2O_5 molecule diffused

into ITO. This implied that V_2O_5 molecules were able to diffuse into the ITO matrix either during deposition or/and thermal annealing process of the samples. According to the RBS spectra, we found a very thin layer V_2O_5 thin film with an average thickness of 6 nm in almost all samples above the indium tin oxide layer. However, as we go into ITO depth profile the concentration of vanadium monotonically decreases with depth in all the samples. For example, in a sample annealed at 350°C after deposition, the concentration of vanadium were found to be 32%, 2.4% 1.9% and 1.3% corresponding to the layers 6.4 nm beneath the surface, then goes to 18 nm depth, 25 nm depth and another 25 nm, respectively. The depth profile analysis of the RBS experiment clearly showed that significant amount V_2O_5 molecules were infiltrated into the ITO layer which definitely alter the optical and electrical properties of the medium. The concentration of V_2O_5 molecules generally decreases from indium tin oxide with sample annealing temperature.

4.5 Conclusions

Solution processed vanadium pentoxide (V_2O_5) thin films has been successfully produced by electrochemical deposition at room temperature. Crystal orientation and surface morphology revealed that the deposited layers have orthorhombic structure and are crystalline, their grains are evenly distributed across substrates surface. Optical absorption measurements indicated that the film has a direct energy band gap structure whose band gap is (2.45 $\pm$ 0.02) nm is transparent enough for the transmission of visible and infrared regions of the solar spectrum. Effective charge separation and reduced recombination rate of excitons can make the films suitable for hole transport buffer layer in OPV devices. According to current investigations the quality of the film and the size of the crystal grain size is dependent on post-

deposition temperatures. According to our investigation, optimum annealing temperature for the high-quality of the film is (400-450)°C.

Acknowledgments

This work is supported by National Research Foundation (NRF), South Africa. Grant numbers: 93562, 92786 and 85589. The authors are also thankful to members of staff of Microscopy and Microanalysis Unit (MMU) at School of Life Sciences, , UKZN, South Africa.

Bibliography

Abbasi, M., Rozati, S.M., Irani, R. & Beke, S. (2015) Synthesis and gas sensing behavior of nanostructured V_2O_5 thin films prepared by spray pyrolysis. Materials Science in Semiconductor Processing **29**, 132–138.

Abramo, M.C., Caccamo, C., Calvo, M., et al. (2011) Molecular dynamics and small-angle neutron scattering of lysozyme aqueous solutions. Philos. Mag. **91**, 2066–2076.

Abramo, M.C., Caccamo, C., Costa, D., Pellicane, G. & Ruberto, R. (2010) Molecular Dynamics of an Embedded-Charge Model of Lysozyme Aqueous Solutions. J. Phys. Chem. B **114**, 9109–9118.

Arbab, E.A.A. & Mola, G.T. (2016) V_2O_5 thin film deposition for application in organic solar cells. Appl. Phys. A: Material Science & Processing, 122:405, DOI: 10.1007/s00339-016-9966-1.

Bao, X., Zhu, Q., Wang, T., et al. (2015) Simple O_2 plasma processed V_2O_5 as anode buffer layer for high-performance polymer solar cells. ACS Appl. Mater. Interfaces, **7**, 7613–7618. **Bouzidi, A., Benramdane, N.,Nakrela, A., Mathieu, C., Khelifa, B., Desfeux, R. & Da Costa, A.** (2002) First synthesis of vanadium oxide thin films by spray pyrolysis technique. Materials Science and Engineering B **95**, 141–147.

Cho, S.P., Yeo, J.S., Kim, D.Y., Na, S. & Kim, S.S. (2015) Brush painted V_2O_5 hole transport layer for efficient and air-stable polymer solar cells. Solar Energy Materials and Solar Cells, **132**, 196–203.

Escobar, G.T., Pampel, J., Caicedo, J.M. & Cantu, M.L. (2013) Low-temperature, solution-processed, layered V_2O_5 hydrate as the hole-transport layer for stable organic solar cells. Energy Environ. Sci., **6**, 3088–3098.

Hu, Y., Li, Z., Zhang, Z. & Meng, D. (2009) Effect of magnetic field on the visible light emission of V_2O_5 nanorods. Appl. Phys. Lett., **94**, 103107-1–103107-3.

Lee, S.J., Kim, H.P., Yusoff, A.R.M. & Jang, J. (2014) Organic photovoltaic with PEDOT:PSS and V_2O_5 mixture as hole transport layer. Sol. Energy Mater. Sol. Cells **120**, 238–243.

Lee, J-K., Kim, G-P., Song, I. K & Baeck, S-H. (2009) Electrodeposition of mesoporous V_2O_5 with enhanced lithium-ion intercalation property. Electrochemistry Communications, **11**, 1571–1574.

Lim, F.J., Ananthanarayanan, K., Luther, J. & Ho, G.W. (2012) Influence of a novel fluorosurfactant modified PEDOT:PSS hole transport layer on the performance of inverted organic solar cells. J. Mater. Chem. **22**, 25057–25064.

Litzov, I. & Brabec, C.J. (2013) Development of Efficient and Stable Inverted Bulk Heterojunction (BHJ) Solar Cells Using Different Metal Oxide Interfaces. Materials **6** (12), 5796–5820.

Liu, Y., Zhang,W., Zou, Y., Xie, G., Fang, J. & Yang, C. (2016) Improved performance of inverted polymer solar cells by utilizing alcohol-soluble oligofluorenes as efficient cathode interlayers. Organic Electronics **30**, 182–190.

Meyer, J., Hamwi, S., Krger, M., Kowalsky, W., Riedl, T. & Kahn, A. (2012) Transition Metal Oxides for Organic Electronics: Energetics, Device Physics

and Applications. Adv. Mater., **24**, 5408–5427.

Ramana, C.V., Smith, R.S., Hussain, O.M, Chusuei, C.C & Julien, C.M. (2005) Correlation between Growth Conditions, Microstructure, and Optical Properties in Pulsed-Laser-Deposited V_2O_5 Thin Films. J. Chem. Mater. **17**, 1213–1219.

Pellicane, G. & Pandaram, O.D. (2014) Gibbs ensemble Monte Carlo of nonadditive hard-sphere mixtures. J. Chem. Phys. **141**, 044508-1–044508-13. **Raj, D.V., Ponpandian, N., Mangalaraj, D. & Viswanathan, C**. (2013) Effect of annealing and electrochemical properties of sol–gel dip coated nanocrystalline V_2O_5 thin films. J. Mater. Sc. & Semiconductor Processing, **16** (2), 256–262.

Sun, Y., Seo, J.H., Takacs, J. Seifter, J. & Heeger, A. J. (2011) Inverted Polymer Solar Cells Integrated with a Low-Temperature-Annealed Sol-Gel-Derived ZnO Film as an Electron Transport Layer. Adv. Mater. **23**, 1679–1683.

Taleatu, B.A., Fasasi, A.Y., Di Santo, G., et al. (2011) Electro-chemical deposition of zinc oxide nanostructures by using two electrodes. AIP Advances **1**, 032147-1–032147-10.

Taleatu, B.A., Arbab, E.A.A. & Mola, G.T. (2015) Stable α-MnS thin film deposited by two-electrode cell: synthesis, structural characterization and photoemission spectroscopic studies. Appl. Phys. A **120** (3), 959– 965.

Tan, Z., Zhang, W., Zhang, Z., Qian, D., Huang, Y., Hou, J., Li, Y. (2012) High-Performance Inverted Polymer Solar Cells with Solution- Processed Titanium Chelate as Electron-Collecting Layer on ITO Electrode. Adv. Mater. **24**, 1476–1481. Wu, J., Zhang, Y., Xua, P., Guoa, W., Shena, L. & Ruan, S. (2013) Role of solution-processed V_2O_5 in P3HT:PCBM based inverted polymer solar cells. SyntheticMetals, **170**, 7–10.

Voroshazi, E., Verreet, B., Aernouts, T., & Heremans, P. (2011) Long-term

operational lifetime and degradation analysis of P3HT:PCBM photovoltaic cells. Sol. Energy Mater. Sol. Cells, **95** (5), 1303–1307.

Vernardou, D., Sapountzis, A., Spanakis, E., Kenanakis, G., Koudoumas, E. & Katsarakis, N. (2013) Electrochemical Activity of Electrodeposited V_2O_5 Coatings. Journal of Electrochemical Society **160** (1), D6–D9.

Zhao, D.W., Tan, S.T., Ke, L., et al. (2010) Optimization of an inverted organic solar cell. Sol. Energy Mater. Sol. Cells **94**, 985–991.

Chapter 5

SYNTHESIS AND SOME SURFACE STUDIES OF LAMINATED ZnO/TiO_2

TRANSPARENT BILAYER BY TWO-STEP GROWTH

Materials Science in Semiconductor Processing 44 (2016) 85–90

Contents lists available at ScienceDirect

Materials Science in Semiconductor Processing

journal homepage: www.elsevier.com/locate/mssp

Synthesis and some surface studies of laminated ZnO/TiO_2 transparent bilayer by two-step growth

Bidini A. Taleatu [a,b,*], Elhadi A.A. Arbab [a], Genene T. Mola [a]

[a] School of Chemistry and Physics, University of KwaZulu-Natal, P Bag X01 Scottsville, 3209 Pietermaritzburg, South Africa
[b] Department of Physics and Engineering Physics, Obafemi Awolowo University, Ile-Ife, Nigeria

ARTICLE INFO

Article history:
Received 28 August 2015
Received in revised form
25 November 2015
Accepted 26 December 2015

Keywords:
Bilayer
Electrodeposition
Diffraction
Transparent
Morphology
Energy band gap

ABSTRACT

A laminated bilayer was prepared by first depositing titanium dioxide (TiO_2) nanocrystals on indium tin oxide (ITO) coated glass by a two-electrode cell. Zinc oxide (ZnO) thin film was thereafter deposited on the TiO_2 by two different techniques: electrochemical deposition and vacuum evaporation. The films were characterized by some surface probing techniques. Morphological study revealed that particle size of the TiO_2 underlayer increases between 110 and 138 nm with increase in deposition voltage. It also showed that ZnO thin film (overlayer) completely covered the underlying TiO_2 without chemical interaction between constituents of both layers. Cross-sectional FESEM study gave values of layered film thickness below 55 μm. Exhibition of strong diffraction peak at plane (121) indicated preference of TiO_2 film's growth orientation. It also suggested a feature of phase-pure brookite. Optical studies showed that each film exhibited strong absorption edge at $\lambda = \sim 330$ nm and transmitted fairly across visible light region. Energy band gap lied between 3.24 and 3.43 eV. This study demonstrated successive layer deposition of transparent metal oxide structures from inorganic reagents. It also reaffirmed TiO_2 as a recipe for barrier layer that can hinder transition of holes from absorber to transparent front contact of nanostructured photonic devices.

5.1 Abstract

A laminated bilayer was prepared by first depositing titanium dioxide (TiO_2) nanocrystals on indium tin oxide (ITO) coated glass by a two-electrode cell. Zinc oxide (ZnO) thin film was thereafter deposited on the TiO_2 by two different techniques: electrochemical deposition and vacuum evaporation. The films were characterized by some surface probing techniques. Morphological study revealed that particle size of the TiO_2 underlayer increases between 110 and 138 nm with increase in deposition voltage. It also showed that ZnO thin film (overlayer) completely covered the underlying TiO_2 without chemical interaction between constituents of both layers. Cross-sectional FESEM study gave values of layered film thickness below 55 μm. Exhibition of strong diffraction peak at plane (121) indicated preference of TiO_2 film's growth orientation. It also suggested a feature of phase-pure brookite. Optical studies showed that each film exhibited strong absorption edge at $\lambda =$ 330 nm and transmitted fairly across visible light region. Energy band gap lied between 3.24 and 3.43 eV. This study demonstrated successive layer deposition of transparent metal oxide structures from inorganic reagents. It also reaffirmed TiO_2 as a recipe for barrier layer that can hinder transition of holes from absorber to transparent front contact of nanostructured photonic devices.

Keywords: bilayer, electrodeposition, diffraction, transparent, morphology, energy band gap

5.2 Introduction

Transition metal oxide interfacial layers are robust films with outstanding optoelectronic properties suitable for fabrication of efficient energy conversion and semiconductor devices.

Critical components in photovoltaic system are charge selective interfaces that enable pathway through photoactive layer to a metallic contact electrode (external circuit) [1]. Nanostructured configuration of most photovoltaic devices comprises a three-component porous heterojunction described as n-a-p "n" means n-type, "a" means absorber and p" means p-type). The base layer is usually a porous film made of transparent n-type semiconductor onto which a thin layer of inorganic absorber is deposited. Photons are absorbed by the absorber layer and electron/hole pairs are generated, the generated charges are injected into the two separate transparent phases (n and p-type) to minimize chances of charge recombination [2]. Since coating of absorber layer is applied on front side where light enters the cell, materials with high refractive index ($n \geqslant 2.3$) are desirable for good anti-reflection properties [3]. ZnO and TiO_2 are some of such promising candidates. For multilayer nanostructures, thin films of ZnO and TiO_2 are suitable partners because of their comparable functional properties such as wide band gap, good optical transmittance, high refractive index, work function, grain size and distribution, porosity or crystallinity, texture and high stability [4, 5]. Growth of thin ZnO layer over a porous TiO_2 electrode can aid surface charge mobility required for development of efficient high-powered solar cells, energy storage and optical devices [5]. According to Nakade et al., 2003 [6], some surface characteristics of nanoporous TiO_2 such as trap sites distribution and density can largely influence electron recombination lifetime in dye-sensitized solar cell. TiO_2 could also serve as buffer layer to limit lattice and thermal mismatches between ZnO and substrate materials [5]. For effective soft x-ray reflectivity, potential use of ZnO/TiO_2 mirror structure at "water-window" wavelength in multilayer optics has been indicated [7]. In this work, the authors are reporting some surface properties of bilayer structure consisting of ZnO thin absorber (overlayer) and nanocrystalline TiO_2 underlayer. The samples were prepared by two successive growth techniques; electrochemical deposition and vacuum evaporation. To our knowledge, production of transparent lami-

nated bilayer via such two-step growth method is new and it sets to offer some comparative advantages such as durability and reproducibility over the popular atomic layer deposition (ALD). Other advantages include low process temperature, low cost of raw materials, ease of tuning cell parameters to control composition and morphology, and ability to deposit films on substrates with desired dimensions and orientation [4, 8]. Formation of this bilayer is an approach that is easily scalable to industrial processes.

5.3 Experimental:

Schematic diagram of a two-step synthesis of ZnO/TiO_2 bilayer is presented in scheme 1. In the process, TiO_2 nanostructures were first deposited on ITO coated glass (15 mm x 10 mm x 0.7 mm, surface ρ = 15.3 Ω-cm, Lumtec Inc.) by two-electrode electrochemical cell described somewhere [8]. The electrolyte was made from titanium disulphate ($Ti(SO_4)_2$) and NaOH reagents. $Ti(SO_4)_2$ solution (0.2 M) was prepared in 100 ml standard flask and heated at 80^0C for 30 minutes with constant stirring. After heating, the solution was allowed to cool and filtered. Prior to sample deposition, 20 ml of freshly prepared NaOH (0.1 M) was added to 40 ml of the filtrate in the cell. Ultrasonically cleaned ITO substrate was mounted as working electrode and graphite piece served as counter electrode. The cell was coupled and two different cathodic potentials were selected to grow two sets of TiO_2 samples (T1 and T2). The as-grown samples were rinsed with distilled water and dried (preheated) for 5 minutes in furnace at 150^0C. This treatment was carried out to activate sample's surface passivation in preparation for overlayer deposition [5]. For the fact that certain indispensable features such as large particle size of nanostructures, high surface area, long electron diffusion length and pronounced light-scattering are not often completely

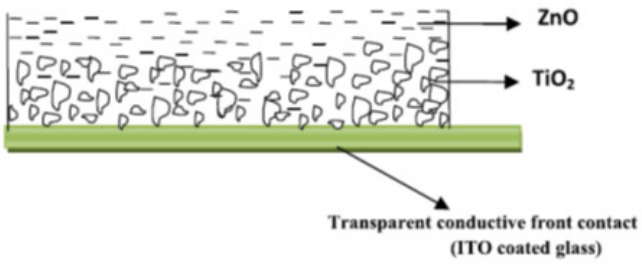

Scheme 1: Surface arrangement of laminated ZnO/TiO_2 transparent bilayer.

possessed by most single-layer surface, hence, the need for additional layer(s) [9]. Therefore, we developed a bilayer structure consisting of ZnO thin film deposited on preheated TiO_2 nanocrystals. Experimental conditions are stated in Table 1. On the first TiO_2 sample (T1), 10 nm thick of ZnO film was deposited in vacuum by Auto 306 vacuum evaporator. The obtained bilayer structure (ZnO/TiO_2) is tagged B1. The second bilayer sample (B2) was formed by electrodepositing ZnO film on the other TiO_2 sample (T2) from 0.2 M of zinc nitrate solution (electrolyte). The growth conditions included cathodic potential (2.0 V) and deposition period (30 minutes). After the deposition, the sample (ZnO/TiO_2) was rinsed with distilled water and dried in furnace at 120^0C for 10 minutes.

5.4 Post-deposition heat treatment and samples characterization:

All the samples were annealed in air at 300^0C for 1 hour. This treatment gave adequate energy to sufficiently orient film particles in proper equilibrium site [10]. It also enhanced relative interfacial roughness, inter-diffusion between layers and conformality which are some

of factors required for formation of high quality nanolaminate [5]. Surface morphology was investigated by Zeiss EVO LS 15 ultra plus FESEM and JEM 1400 transmission electron microscope (TEM). Diffraction patterns were collected by powder X-ray diffractometer with CuKα radiation (λ= 0.15406 nm). Optical absorption across ultraviolet/visible spectrum was studied using Perkin Elmer double beam UV/VIS spectrophotometer respectively.

5.5 Results and discussion

5.5.1 Surface morphology

Surface structure and particle distribution of the TiO_2 and ZnO/TiO_2 (bilayer) films were examined at two different magnifications. Scanning electron microscope (SEM) images are shown in Fig. 5.1. Considering images in Fig. 5.1a(i-ii), it can be seen that particles of both TiO_2 samples (T1 and T2) are evenly distributed across substrate's surface. The films are crystalline and possess few pores. Film thickness was estimated from their respective cross-sectional images as 54.26 μm and 22.69 μm. Average particle sizes were also determined as 137.09 nm and 110.51 nm accordingly (Fig. 5.1a(iii-iv)). Variation in these values can be attributed to difference in growth cathodic potential. These results suggest that an increase in applied voltage can influence growth height and particle size of thin film structure.

Similar to this observation, Sun et al., 2013 [9] have reported a 3-D TiO_2 nanostructure that possesses high specific surface area desirable for strong and effective light scattering in high performing photoanode. Thus, a TiO_2 structure that can enhance efficiency of nanostructured photovoltaic cell must possess (i) average internal surface that can enable sufficient absorber and (ii) minimum pore size that can allow continuous pathway [2]. In bilayer

Table 5.1: Applied deposition voltages, estimated structural properties and energy band gap of ZnO/TiO_2 bilayer films.

Sample	Catodic potential (v)	Film thickness (μm)	Particl size (nm)	FWHM (deg)	Crystallite size (nm)	Energy band gap (eV)
T1(TiO_2)	2.20	54.26	137.01	0.49	17.5	3.43
T2(TiO_2)	2.10	22.69	110.51	0.46	16.6	3.24
B1(ZnO/TiO_2)	-	54.27	-	-	-	3.41
B2(ZnO/TiO_2)	2.00	51.86	-	-	-	3.40

sample B1, uniform distribution and thinness of ZnO overlayer (10 nm) can be appraised by comparing image in Fig. 5.1b(i) with image of underlying TiO_2 nanostructure taken at equal magnification (Fig. 5.1a(i)). First, there is marked difference in their appearance and second, the ZnO layer completely laminated the underneath structure. It also filled all the existing pores. From the image of second bilayer sample B2, it can be clearly seen that ZnO layer produced by electrochemical deposition was fairly thick (Fig. 5.1b(ii)). One of limitations of this technique is remote chance of controlling film thickness during growth process. However, it can be appreciated that the electrodeposited ZnO film also completely laminated the underneath TiO_2 nanostructure (see Fig. 5.1a(ii)). Cross-sectional SEM studies gave thickness of the electrodeposited ZnO overlayer as 29.17 μm. Image acquired at higher magnification (Fig. 6.1b(iii)) revealed clearly that there was no significant chemical interaction between ZnO overlayer and the proximate surface. Particle distribution of TiO_2 underlayer remains unaltered. In solid state photovoltaic concept, this kind of structure can enhance efficiencies because the TiO_2 underlayer can act as barrier against transition of holes from absorber to conductive front contact [2]. Consequently, TiO_2 influences recombination

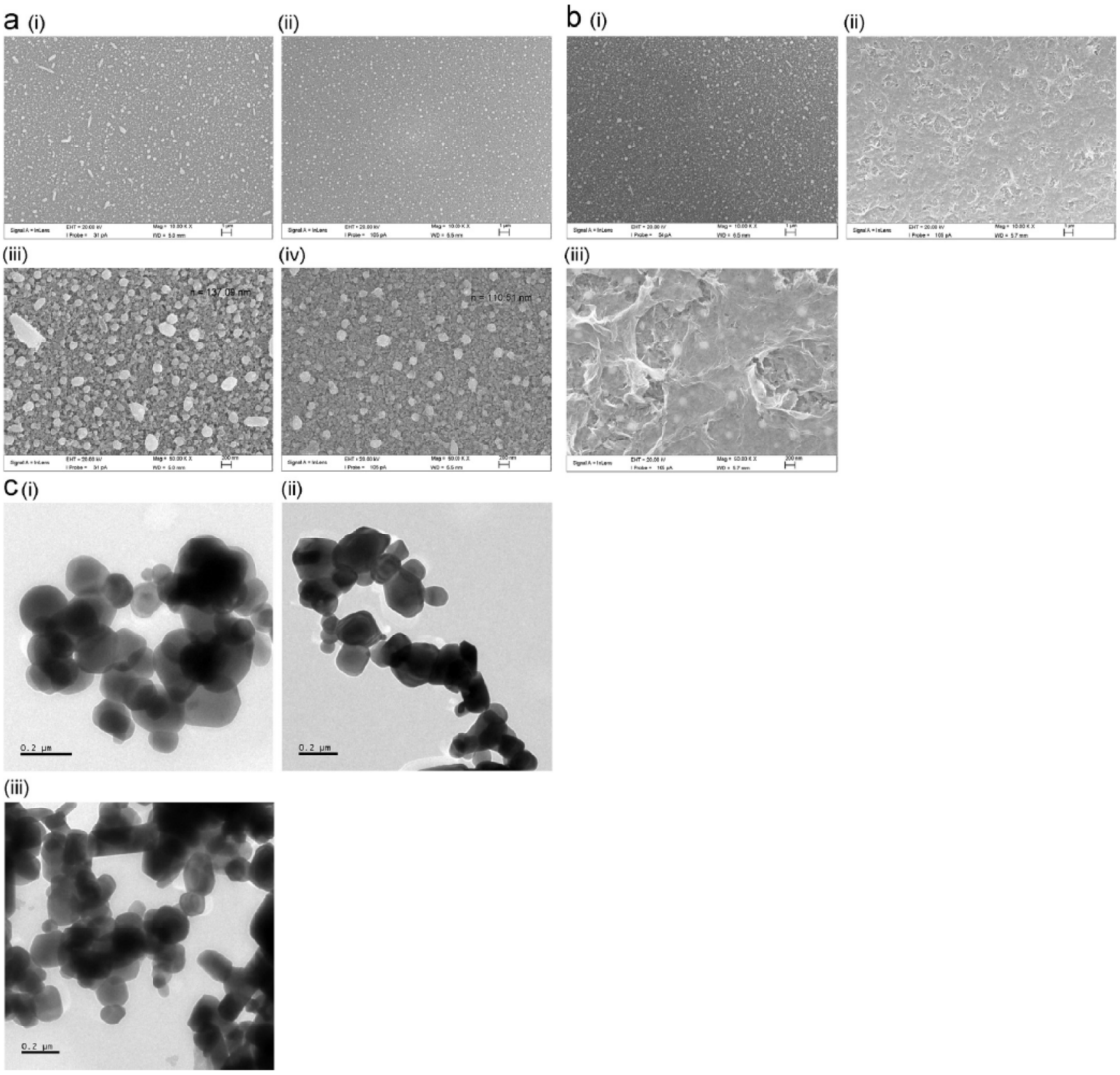

Fig. 5.1. a (i): SEM of TiO2 nanostructure electrodeposited at 2.2 V (Sample T1) (Mag. x10 k), (ii) SEM of TiO2 nanostructure electrodeposited at 2.1 V (Sample T2) (Mag. x10 k), (iii) SEM of TiO2 nanostructure electrodeposited at 2.2 V (Sample T1) (Mag. x50 k), and (iv) SEM of TiO2 nanostructure electrodeposited at 2.1 V (Sample T2) (Mag. x50 k). b (i): SEM of ZnO/TiO2 bilayer laminated in vacuum (Sample B1) (Mag. x10 k), (ii) SEM of ZnO/TiO2 bilayer obtained at 2.0 V (Sample B2) (Mag. x10 k), and (iii) SEM of ZnO/TiO2 bilayer obtained at 2.0 V (Sample B2) (Mag. x50 k). c (i) TEM of electrodeposited TiO2 nanostructre, (ii) TEM of ZnO/TiO2 bilayer laminated in vacuum and (iii) TEM of ZnO/TiO2 bilayer obtained by electrodeposition.

rate because electron lifetime could be related to its probability to encounter holes or it may be determined by the energy level of surface trap sites according to Shockley-Read model [6]. Further investigations of morphologies were carried out by TEM. Since no significant difference was observed in the structure and particle distribution of samples T1 and T2 (see SEM images), results of TEM studies of only samples T1, B1 and B2 are presented (Fig. 5.1c(i-iii)). All the images were acquired at the same scale (Fig. 5.1c (i-iii)). In each sample, particles orientation and agglomeration were examined. Particles were generally found to be polyhedral and orthorhombic lattice feature (a≠b≠c) could easily be identified. Crystalline plains were not seen and particle shapes are not very distinct. These might be due to poor homogeneity of the solution electrolyte. Irregular shape of TiO_2 particles and wide range of size distribution have been attributed to poor homogeneity of starting precursor [11]. From sample T1 (Fig. 5.1c(i)), particle size distribution lies between 0.12 – 0.15 μm. This is consistent with results of SEM. In fig. 5.1c(ii and iii), certain features attributable to ZnO are identified. Some dark hexagonal features found atop the polyhedral shaped particles confirm the presence of ZnO. As a matter of fact, higher proportion of these features in Fig. 5.1c(iii) indicates formation of larger thickness of ZnO overlayer. To study the samples' composition, full scale EDX spectroscopic scan was done at beam kinetic energy of 20 KeV. The study was carried out using INCA Point ID software for quant optimization. Spectra shown in Fig. 5.2 (a and b) represent elements present in TiO_2 and bilayer films respectively. It can be seen that apart from constituents of ITO coated glass (substrate), the samples are free of impurity. Since this facility is not exclusive in quantitative analysis, it could only be used for identification of film composition.

a

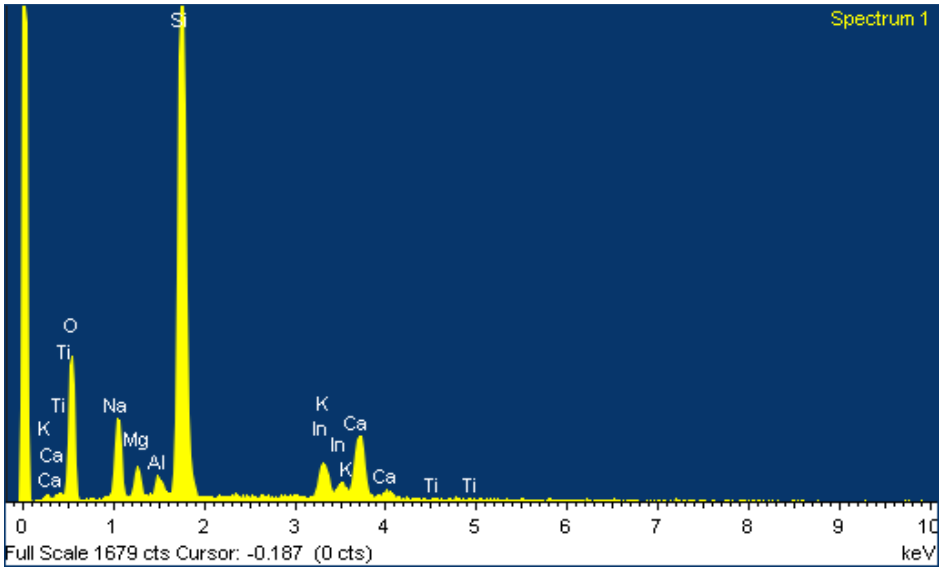

b

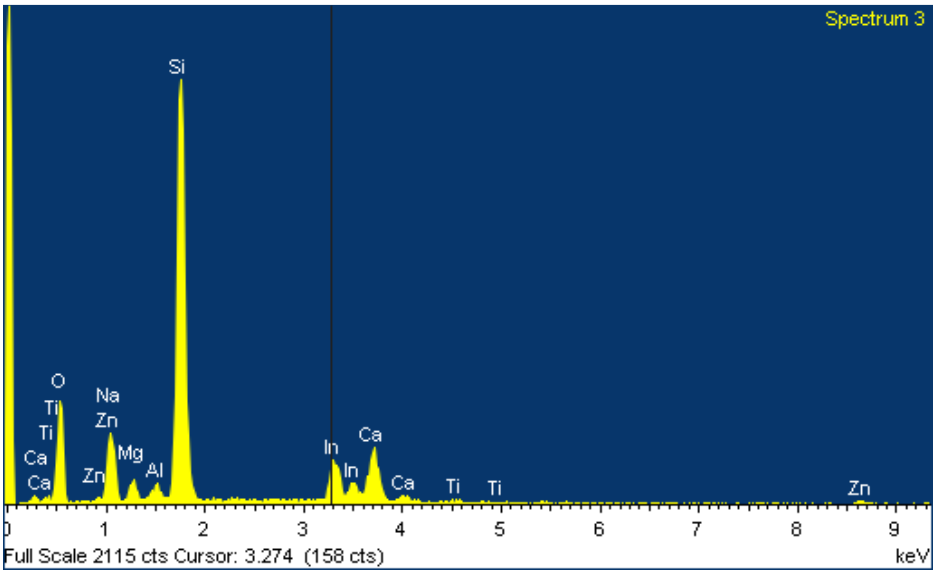

Fig. 5.2. a: EDX spectrum of TiO_2 (sample T1) deposited at 2.2 V. Elemental composition of coated glass substrate and TiO_2 are identified, b: EDX spectrum of ZnO/ TiO_2 (sample B1) laminated in vacuum. Elemental composition of coated glass substrate, TiO_2 and ZnO are identified.

5.5.2 Crystal structures

Diffraction patterns of all the samples are shown in Fig. 5.3. All the patterns are indexed according to ICDD (00-029-1360). Apart from peaks emanating from ITO coated glass and ZnO, three diffraction peaks of TiO_2 brookite orthorhombic structure are observed in all the samples: one prominent peak appears at $2\theta = 30.70$ and two small peaks occur at 37.80 and 55.80 respectively. The former corresponds to diffraction from (121) plane while the later are attributed to diffraction from (131) and (151) planes respectively. Exhibition of strong peak at plane (121) indicates preferred growth orientation. Reyes-Coronado et al., 2008 [12] have earlier obtained such preference in phase-pure brookite nanoparticles prepared by hydrothermal treatment. Comparing the two diffraction patterns (samples T1 and T2), there is no remarkable difference in their peaks, indicating that slight difference in cathodic potential ($\pm$ 0.1 V) may not be sufficient to achieve different crystallinity. In the bilayer samples (B1 and B2), major characteristic peaks of ZnO corresponding to diffraction from planes (002) and (101) are identified [5, 8]. A mixed phase of TiO_2 and ZnO is also observed; this could have arisen because of two reasons: (i) brief heating of as-grown TiO_2 films might not be sufficient to prevent some interactions between the TiO_2 layer and zinc nitrate (electrolyte) during deposition of ZnO overlayer; and (ii) during post-deposition annealing, there could also be some interactions between the two layers (TiO_2 and ZnO) because TiO_2 film does not become crystalline until annealing temperature nears 300^0C [4]. On diffraction pattern of sample B2, a small peak of $Zn(OH)_2$ corresponding to diffraction from plane (002) is noticed (ICDD 01-072-2032). This could be due to a little concomitant residue from sample preparation. According to Bragg's law, interplanar spacing, d, for TiO_2 (121) was calculated as 2.9 Å. A crystallite size of 16.6 and 17.5 nm were estimated from FWHM of

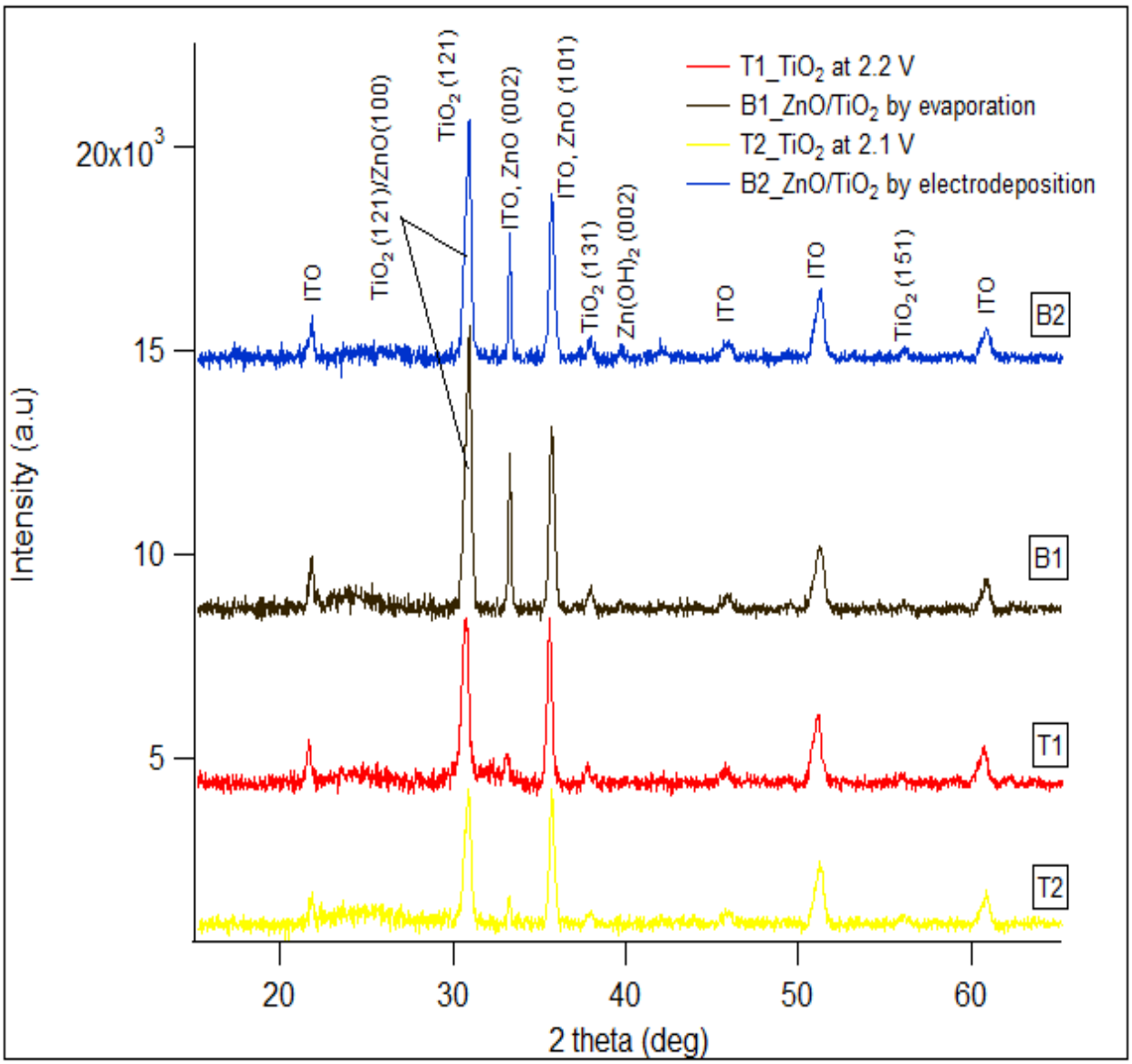
T1_TiO2 at 2.2 V
B1_ZnO/TiO2 by evaporation
T2_TiO2 at 2.1 V
B2_ZnO/TiO2 by electrodeposition
ITO
TiO2 (121)/ZnO(100)
TiO2 (121)
ITO, ZnO (002)
ITO, ZnO (101)
TiO2 (131)
Zn(OH)2 (002)
ITO
ITO
TiO2 (151)
ITO
B2
B1
T1
T2
20x10^3
15
10
5
Intensity (a.u)
20
30
40
50
60
2 theta (deg)

Fig. 5.3

the (121) peaks of both TiO_2 films using Scherrer's equation [5].

$$D = \frac{\lambda}{2sin\theta} \tag{5.1}$$

$$D = \frac{K\lambda}{\beta cos\theta} \tag{5.2}$$

Where D is average crystallite size, K (0.89) is a constant, λ is wavelength of CuKα radiation, β is FWHM (measured in degree) of the peak, and θ is Bragg's angle. Comparing the estimated values of crystallite size with that of particle size obtained from SEM, it can be suggested that particles agglomerated faster in sample T1 than in T2 (see Fig 5.1a(i) and 1a(ii)).

5.6 Optical studies

5.6.1 Absorption edge and Transmittance

Optical measurement was carried out in air. Absorption spectra of all the samples were taken from ultraviolet to visible region. The plots are presented in Fig. 5.4a. The samples generally have strong absorption peak in UV region and they significantly exhibit absorption edge at $\lambda = \sim 330nm$. This feature has been reported as an indication of intrinsic band gap absorption (electron-trapping potential by oxygen vacancies) of TiO_2 structure [5, 13]. It can inhibit recombination rate of photo-induced $e^- - h^+$ pairs and increase photocatalytic performance. It also emphasizes role of some metal oxide as buffer layer for charge separation in photovoltaic devices [14, 15]. In both bilayer samples, there is a slight shift or extension of absorption edge towards visible region (see inset in Fig. 5.4a). This behaviour could be attributed to increase in film thickness due to ZnO lamination. It could also be due to the fact that absorption edge of ZnO thin film mostly occurs at a wavelength higher than 400

nm [16]. Such shift has been found to improve photocatalytic activity of doped mesoporous TiO_2 under visible light illumination [13]. Fig. 5.4b shows films' transmittance. In UV region, value of spectra transmittance decreases intensively with increase in photon energy, this can be attributed to strong absorption from fundamental band gap and high-energy critical point transition [5]. Across visible light region (λ = 380–900nm), the films are fairly transparent with respect to the highly transmitting blank ITO substrate. Average transmittance is above 60% and it increases across the spectrum. Due to thinness of vacuum deposited ZnO overlayer, there is no noticeable difference between transmittance of bilayer sample B1 and the TiO_2 underlayer (T1).

5.6.2 Energy band gap

Absorption coefficient was generated from measured optical data using equation 5.3 assuming that film reflectance is very negligible (R<<1) [16].

$$\alpha = \frac{-1}{d} lnT \tag{5.3}$$

For a semiconducting material, optical band gap can be expressed by tauc model and parabolic band [14, 15]:

$$\alpha = A(h\nu - E_g)^{n/2} \tag{5.4}$$

Where n = 1 and 4 for direct and indirect energy band gap respectively. α is absorption coefficient, T is film transmittance, d is film thickness, A is empirical constant, $h\nu$ is photon energy and E_g is energy band gap. Values of α^2 are plotted against photon energy ($h\nu$). The energy gap is determined by extrapolating linear region of the tauc plot to energy axis where $\alpha^2 = 0$. From the plots (Fig. 5.4c), all the films have direct allowed energy transition. Estimated energy band gaps of the two TiO_2 nanostructures (T1 and T2) are

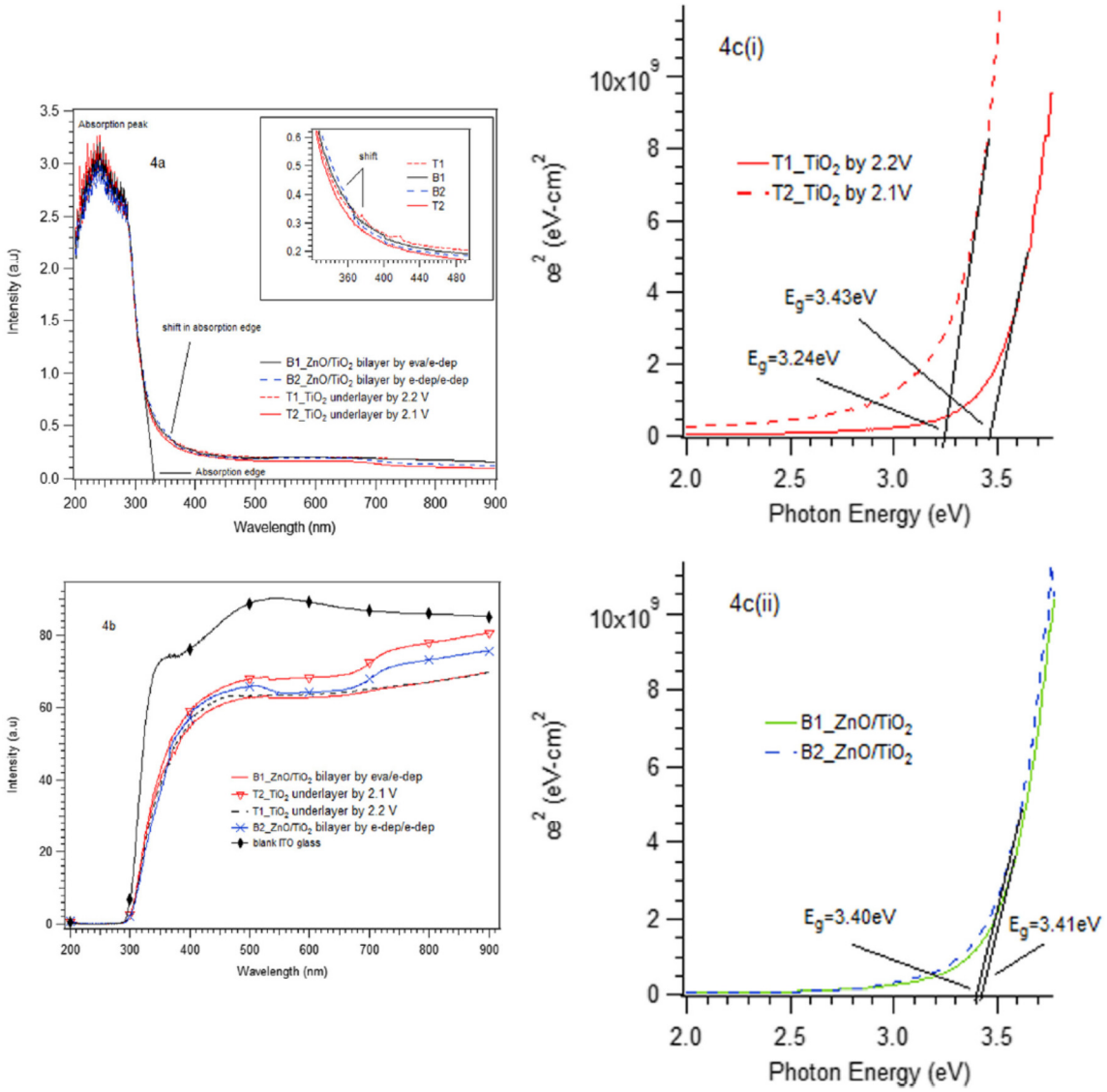
4a
Absorption peak
shift in absorption edge
Absorption edge
Intensity (a.u)
Wavelength (nm)
B1_ZnO/TiO2 bilayer by eva/e-dep
B2_ZnO/TiO2 bilayer by e-dep/e-dep
T1_TiO2 underlayer by 2.2 V
T2_TiO2 underlayer by 2.1 V
shift
T1
B1
B2
T2
4b
B1_ZnO/TiO2 bilayer by eva/e-dep
T2_TiO2 underlayer by 2.1 V
T1_TiO2 underlayer by 2.2 V
B2_ZnO/TiO2 bilayer by e-dep/e-dep
blank ITO glass
4c(i)
T1_TiO2 by 2.2V
T2_TiO2 by 2.1V
Eg=3.43eV
Eg=3.24eV
Photon Energy (eV)
4c(ii)
B1_ZnO/TiO2
B2_ZnO/TiO2
Eg=3.40eV
Eg=3.41eV
Photon Energy (eV)

Fig. 5.4

3.43 and 3.24 eV respectively. These values are in accordance with some energy band gaps in literatures [12, 17, 18]. It is also noteworthy that difference in these values may be due to difference in sample's thickness (see Table 1). With overlaying ZnO film, energy band gap of bilayer sample B1 shifts to 3.41 eV indicating a slight narrowing of about 20 meV. This shift conforms to thinness of deposited ZnO overlayer. In the second bilayer (B2), a higher value of energy band gap (3.40 eV) compared to that of TiO_2 underlayer (T2) (3.24 eV) was obtained. This observation is not in accordance with principle of optical energy band gap theory. The irregularity might be due to some surface microstructural differences between electrodeposited TiO_2 underlayer (T2) and electrodeposited ZnO top layer. Owing to the fact that this ZnO film is relatively thicker ($\sim 29.17\ \mu$m) than the proximate TiO_2 ($\sim 22.69\ \mu$m), this bilayer sample might not be well thermally stabilized during post-deposition annealing treatment and thereby had more defects and structural disorder. Further investigations are in progress.

5.7 Conclusion

Room temperature growth and some surface characterization of ZnO/TiO_2 bilayer structure have been carried out. Effective lamination of thin absorber layer (ZnO) on porous n-type semiconductor nanostructure (TiO_2) has been demonstrated by two comparable techniques. Porous aggregates shown by morphological features suggest that brookite nanocrystals can be suitable for application in photocatalysis, sensor and solar devices. This layer-by-layer investigation generally reveals arrangement of some metal oxides nanostructures considerable for effective charge absorption as well as buffer between photoactive layer and contact electrodes in a design of optoelectronic devices.

5.7.1 Acknowledgments

This work is supported by University of KwaZulu-Natal, South Africa through postdoctoral scholarship. The authors are grateful to colleagues at Microscopy and Microanalysis Unit (MMU) of School of Life Science, UKZN Durban and Pietermaritzburg for SEM and EDX measurement and analysis. Effort of staff of iTHEMBA Lab, Sommerset West is appreciated on XRD studies.

Bibliography

[1] K.H. Wong, Mason, C.W., Devaraj, S., Ouyang J. and Bayala, P. (2014). Low temperature aqueous electrodeposited TiO_x thin films as electron extraction layer for efficient inverted organic solar cells. J. Appl. Materials and Interfaces, 6, 2679 – 2685.

[2] Larramona, G., Chone, C., Jacob, A., Sakakura, D., Delatouche, B., Pere, D., Cieren, X., Nagino, M. and Bayon, R. (2006). Nanostructured photovoltaic cell of the type titanium dioxide, cadmium sulfide thin coating, and copper thiocynate showing high quantum efficiency. J. Chem Mater, 18, 1688-1696.

[3] Lee, B.G., Skarp, J., Malinen, V., Li, S., Choi, S. and Branz, H.M. (2012). Excellent passivation and low reflectivity Al2O3/TiO_2 bilayer coatings for n-wafer silicon solar cells. IEEE Photovoltaic Specialists Conference, Texas. NREL/CP-5200-54121, 1-3.

[4] Karuppuchamy, S., Iwasaki, M. and Minoura, H. (2006). Electrochemical properties of electrosynthesized TiO2 thin films. J. Appl Surf. Sci. 253. 2924-2929.

[5] Gu, Y-Z., Lu, H-L., Geng, Y., Ye, Z-Y., Zhang, Y., Sun, Q-Q., Ding, S-J. and D.W Zhang. (2013). Optical and microstructural properties of ZnO/TiO_2 nanolaminates prepared by atomic layer deposition. Nanoscale Res Lett 8:107, 1-5.

[6] Nakade, S., Saito, Y., Kubo, W., kitamura, T., Wada, T. and Yanagida, S. (2003). Influence of TiO_2 nanoparticle size on electron diffusion and recombination in dye-sensitized TiO2 solar cells. J. Phys. Chem. B, 107, 8607-8611.

[7] Kumagai, H., Tanaka, Y., Murata, M.m Masuda, Y. and Shinagawa, T. (2010). Novel TiO_2/ZnO multilayer mirrors at 'water-window' wavelengths fabricated by atomic layer epitaxy. J. Phys. Condens. Matter 22, 474008, 1-7.

[8] Taleatu, B.A., Fasasi, A.Y., Di Santo, G., Bernstorff, S., Goldoni, A., Fanetti, M., Floreano, L., Borghetti, P., Casalis, L., Sanavio B. and Castellarin-Cudia, C. (2011). Electro-chemical deposition of zinc oxide nanostructures by using two electrodes. AIP Advances 1, 032147 (10).

[9] Sun, Z., Kim, J.H., Zhao, Y., Attard D. and Dou, S.X. (2013). Morphology-controlled 1D-3D nanostructured TiO_2 bilayer photoanodes for dye-sensitized solar cells. Chem. Commun. 49, 966-968.

[10] Jundale D, Pawar S, Chougule M, Godse P, Patil S, Raut B, Sen S and Patil V. Nanocrystalline CuO thin films for H2S monitoring: Microstructural and opoelectronic characterization. J. sensor Technology, 1, 36-46, 2011.

[11] Paulauskas, I.E., Modeshia, D.R., Ali, T.T., El-Mossalamy, E.E., Obaid, A.Y., Basahel, S.N., Al-Ghamdi, A.A. and Sartain, F.K. (2013). Photocatalytic activity of doped and undoped titanium dioxide nanoparticles synthesized by flame spray pyrolysis. Platinum Metals Rev., 57, 1, 32-43.

[12] Reyes-Coronado, D., Rodriguez-Gattorno, G., Espinosa-Pesqueira, M.E., Cab, C., de Coss, R. and Oskam, G. (2008). Phase-pure TiO_2 nanoparticles: anatase, brookite and rutile. Nanotechnology 19, 145605 (10).

[13] Fan, X., Chen, X., Zhu, S., Li, Z., Yu, T., Ye, J. and Zou, Z. (2008). The structural, physical and photocatalytical properties of the mesoporous Cr-doped TiO_2. J. Molecular Catalysis A: Chemical 284, 155-160.

[14] Peng, Y-H., Huang, G-F. and Huang, W-Q. (2012). Visible-light absorption and photocatalytic activity of Cr-doped TiO_2 nanocrystal films. Advanced Powder Technol. 23, 8-12.

[15] Taleatu, B.A., Makinde, W.O., Eleruja, M.A. and Fasasi. A.Y. (2013). Band alignment and charge transport characteristics of TPP/ZnO hybrid for photovoltaic cell potential. Current Appl. Phys. 13, 97-102.

[16] Cho, S. (2009). Effects of growth temperature on the properties of ZnO thin films grown by Radio-frequency magnetron sputtering. Transitions on Electrical and Electronic Mater. 10, 6, 185-188.

[17] Ayouchi, R., Casteleiro, C., Schwarz, R., Barrado, J.R. and Martin, F. (2010). Optical properties of TiO_2 thin films prepared by chemical spray pyrolysis from aqueous solutions. Phys. Status Solidi C, 7, No. 3-4, 933-936.

[18] Di Paola A, Bellardita M. and Palmisano L. (2013). Brookite, the Least Known TiO_2 Photocatalysit. Catalysts 3, 36-73.

Chapter 6

TERNARY MOLECULES BLEND ORGANIC BULK HETEROJUNCTION

SOLAR CELL

Materials Science in Semiconductor Processing 40 (2015) 158–161

Contents lists available at ScienceDirect

Materials Science in Semiconductor Processing

journal homepage: www.elsevier.com/locate/matsci

Ternary molecules blend organic bulk heterojunction solar cell

Elhadi A.A. Arbab [a], Bidini A. Taleatu [a,b], Genene Tessema Mola [a,*]

[a] School of Chemistry & Physics, University of KwaZulu-Natal, Pietermaritzburg Campus, Private Bag X01, Scottsville 3209, South Africa
[b] Department of Physics and Engineering Physics, Obafemi Awolowo University Ile-Ife, Nigeria

ARTICLE INFO

Article history:
Received 8 April 2015
Received in revised form
4 June 2015
Accepted 24 June 2015

Keywords:
Organic PV cells
Conducting Polymer
PTB7:PCBM blend
Bulkheterojunction

ABSTRACT

The ternary molecules blend organic photovoltaic cell using poly(3 hexylthiophene) (P3HT), poly[[4,8-bis [(2-ethyhexyl)oxy] benzo(1, 2 – b: 4, 5 – b')dithiophene-2,6-diyl][3-fluoro-2-[(2 ethylhexyl)carbonyl] thieno[3,4-b]thiophenediyl]] (PTB7) and [6,6]-phenyl-C61-butyric acid methyl ester (PCBM) were investigated. The performance of the ternary blend was compared with two binary molecules based photoactive layers such as P3HT:PCBM and PTB7:PCBM. It was found that the ternary molecules photovoltaic cell performs better than those with P3HT:PCBM composition. The optical and morphological properties of the ternary blend active layers were investigated, and the results suggest that better photon harvesting medium can be achieved by blending two donor molecules.

6.1 Abstract

The ternary molecules blend organic photovoltaic cell using poly(3 hexylthiophene) (P3HT), poly[[4,8-bis[(2-ethyhexyl)oxy] benzo(1,2-b:4,5-b') dithiophene -2,6-diyl] [3-fluoro-2-[(2 ethyl-hexyl) carbonyl]thieno[3,4-b] thiophenediyl]] (PTB7) and [6,6]-phenyl-C61-butyric acid methyl ester (PCBM) were investigated. The performance of the ternary blend was compared with two binary molecules based photoactive layers such as P3HT:PCBM and PTB7:PCBM. It was found that the ternary molecules photovoltaic cell perform better than those with P3HT:PCBM composition. The optical and morphological properties of the ternary blend active layers were investigated and, the results suggest that better photon harvesting medium can be achieved by blending two donor molecules.

keywords: Organic PV cells, Conducting Polymer; PTB7:PCBM blend, bulkhetero-junction.

6.2 Introduction

In rapidly increasing global atmospheric temperature together with the growing energy demand globally have brought intensive research efforts towards achieving viable and sustainable energy sources. Solar energy is one of the alternative green energy options that remain untapped potential at present. However, the search for efficient mechanism to convert solar energy into electricity has been the challenge ever since the realization of the concept of solar energy. In the last few decades silicon based solar panel has been successfully used in the generation of electric power, but, the cost of device fabrication is still expensive in spite of the recent declining trend. Meanwhile, the discovery of electrical conduction in polymer molecules, which are traditionally known as an insulator, has opened up a new dimension for

application in organic photovoltaic (OPV) cell [1-10].The advantages of organic molecules based solar cell over the inorganic ones are low fabrication cost, the ease of device fabrication such as roll-to-roll techniques, and flexibility of the substrates [8-14]. However, organic semiconductors are environmentally unstable under exposure to light and humidity which generally requires protection for better performance. The degradation of polymer molecules is caused by photosensitized generation of singlet oxygen which then reacts with the polymer chains [12-16]. Therefore, the preparation of devices in controlled environment such as glove box followed by encapsulation have significantly increased the power conversion efficiency and life span of OPV devices.

The most efficient device architecture in the preparation of organic molecule based solar cell is the binary molecules bulk heterojunction (BHJ) design in which an acceptor and a donor type of organic molecules are blended in the photoactive medium to create donor/acceptor interfaces at the molecular level. Such bulk heterojunction design has significantly improved the efficiency of exciton dissociation and charge transport in the medium. The harvesting of photons in OPV cell mainly depends on the optical absorption bands of the donor and acceptor molecules used as an active layer [17-20]. In order to enhance the optical absorbance and spectral sensitivity of the photoactive medium in OPV; it is customary to blend molecules of different absorption bands together. A typical example of such method is the ternary molecules blend BHJ solar cell in which the active layer is composed of either two donor (D1,D2) and an acceptor (A) molecules or one donor(D) and two acceptor (A1, A2) molecules, with different stoichiometric ratio by weight [21-25]. In this work, we employed two donors and an acceptor molecules in the preparation OPV devices using P3HT and PTB7 as donor and PCBM as an acceptor. Figure 6.1 shows the chemical structure of all the molecules involved in the preparation of photoactive layer of OPV devices which are fabricated and characterized under ambient environment. Generally, the performance of such

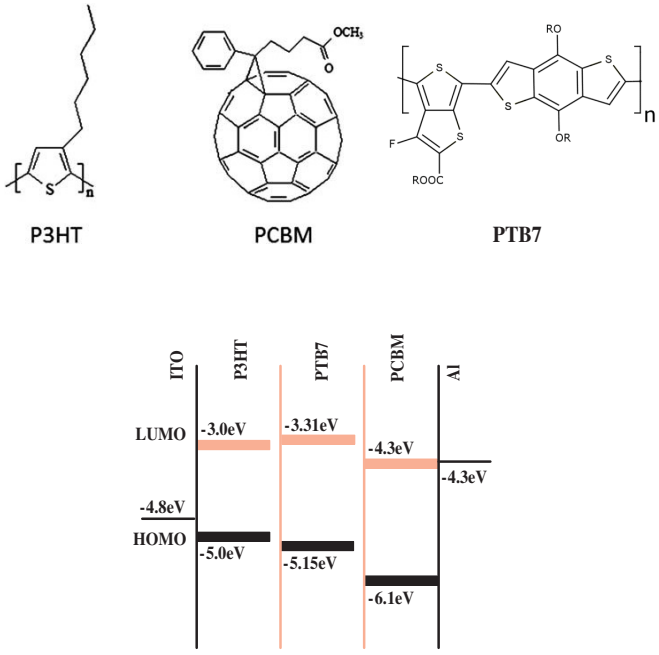

Figure 6.1: Chemical structures of the molecules used in the preparation of the photoactive layers.

organic molecules blend (P3HT:PTB7:PCBM) relies on a good control of the morphology of the active layer such as the crystallinity of the polymer chains as well as the miscibility of the polymers in the medium. This article consists of experimental observation of the ternary molecules blend BHJ solar cell followed by discussion of the results.

6.3 Experimentals

6.3.1 Device Preparation

Bulk heterojunction type organic solar cell devices were prepared from chloroform based solution. The device preparation begins by partially etching the unpatterned ITO coated glass substrate using acid solution containing HCl:H_2O : NHO_3[48%:48%:4%] by volume.

The substrates were then cleaned thoroughly by successive sonication in detergent, deionized water, acetone and isopropanol, respectively. The substrates were then dried in an oven at 150^oC for 30 min prior to the coating of thin layer of PEDOT:PSS at 3500 rpm. They were immediately baked in an oven again at 150^oC for 30 min. The binary and ternary molecules blend solutions were separately prepared in chloroform solvent from the mixture of (P3HT:PCBM), (PTB7:PCBM) and (P3HT:PTB7:PCBM). The concentration of the solution used in this experiment was 20 mg/ml. In all the cases, the donor to acceptor weight ratio maintained at a constant 1:1. The solution was sonicated at a temperature of 40°C for 3 Hrs in order to allow homogeneity and inter-dispersion of the molecules. The active layers from the solution blends were spin coated on dried PEDOT:PSS layer at the spin rate of 1200 rpm for 40 sec. The samples were immediately loaded into the vacuum chamber (Edward Auto 306 deposition unit) at a base pressure of 10^{-6}mbar. Finally, a thin buffer layers of LiF and the Al electrode were deposited on the sample for thickness 0.5 nm and 60 nm respectively. The electrical characterization of the devices were carried out using computer interfaced Keithley HP2400 source-meter under AM1.5 solar simulator (model SS50AAA) operating at an integrated power intensity of 100 mW/cm^2. The effective area of the diodes was 0.15 cm^2. The surface morphology and chemical composition of the active layer was studied using scanning electron microscope (SEM)(Zeiss crossbeam series with Gemini FE-SEM), fluorescence light microscope(FLM)(Olympus AX70 Compound) with camera (Nikon, DS-Ri1). The UV-VIS absorption and transmittance spectra of blend thin film were recorded with UV/VIS double beam spectrometer (T 80-PG-Instruments Ltd.)

The current-voltage characteristics of the solar cell diode obeys a simple diode equation given by :

$$J = J_s(e^{qV/KT} - 1) - J_{ph} \tag{6.1}$$

where J_s and J_{ph} are the saturation and photo-generated currents, respectively. From the diode equation one can derive all important parameters of the solar cell. The power conversion efficiency (PCE), for example, is defined as:

$$\eta = \frac{P_{max}}{P_{in}} = \frac{J_{sc} \times V_{oc}}{P_{in}} \times FF \tag{6.2}$$

where P_{in} and P_{max} are the incident power and the maximum extractable power by the solar cell, respectively. The fill factor (FF) is defined as:

$$FF = \frac{J_{max} \times V_{max}}{V_{oc} \times J_{sc}} \tag{6.3}$$

In device preparation of OPV often the FF is mainly affected by laboratory condition and the morphology of the active layer[4, 14, 16].

6.4 Results and Discussion

6.4.1 Optical Absorption

The optical absorption spectra of the two donor polymers (P3HT and PTB7) are given in Fig. 6.2 which shows a distinct optical absorption bands of the two molecules. The P3HT molecule has an optical absorption band in the region between 400 nm up to 650 nm while the PTB7 absorption band extends from nearly 400 nm to 750 nm. The two absorption spectra clearly overlap between 400 nm to 650 nm but separated beyond 650 nm. The PTB7 optical absorption covers an additional spectral range from 650 nm up to 750 nm which in principle is expected to boost photons harvesting in the medium and became the reason for this investigation. A series of optical absorption measurement were also taken from thin films composed of P3HT, PTB7 & PCBM molecules blend at different stoichiometric ratio of P3HT

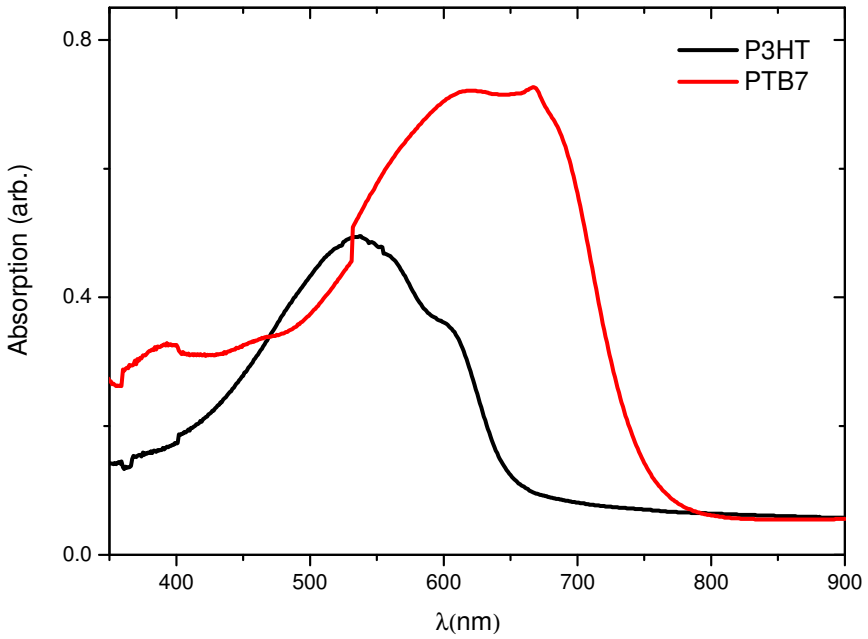

Figure 6.2: Optical absorption spectra of P3HT and PTB7

and PTB7(see Fig. 6.3). According to the absorbance given Fig. 6.3 the peak absorbance of the ternary blend is centered around 520 nm close to the maximum absorbance of the P3HT molecule. A small bump near the tail of the spectrum is evident around 680 nm which is associated with the existence of PTB7 in the film. The strong vibronic shoulder near 590 nm of the P3HT:PCBM is still evident in the ternary blend molecules which diminishes as the amount of P3HT molecule decreases in the blend. These shoulders are common to P3HT thin films and are attributed to inter-chain vibrational and electronic absorptions induced by a high degree of ordering and strong inter-chain interactions. The absorbance of the ternary blend film generally covers wide range of visible spectrum ranging from 400 nm to 750 nm and extends to some parts of UV and NIR regions (see Fig. 6.3). The absorbance peak of the ternary blend remain almost unchanged around 520 nm for all stoichiometric ratio used in this study. However, the peak width broadens and gets red-shifted as the concentration

of P3HT reduces in the blend. The tendency of the absorbance towards red-shift is an encouraging sign for the creation of better photon harvesting medium [26-29].Therefore, the ternary BHJ solar cells with broadened absorption band would likely improve device performance.

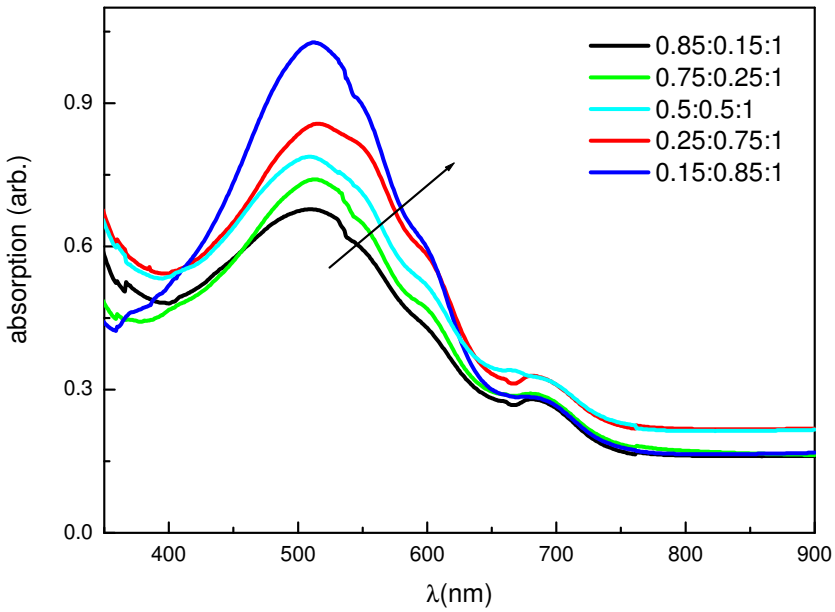

Figure 6.3: Optical absorption of the P3HT:PTB7:PCBM blend at various stoichiometric ratio of the polymers in the same order.

6.4.2 Electrical Measurement

A number of binary and ternary BHJ organic photovoltaic cell have been fabricated under ambient laboratory conditions where all samples were prepared and tested in laboratory atmosphere. We employed sandwich type device structure designed according to a sequence

of layers ITO/PEDOT:PSS/Active Layer/LiF:Al. In the case of binary BHJ devices the active layer is ether P3HT:PCBM or PTB7:PCBM blend while in the ternary devices the active layer is composed of P3HT:PTB7:PCBM mixture at various stoichiometric ratio by weight. A representative current-voltage characteristics of the devices is shown in Figure 6.4 for both types of active layers. The J-V curves are generally characterized by low fill factor associated with existence of high series resistance in the devices. The measured parameters of those better performing devices are given in Table I for three types active layers under investigations.

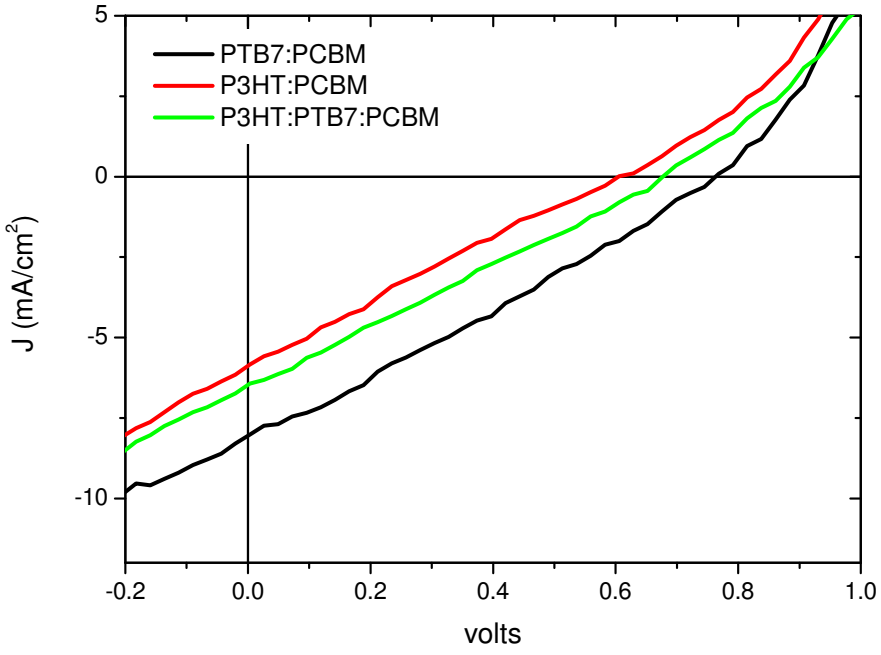

Figure 6.4: J-V characteristics of binary and ternary blend BHJ for the best performed diodes.

The short circuit currents(J_{sc}), for instance, are 5.8 mA/cm^2, 6.4 mA/cm^2 8.1 mA/cm^2 for layers P3HT:PCBM, P3HT:PTB7:PCBM and PTB7:PCBM, respectively. The correspond-

ing power conversion efficiencies (PCE) are 1.0% 1.2% and 1.9% in the same order. The ternary blend devices open circuit voltage has grown by 11% from the P3HT:PCBM composition and lowered by nearly 11% from PTB7:PCBM OPV devices. The PTB7:PCBM binary blend bulk heterojunction photovoltaic cell exhibited better device performance than both ternary blend and P3HT:PCBM as can be seen from Table 6.1. The ternary blend photoactive layer showed intermediate behavior between PTB7:PCBM and P3HT:PCBM binary devices but it is close to the parameters of P3HT:PCBM active layer. The results suggest that the behavior of P3HT in the ternary blend is relatively dominant compared to PTB7 because of the higher density of the later. The lower power conversion efficiency of ternary blend devices is attributed to the poor miscibility of the two donor polymers in the photoactive medium which will be discussed in the following section. The observed low fill factor associated with high resistance across the electrodes of the devices seriously affected the shape of the J-V curve. The origin of such high series resistance may be attributed to the ambient environmental conditions under which devices were prepared [18-20].

Active Layer	V_{oc} (volts)	J_{sc} (mA/cm^2)	FF	PCE (%)	R_s Ohms
P3HT:PCBM (1:1)	0.61	5.8	0.25	1.0	510
P3HT:PTB7:PCBM (0.5:0.5:1)	0.68	6.4	0.25	1.2	375
PTB7:PCBM (1:1)	0.76	8.1	0.30	1.9	140

Table 6.1: The cell parameters for best performed diodes.

6.4.3 Surface Morphology

The scanning electron microscopy(SEM) and fluorescence light microscope(FLM) were used to study the surface morphology of the photoactive films produced by spin coating on glass substrate (see Fig. 6.5). The EDX elemental analysis was also conducted on the various features of the surface of the film. Based on the morphology and the elemental analysis we were able to identify the different structures on the surface. Both SEM and FLM images clearly captured the crystal type parallel lines and white spots which are often associated with P3HT and PCBM molecules, respectively [12, 13]. Apart from P3HT and PCBM there are different sized islands widely distributed over the surface on the background of P3HT microcrystalline features which are most likely due to the presence of PTB7 molecules (Fig. 6.5). The EDX data taken from such islands are indicating the existence of peaks associated with sulfur and fluorine among others which are the elements found in PTB7 molecule. Therefore, both SEM and FLM images have confirmed the existence of PTB7 cluster with

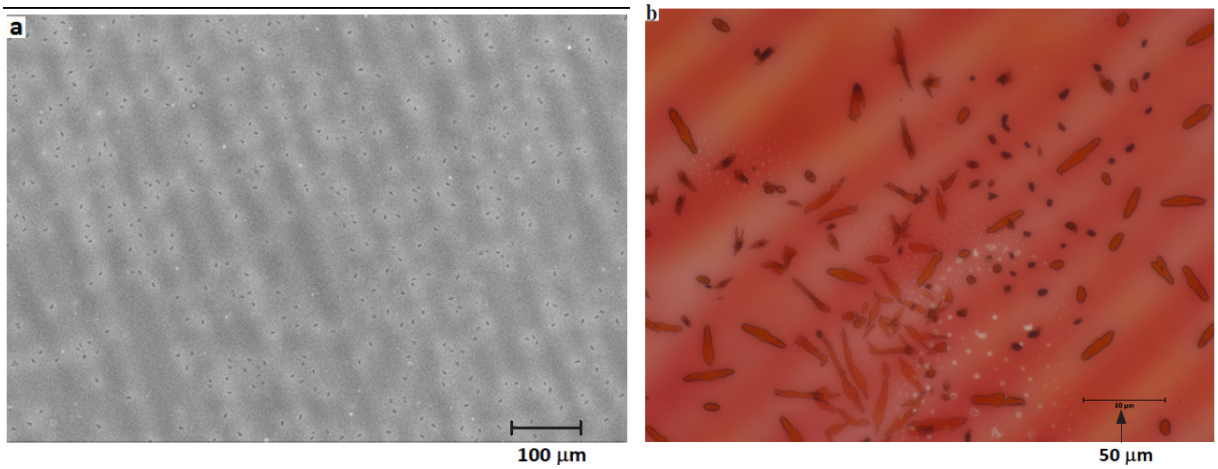

Figure 6.5: The surface morphology of the ternary molecules blend film taken using a) SEM and b) FLM.

in the P3HT matrix in the film. However, the PTB7 molecules in ternary blend tend to

segregate themselves from the rest of the molecules and form large cluster and islands as large as 20μm (Fig. 6.5). This suggest that the PTB7 are rather less crystalline in the P3HT ternary blend solution. The bottom panel in Figure 6.5 shows that the PCBM molecules tend to be attracted more to the PTB7 molecules and clusters which would definitely affect the uniformity of the distribution of the acceptor molecules in the medium. Such uneven distribution of the PCBM in the photoactive layer would definitely hinder the charge dissociation and transportation. Therefore, the reduced performance of the ternary blend molecules (compared with PTB7) could be due to poor miscibility of the donor molecules and uneven distribution of PCBM in the active layer. The less crystalline nature of PTB7 molecules in the ternary blend could also negatively contribute to the performance of the devices.

6.5 Conclusions:

Both ternary and binary bulk heterojunction solar cells were fabricated using P3HT, PTB7 and PCBM polymer molecules. The OPV devices were produced by solution processing method in ambient laboratory environment. The optical absorbance of the ternary blend indicated the broadening of the absorption band centered around 520 nm. However, the ternary blend devices were found to be less efficient than those devices with PTB7:PCBM active layer but better than the P3HT:PCBM. According to the SEM and FLM images we found PTB7 molecule is less crystalline than P3HT and forms varied sized clusters in the photoactive medium. The existence of such islands in the active layer would certainly reduces the efficient dissociation of exciton and transport of charges. It was also found that the open circuit voltage of the ternary blend grew by 11% from P3HT:PCBM devices and lowered by the same magnitude from PTB7:PCBM. Generally, it is to be noted that there are

improvements on the solar cell parameters of the ternary blend molecules compared to those P3HT based devices. This needs further investigations using clean room device preparation and thermal annealing.

6.5.1 Acknowledgments

This work is based on the research supported by the National Research Foundation (NRF) (Grant No.: 92786 & 85589), South Africa. The authors are also grateful to the staffs at Microscopy and Microanalysis Unit (MMU) of the University of KwaZulu-Natal for SEM, FLM and EDX studies and analysis.

Bibliography

[1] W. Zhou, H. X. Yang, Z. H. Fang, Applied Energy, (2007), 84, 1187-1198.

[2] K. S. Liao, S. D. Yambem, A. Haldar, N. J .Alley and S. A. Curran, Energies,(2010), 3, 1212-1250.

[3] E. Kymakis, N. Kornilios and E. Koudoumas, J. Phys. D: Applied Physics., (2008), 41, 165110-165115.

[4] B. Ratier, J. M. Nunzi, M. Aldissi, T. M. Kraft and E. Buncel, Polym. Int.,(2012), 61, 342-354.

[5] G .Zhao, Y. He, and Y. Li, Adv. Mater.,(2010), 22, 4355-4358.

[6] K. Kawano, J. Sakai, M. Yahiro, and C. Adachi, Solar Energy Materials and solar cells,(2009),93, 514-518.

[7] F. Padinger, R. S. Rittberger, and N. S. Sariciftci, Adv. Funct. Mater., (2003), 13(1), 85-88.

[8] J. H. Park, J. S. Kim, J. H. Lee, W. H. Lee, and K. Cho, J.Phys. Chem. C., (2009), 113, 17579-17584.

[9] J. Y. Kim, S. H. Kim, H. H. Lee, K. Lee, W. Ma, X. Gong, and A. J.Heeger, Adv. Mater., (2006), 18, 572-576.

[10] S. V. D. Prasad, V. Krishnanaik, K. R. Babu, Int. J. Science and Modern Engineering (IJISME), (2013), 1(9), 2319-6386.

[11] A. L. Ayzner, C. J. Tassone, S. H. Tolbert, and B. J. S chwartz, J. Phys. Chem. C.,(2009), 113, 20050-20060.

[12] J. T. Bell and Genene T. Mola, Physica B:Condensed Matter, (2014), 437, 63-66.

[13] Y. W. Su, S. C. Lan, and K. H. Wei, Materials today, (2012), 15(12), 554-562.

[14] G. Dennle, M. C. Scharber and C. J. Brabec, Adv. Mater., (2009), 21, 1323-1338.

[15] J. Nelson, Materials today, (2011), 437, 14(10), 462-469.

[16] B. Qi and J. Wang, Phys. Chem. Chem. Phys., (2013), 15, 8972-8982.

[17] C. Deibel, V. Dyakonov, Rep. Prog. Phys., (2010), 73, 396-401.

[18] G. Kalita, M. Masahiro, W. Koichi and M. Umeno, Solid-State Electronic, (2010), 54, 447-451.

[19] D. Gao, M. G. Helander, Z. B. Wang, D. P. Puzzo, M. T. Greiner, and Z. H. Lu, Adv. Mater., (2010), 22, 5404-5408.

[20] L. Yang, L. Yan, and W. You, J. Phys. Chem. Lett.,(2013), 4, 1802-1810.

[21] T. Ameri, P. Khoram, J. Min, and C. J. Brabec, Adv. Mater., (2013), 25, 4245-4266.

[22] R. A. Street, D. Davies, P. P. Khlyabich, B. Burkhart, and B. C. Thompson, J. Am. Chem. Soc., (2013), 135, 986-989.

[23] P. P. Khlyabich, A. E. Rudenko, R. A. Street, and B. C. Thompson, ACS Appl. Mater. Interfaces, (2014), 6, 9913-9919.

[24] Q. An, et al., Solar Energy Materials and Solar Cells, (2013), 118, 30-35.

[25] S. J. Lee, H. P. Kim, A. R. M. Yusoff, and J. Jang, Solar Energy Materials and Solar Cells, (2014), 120, 238-243.

[26] Y. J. Suh, S. Y. Park, T. H. Lee, W. S. Chung, K. K. Kim, Microscopy and Microanalysis, (2010), 16, 1378-1379.

[27] K. Norrman, M. V. Madsen, S. A. Gevorgyan, F. C. Krebs, J. Am. Chem. Soc., (2010), 132, 16883-16892.

[28] T. Aernouts, W. Geen, and J. Poortmans, Thin Solid Films, (2002), 297-301, 403-404.

[29] G. Li, Adv. Funct. Mater., (2007), 17, 1636.

Chapter 7

ENVIRONMENTAL STABILITY OF PTB7:PCBM BULK HETEROJUNCTION

SOLAR CELL

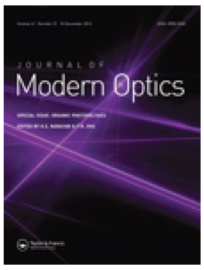

Journal of Modern Optics
Publication details, including instructions for authors and subscription information:
http://www.tandfonline.com/loi/tmop20

Environmental stability of PTB7:PCBM bulk heterojunction solar cell

Elhadi A.A. Arbab[a], Bidini Taleatu[a] & Genene T. Mola[a]
[a] School of Chemistry & Physics, University of KwaZulu-Natal, Scottsville, South Africa.
Published online: 23 Jul 2014.

Journal of Modern Optics, 2014
Vol. 61, No. 21, 1749–1753, http://dx.doi.org/10.1080/09500340.2014.941428

Taylor & Francis
Taylor & Francis Group

Environmental stability of PTB7:PCBM bulk heterojunction solar cell

Elhadi A.A. Arbab, Bidini Taleatu and Genene T. Mola*

School of Chemistry & Physics, University of KwaZulu-Natal, Scottsville, South Africa

(*Received 13 March 2014; accepted 30 June 2014*)

The short life span of organic photovoltaic (OPV) cell in an ambient laboratory condition is one of the challenges hindering the realization of organic-based devices. The presence of moisture and oxygen in conjugated polymer matrix is the major factors responsible for the degradation of organic molecules. The chemical degradation of OPV cell generally depends on the nature of the semiconductor polymer used in the preparation of the devices. However, the lifespan of unprotected OPV cells often ranges in the order of few hours in simple laboratory environment. We are reporting here the lifetime of organic photovoltaic cell in ambient laboratory condition whose active layer is composed of PTB7:PCBM blend.

Keywords: organic PV cells; polymer; PTB7:PCBM bulk heterojunction

7.1 Abstract

The short life span of organic photovoltaic (OPV) cell in an ambient laboratory condition is one of the challenges hindering the realization of organic based devices. The presence of moisture and oxygen in conjugated polymer matrix is the major factors responsible for degradation of organic molecules. The chemical degradation of OPV cell generally depends on nature of the semiconductor polymer used in the preparation of the devices. However, the life span of unprotected OPV cells often ranges in the order of few hours in simple laboratory environment. We are reporting here the life time of organic photovoltaic cell in ambient laboratory condition whose active layer is composed of PTB7:PCBM blend.

keywords: Organic PV cells, Polymer, PTB7:PCBM bulkhetrojunction.

7.2 Introduction

Gross mitigation of environmental degradation and global warming can be largely achieved through the use of renewable sources of energy. The renewable sources are environmentally friendly and inexhaustible. Solar energy is the most abundant and untapped energy sources in nature which can be converted into electricity by means of photovoltaic cell. Solar panels based on inorganic molecules have gained rapid growth in energy market since the past few decades because of the utilization of solar energy. However, the cost of these solar panels is still expensive and unaffordable for many around the globe. Organic photovoltaic(OPV) cells came into picture with the view of reducing the cost of device preparation by way of roll to roll printing technique [1-4]. They have attracted huge research attention both in

academia and industry because of their inexpensive approach of device fabrication, flexibility and light weight [5-14]. However, the low power conversion efficiency, environmental instability and short lifetime are still the major challenges of organic molecule based solar cells to compete with others in the energy market [11-20]. The mechanisms of solar energy conversion in OPV cell begin with the generation of excitons by absorption photons in the photoactive medium. This is followed by exciton relaxation into a charge transfer exciton state and simultaneous dissociation into free charge carriers electrons and holes. The design of device structure play an important role on the performance of organic solar cell though the optical and electrical properties of the polymer molecules are the major factors. The most effective device architecture in the preparation of OPV cell is the bulk heterojunction design which consists of acceptor and donor polymers blend sandwiched between two electrodes [1, 9-12]. This design enhances photon harvesting by creating intermolecular acceptor/donor interfaces for an efficient dissociation of excitons. The generated free charge carriers are then transported via percolating path ways to the electrodes. It is to be noted that the transport of charges is highly influenced by the morphology of the active layer which often can substantially improve by post fabrication heat treatment. However, the life time of the active layer remain susceptible to external environment.

An important progress has been made to increase the life time of OPV by way of encapsulation or lamination of the active layer of the devices to prevent from exposure to moisture and oxygen [4]. However, under ambient environment the life span of OPV cells is very short because of the instability of the organic molecules in air. Although it is not unusual to observe fast degradation of organic solar cell in the laboratory; there hasn't been much reports on how quickly the active layer degrades under ambient environment. The purpose of this investigation is to measure how quick the PTB7:PCBM active layer degrades in ambient condition. The degradation of OPV cells involves the chemical and physical transformations

of the organic molecules which lose its electrical conduction by absorbing moisture and oxygen [20-23]. Such transformation would indeed change the parameters of the cell. We are presenting here the degradation of organic photovoltaic cell beginning from fabrication to the point where the efficiency reduced by more than 80% of its initial value.

7.3 Experimental

The OPV devices were prepared on unpatterned ITO coated glass substrate which were partially etched by acid solution containing HCl:H_2O:NHO_3 [48%:48%:4%]. The substrates were cleaned thoroughly by successive sonication bath in detergent, deionized water, acetone and isopropanol for 10 minutes, respectively. They were then dried in an open furnace at 120°C for 20 minutes prior to the coating of PEDOT:PSS thin layer at 3500 rpm. The samples were immediately baked in an oven at 120^{o}Cfor 30 minutes. Following PEDOT:PSS the active layer composed of PTB7 and PCBM was coated from chloroform based solution (see Fig. 7.1). The solution of the polymer blend was prepared from PTB7 and PCBM at 1:1.5 stoichiometric ratio by weight. The concentration of the solution used in this experiment was 20 mg/ml. In order to allow homogeneity and inter-dispersion of donor/acceptor molecules the solution was sonicated for 3 hrs at a temperature between 35°C to 40°C. After coating the active layer the samples were again dried at 100°C for 10 minutes. They were then immediately loaded into the vacuum chamber for the depositions of LiF and aluminium electrodes. A very thin layer of LiF (0.3 nm) was first evaporated and followed by 100 nm thick Al electrode at base pressure of 7.6×10^{-7} mbar. A standard device structure as depicted in Fig. 7.2 shows the various layers of the organic solar cell. Except the deposition of aluminium electrode, the preparation of the devices were carried out under ambient lab-

oratory conditions without the use of glove box or clean room. The electrical properties of the devices was measured using Keithely 2400 source meter under AM1.5 solar simulator of integrated power density of 100 mW/cm^2. The power conversion efficiency (PCE) was determined from the J-V data under illumination condition. The electrical properties of organic molecules based solar cell follows a simple diode equation which can be expressed as:

$$J = J_s(e^{qV/kT} - 1) - J_{ph} \tag{7.1}$$

where V is the applied voltage. J_s and J_{ph} are the saturation and photon generated currents, respectively. The power conversion efficiency is defined as the ratio of the maximum generated power by the cell to that of the input power, given by

$$PCE = \eta = \frac{P_{max}}{P_{in}} = FF \cdot \frac{V_{oc} \times J_{sc}}{P_{in}} \tag{7.2}$$

The open circuit voltage (V_{oc}) and short circuit current (J_{sc}) can be determined from J-V data. The fill factor(FF) is determined from the expression:

$$FF = \frac{J_{max} \times V_{max}}{V_{oc} \times J_{sc}} \tag{7.3}$$

It is a measure of the squareness of the J-V curve which depends on the device architecture as well as the morphology of the active layer of the cell [19].

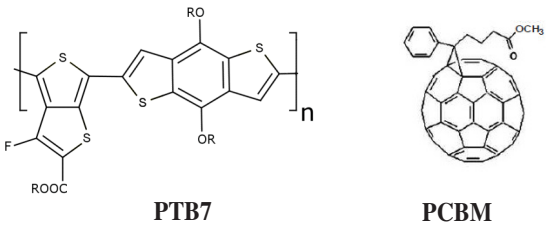

PTB7 **PCBM**

Figure 7.1: Chemical structures of the donor and acceptor molecules.

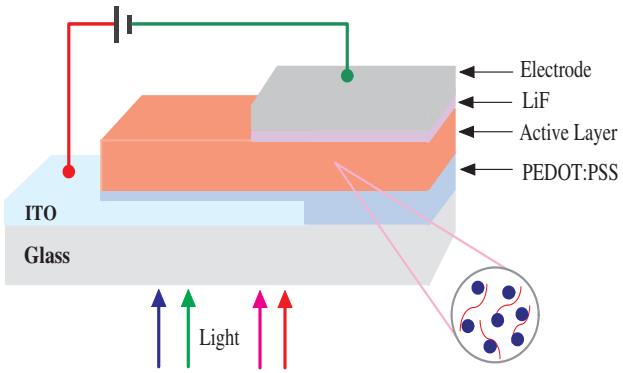

Figure 7.2: Schematic diagram for bulk heterojunction organic solar cell.

7.4 Results and Discussion

Several organic solar cells have been prepared under ambient laboratory condition where the samples are exposed to atmospheric air. The photoactive layers of the devices were composed of PTB7:PCBM blend which appeared for us more environmentally stable compared to the most common conducting polymers P3HT. The performance of the devices was studied using the electrical measurements taken both under illumination and dark conditions. The current-voltage characteristics given in Fig. 7.3 are taken from OPV devices prepared in this experiment. The J-V data represents a typical diode behavior of organic solar cell. The parameters derived from the data show that the mean values of the open circuit voltage, short circuit current, fill factor and power conversion efficiency (PCE) are found to be V_{OC}= 0.71 volts, J_{SC}= 17.2 mA/cm^2 FF=35%, and PCE = 4.3%, respectively. These values are consistent with the parameters reported in literatures except the fact that the recorded fill factor is relatively low in the present experiment. Such low fill factor is associated with the presence of high series resistance between the active layer and the electrodes which severely affects the shape of the J-V curve. The large series resistance could be attributed to the formation of oxide layers between the active layer and the electrodes as well as other defects

in the photoactive medium. However, inspite of such large series resistances in the samples, we have measured high current densities suggesting that there exist better donor/acceptor molecules miscibility in the photoactive medium.

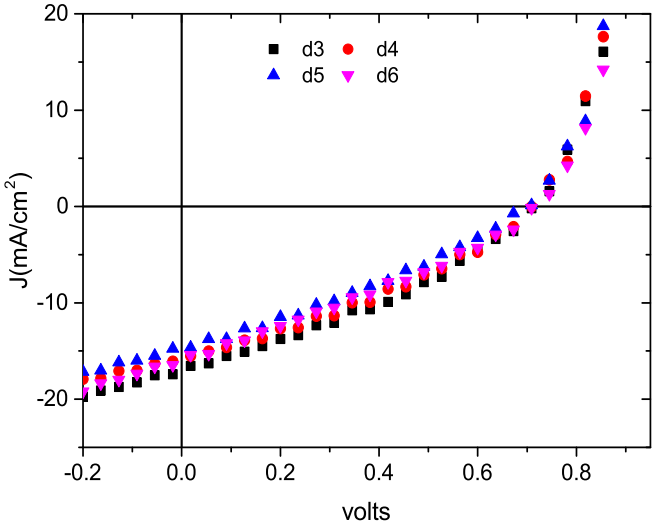

Figure 7.3: The current-voltage characteristics of bulk heterojunction organic solar cell whose active layer is composed of PTB7:PCBM blend. The symbols d3 to d6 denote the diode numbers in the sample solar cell.

A series of measurements were conducted on the samples at a constant time interval in order to be able to understand the rate at which the fabricated devices lose their power conversion efficiency under ambient laboratory condition. The laboratory temperature and humidity level were 24^{o}C and 62%, respectively. We have measured the J-V data under illumination from each diode to be able to determine the parameters of the cells. It is to be noted that the devices were kept under dark after each illumination measurement carried out at every 20 minutes interval. The power conversion efficiency of the solar cell, as depicted in Fig. 7.4, decreases slightly by changing from 4.3% to 4.09% in the first 40 minutes. After a 40 minutes

mark the efficiency decreases monotonically with time and lost nearly 60% of its efficiency in the second 40 minutes interval. At 200 minutes the efficiency of the device dropped to 0.4% which eventually disappear from the J-V data. Finally, the devices were no more active after 10 hours from discharging the solar cells from the vacuum chamber. The rate of PCE reduction was slow in the first 40 minutes when the device only lost only 5% of the initial value but drastically lowered within the second 40 minutes of its existence.

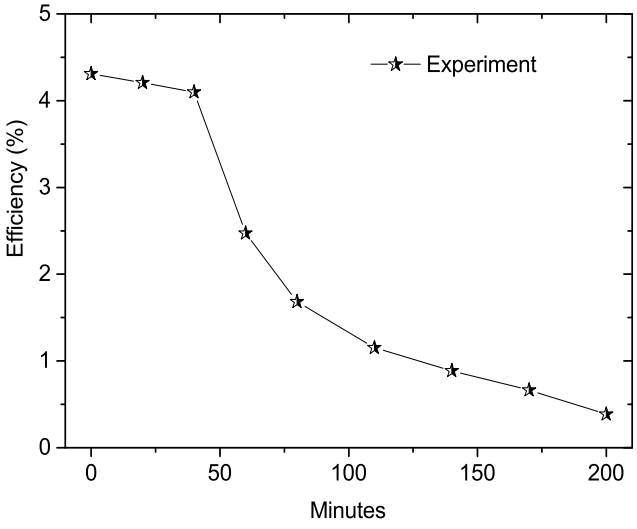

Figure 7.4: Power conversion efficiency of the solar cell as function of time.

Similar variations with time are observed on the open circuit voltage and short circuit current of the devices. These parameters are particularly important since both depend on the chemical and physical properties of the photoactive layer as well as the interfaces between the electrodes and the various layers of the OPV cell. The morphology of the medium for example plays a significant role in the determination of the transport properties of the free charge carriers across the electrodes which in turn affects the magnitude of the short circuit current. On the other hand, chemical transformation between the active layer and the

electrodes could ultimately change the value of the open circuit voltage. According to the data presented in Fig. 7.5 the open circuit voltage shows no significant variation for nearly 2 hours after the devices were produced (see Fig. 7.5). In fact, the mean value of V_{OC} was 0.68 volts at the beginning and then grew by 6% to 0.72 volts at 40 minutes mark. The growth of the V_{OC} at the early stage of the device operation could be attributed to the improved morphology of the interfaces between the photoactive layer and the electrodes due to the heat generated by the light illumination of the devices. After a 40 minutes mark the magnitude of the V_{OC} monotonically decreases with time and reaches to 0.57 volts at 200 minutes.

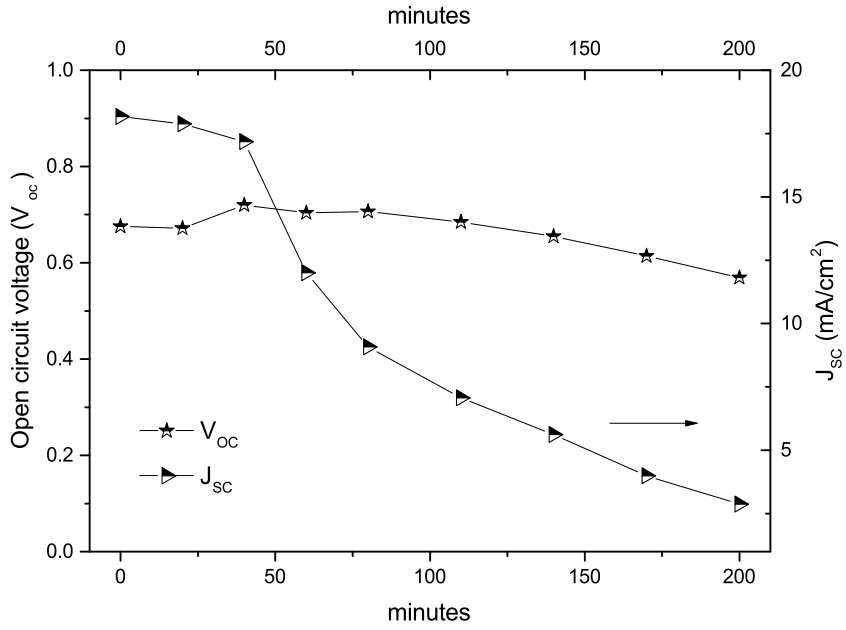

Figure 7.5: The open circuit voltage and short circuit current as a function of time for PTB7:PCBM active layer OPV.

The short circuit current meanwhile follows the same pattern of variation in time compared with that of the power conversion efficiency of the samples. The values of the short circuit

current decreases by nearly 5.5% in the first 40 minutes and then drops exponentially with time. The short circuit current reduced by 61% at 110 minutes, and further dropped to only 15% of the initial value at 200 minutes. Another parameter of the photovoltaic cell which was affected by the degradation process is the series resistance. Initially, the series resistance appeared to change linearly with time which grows from 72 ohms to 110 ohms in the first 40 minutes. Like the rest of the parameters discussed above the series resistance also drastically increases after the 40 minutes mark (see Table 7.1).

Time Min.	V_{oc} (volts)	J_{sc} (mA/cm^2)	FF	PCE (%)	R_s Ohms
0	0.68	18.2	0.34	4.3	72
20	0.67	17.8	0.33	4.2	94
40	0.72	17.2	0.33	4.1	110
80	0.71	9.1	0.25	1.7	458

Table 7.1: The cell parameters for best performed diodes.

This suggests that there are indeed chemical transformations of the molecules in the device which are responsible for preventing the generation and transportation of charges in the photoactive medium. The absorption of oxygen and moisture combined with photon induced chemical reactions are some of the mechanisms for the chemical transformation of the molecules in the active layer. However, it is not possible to distinguish the contribution of each of these factors on the over all performance of the device in this experiment. Therefore, the observed degradation is the result of the collective influences of all possible factors affecting the performance of organic photovoltaic cell. For instance, the creation of aluminium oxide between aluminium and the active layer will cause among others high series resistance.

In this experiment, in fact, we have observed high initial value of series resistance ($R_s = 72$ ohms) which is attributed to the ambient environment device preparation condition. Such high value of R_s severely affects the fill factor and the performance of the devices [19].

In addition to the electrical measurements discussed above the optical absorption measurements were also conducted on the samples. Fig. 7.6 shows the absorption spectra of PTB7 with and with out PCBM. The stronger absorption peak is representing the pure PTB7 polymer molecule which covers wide range of the visible spectrum as well as part of the infra-red regions. According to the data given in the figure one can clearly see that the absorption peak of PTB7 with PCBM is significantly lower than with out PCBM which is an indication of the miscibility of the two molecules in the photoactive medium. The quenching of the optical absorption in PTB7:PCBM blend is attributed to the interaction between PTB7 and PCBM molecules where the presence of PCBM in PTB7 matrix disrupts the crystallinity of PTB7 by hindering inter molecular interactions between PTB7 molecules [24, 25].

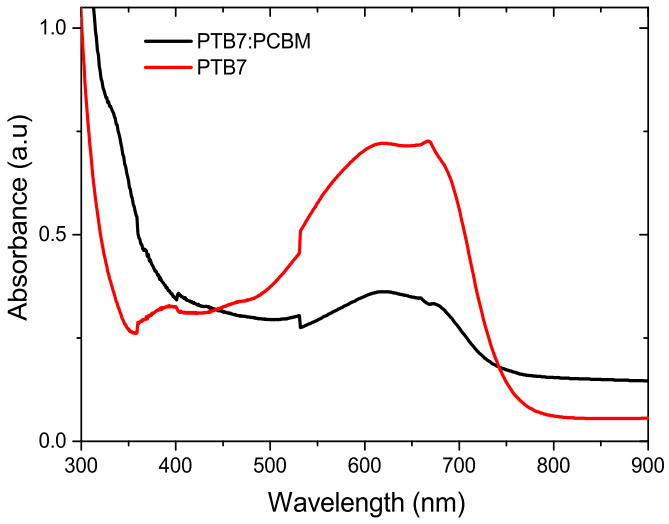

Figure 7.6: Optical absorption of PTB7 with and without PCBM.

The optical absorption measurements taken at various time after the preparation of the devices show no difference on the shape of the spectra. In fact, the spectra in Fig. 7.6 are taken after a month from device preparation which is found to be the same as those spectra taken earlier. This suggest that the molecules are optically active to absorb photons but the photoactive layer turned into electrically non-conducting medium as indicated in the electrical measurement.

7.5 Conclusions

The life time of PTB7:PCBM based organic photovoltaic cell was studied under ambient laboratory environment. Most of the cell parameters remain almost intact during the first 40 minutes of existence. However, the values of these parameter drastically dropped after the 40 minutes mark. The power conversion efficiency of the OPV cell reduced by more than 60% of the initial value at 80 minutes of its existence. The short circuit current and the fill factor are reduced by 50% and 25%, respectively, in the same time interval. The value of the open circuit voltage more or less unaffected up until 80 minutes. This suggest that the degradation most likely affected in the bulk of the photoactive medium away from the electrodes than near the electrodes. This is evident by the slow degradation of the open circuit voltage compared with the other parameters of the cell. According to the current result PTB7:PCBM bulk heterojunction photovoltaic cell can perform well for nearly 45 minutes with out any encapsulation under simple laboratory condition(i.e 24^oC and 62% relative humidity). However, the performance of the device is significantly reduced after an hour under such ambient environment.

Acknowledgments

This work is based on the research supported by the National Research Foundation (NRF), South Africa.

Bibliography

[1] C.J. Brabec, S. Gowrianker, J. M. Halls, D. Laird, S. Jia and S. P. William, *Adv. Mater.*,**22** (2010) 3839-3856.

[2] Y. Liang, Z. Xu, J. Xia, S.T. Tsai, Y. Wu, G. Li, C. Ray, L. Yu, *Adv. Mater.*,**22** (2010) E135-E138.

[3] M. C. Scharber, D. Mühlbacher, M. Koppe, P. Denk, C. Waldauf, A. J. Heeger, C. J. Brabec, *Adv. Fun. Mater.*, **18** (2006) 789-794.

[4] F. C. Krebs, *Solar Energy Materials & Solar cells*, **93**(2009)1636-1641.

[5] M. J. Currie, J. K. Mapel, T. D. Heidel, S. Goffri, M. A. Baldo, *Science*,**321** (2008) 226-228.

[6] H. Hoppe and N. S. Sariciftci *J. Mater. Chem.*,**16** (2006) 45-61.

[7] Y.Su, S.L. Lan, K.H. Wei, *Materialstoday*, **15**(2012)554-562.

[8] G. Zhao, Y. He and Y. Li, *Adv. Mater*, **24** (2010) 4355-4386.

[9] K. Kawano, J. Sakai, M. Yahiro and C. Adachi, *Solar Energy Materials & Solar cells*, **93**(2009) 514-518.

[10] G. Tessema, *Apll. Phys. A: Materials Science & Processing*, **106**, (2012) 53-57.

[11] Z. He, C. Zhong, S. Su, M. Xu, H. Wu and Y. Cao, *Nature phtonics*,**6** (2012) 591-595.

[12] C.J. Brabec, *Solar Energy Materials & Solar cells*, **83** (2004) 273-292.

[13] S. C. Jain, T. Aernout, A.K. Kapor, V. Kumar, W. Greens, J. Poortmans and R. Mertens, *Synthetic Metals*, **148** (2005) 245-304.

[14] R. Steim, F. R. Kogler and C. J. Brabec, *J. Mater. Chem.* , **20**(2010) 2499-2512.

[15] A. L. Ayzner, C. J. Tassone, S. H. Tolbert, and B. J. Schwartz, *J. Phys. Chem. C*, **113**(2009) 20050-20060.

[16] G. Dennle, M.C. Scharber and C.J. Brabec, *Adv. Fun. Mater.*,**21** (2009) 1323-1328.

[17] J. Nelson *Materialstoday* , **14**(2011)462-470.

[18] B. Qi, J. Wang, *Phys. Chem. Chem. Phys.*, **15**(2013) 8972-8982.

[19] D. C. Watters, J. Kingsley, H. Yi, T. Wang, A. Iraqi, D. Lidzey, *Organic Electronics*, **13** (2012) 1401-1408.

[20] M. Jorgensen, K. Norrman, S. A. Gevorgyan, T. Tromholt, B. Andreasen and F. C. Krebs *Adv. Mater.*, **24** (2012) 580-612.

[21] M. Jorgensen, K. Norrman, F. C. Krebs, *Solar Energy Materials & Solar cells*, **92**(2008)686-714.

[22] R. Bettignies, J. Leroy, M. Firon, C. Sentein, *Synthetic Metals* **156**(2006)510-513.

[23] F. C. Krebs, *Solar Energy Materials & Solar cells*, **92**(2008)715-726.

[24] V. Shroriya, J. Ouyang, R. J. Tseng, G. Li, Y. Yang, *Chem. Phys. Lett.*, **411**(2005)138-143.

[25] G. Li, V. Shroriya, Y. Yao, J. Huang, Y. Yang, *J. Mater. Chem.* , **17**(2007)3126-3140.

Chapter 8

Conclusion and future work

8.1 Summary

This thesis is composed of an investigation on the fabrication and characterization of organic thin films solar cell using PTB7 and P3HT as electron donor and PCBM as electron acceptor photoactive layer. Finally we studied the ternary molecules blend active medium composed of PTB7, P3HT and PCBM with a view to enhancing the optical absorption band of the medium. Part of the thesis has also dealt with the deposition and characterization of inorganic semiconductor thin films (V_2O_5, ZnO, and TiO_2) on transparent electrodes. All the samples, including the photoactive layers of the BHJ-OSCs devices and thin films, were fabricated by a sol-gel solution processing method in an ambient laboratory environment and using different low-cost techniques such as spin coating and electrochemical deposition.

The PTB7:PCBM binary bulk heterojunction OSC device's performance and lifetime were investigated, where the devices exhibited a PCE as high as 4.3% under ambient laboratory

condition. Other parameters associated with the PCE such as J_{sc}, V_{oc}, and FF were found to be 17.2 mA/cm^2, 0.71 V and 35% respectively. The devices fill factor was relatively low due to the high series resistance. However, the overall device performance was decreased with time due to exposure to ambient laboratory condition, resulting in drastic reduction on the values of the solar cell parameters.

The ternary molecules blend BHJ-OSC devices which were fabricated using P3HT, PTB7, and PCBM polymer and fullerene molecules, respectively, showed interesting results. The electrical and optical properties of the films were investigated and compared with binary molecules blend. The electrical property of ternary devices exhibited intermediate behaviour between the two constituent binary molecules device structures. But its performance is very close to that of the P3HT:PCBM blend due to the fact that the behaviour of P3HT in the ternary blend is more dominant than the PTB7. It was observed that PTB7 had poor miscibility in the solution containing P3HT and PCBM. Although the optical absorption of the ternary blend showed a red-shift when the concentration PTB7 was increased in the blend which led to improved light harvesting, the device performance remained poor due to the poor morphology of photoactive layer which caused high series resistance in the medium. The morphology of the ternary blend films were characterized using SEM, EDX, and FLM images which revealed the distribution of PTB7 and PCBM molecules in the film where PTB7 molecules were segregated from P3HT domain preventing better miscibility.

Furthermore, vanadium pentoxide (V_2O_5) thin films were successfully synthesized and prepared by electrochemical deposition for efficient and stable hole transport layer in the preparation of organic solar cell to replace PEDOT:PSS. The behaviour of the film is found to be dependent on post-deposition treatment such as annealing at different temperatures as well as various types of cleaning procedures used in order to remove residual impurities, thereby

improving the V_2O_5 films quality. We conclude that cleaning procedure by DI water followed by heat treatment at 400 – 450 ^0C showed better OSC devices performance. The V_2O_5 thin films exhibited high optical transmittance over a wide range of solar spectrum, and suitable energy level alignment for hole transport compared to PEDOT: PSS. The crystal orientation and surface morphology of V_2O_5 films were studied using XRD and SEM which showed that the deposited layers are crystalline and have orthorhombic structure. Their grains are also evenly distributed across the surface of the film. The OSCs fabricated on V_2O_5 buffer layer were found to be more stable and effective in the extraction and transportation of charge carriers from P3HT:PCBM photoactive medium.

In the study of layer-by-layer film of ZnO as thin film absorber layer on TiO_2 n-type semiconductor, nanostructure has been demonstrated by two comparable techniques. Porous combinations shown by morphological features suggest that brookite nanocrystals can be suitable for application in solar devices. This bilayer investigation generally revealed the presence of some metal oxides nanostructures which can be considered as effective photon absorber as well as a buffer layer between the photoactive layer and contact electrodes in photonic devices. As result, optical properties and energy band structure of the fabricated thin films indicated that they can be a suitable candidate for light harvesting. Effective charge separation and reduced recombination rate of charge carriers can make the films suitable as buffer layer in OPV devices.

8.2 Future work

The results obtained in this research show that by using solution processing methods of electrochemical deposition technique for transition metal oxides it is possible to deposit

thin films which can be used as buffer layers for OSC devices. This technique has several advantages over other techniques such as cheap device production cost and the possibility of large area deposition.

The transition metal oxides are promising candidates to improve the performance and environmental stability of OSC devices which are major challenges in organic molecules based solar cells.

Moreover, the investigation of synthesis behaviour of high work function TMOS such as V_2O_5 incorporating with PEDOT:PSS and its application in OSC devices are also very promising directions for future work. Also, the synthesis of bilayer thin films of TMOs such as ZnO/TiO_2 can be used as ETLs alternative to LiF. The application of the electrochemical deposition technique for the deposition of TMOs buffer layers in perovskite solar cells is another area of focus for future research. The technique can also be extended to the deposition of the photoactive medium in perovskite solar cell to achieve a controlled thickness and improved morphology of the photoactive medium.

Another avenue of investigation that would be of interest to improve device efficiency is the effect of solvent additive such as 1,8-diiodooctane (DIO), 1-chloronaphthalene (CN) and their mixture in ternary blends on charge transport.